Exploration of an adhesive peel test for failure and crack analysis of overmoulded MEMS packages

Michael Hall

School of Engineering

Thesis submitted for examination for the degree of Master of Science in Technology.
Espoo 31.12.2020

Supervisor

Prof. Sven Bossuyt

Advisor

Dr Sami Nurmi

Aalto University
School of Engineering

Copyright © 2020 Michael Hall

Aalto University
School of Engineering

Aalto University, P.O. BOX 11000, 00076 AALTO
www.aalto.fi
Abstract of the master's thesis

Author Michael Hall

Title Exploration of an adhesive peel test for failure and crack analysis of overmoulded MEMS packages

Degree programme Mechanical Engineering

Major Mechanical Engineering **Code of major** ME.thes

Supervisor Prof. Sven Bossuyt

Advisor Dr Sami Nurmi

Date 31.12.2020 **Number of pages** 107 **Language** English

Abstract

The proliferation of inertial MEMS sensors into automotive safety systems has contributed to annually declining road accidents and deaths. Being the integral sensing components for vehicular safety, the reliability of inertial MEMS is stringently tested in a wide range of thermal conditions, pushing the boundaries of the designs and materials. For this reason, die attach mediums are often subject to cracking or delamination during development qualification. Fully understanding the mechanisms behind these defects is essential in preventing and fixing them. This research set out to develop an adhesive peel test method for identifying and studying die attach adhesive cracks in over-moulded lead frame-based packages. This presented two main challenges, how to expose the die pad for peeling, and how to perform the peel test itself. Various de-capsulation methods were explored, resulting in the samples being ground to the die pad backside and die pad edge to allow access for peeling. Several peel methods were trialled with different levels of success. A manual peel test was successfully implemented, which effectively revealed the die attach surfaces for analysis. The peeled surfaces clearly revealed cracked adhesive surface morphology in three dimensions, which could be studied in detail with a SEM. The peels also revealed other die pad surface artefacts, the relevance of which could be investigated further in future research. All cracks and surface artefacts were clear and could be successfully measured using software tools.

Keywords Adhesive peel test, die attach, adhesive, inertial MEMS, cracking, delamination, over-moulded electronics packages, temperature cycling, silver-filled epoxy

Preface

I want to thank Professor Sven Bossuyt and my advisor Dr Sami Nurmi for their constructive guidance and patience throughout this thesis process.

Otaniemi, 31.12.2020

Michael A. Hall

Contents

Abbreviations

MEMS	Micro-electromechanical systems
CS	Cross-section
SEM	Scanning electron microscope
OM	Over-mould
VSC	Vehicle stability control
ASIL	Automotive safety integrity level
IC	Integrated circuit
SOIC	Small-outline integrated circuit
PCB	Printed circuit board
LCP	Liquid crystal polymer
DA	Die attach
ASIC	Application specific integrated circuit
BLT	Bond line thickness
SAE	Society of automotive engineers
t-dep	Temperature dependency
Tg	Glass transition temperature
CTE	Coefficient of thermal expansion
AEC	Automotive electronics council
TC	Temperature cycling
OEMs	Original equipment manufacturers
NDT	Non-destructive testing
CT	Computed tomography
CSAM	Confocul scanning acoustic microscope
BOM	Bill of materials

1 Introduction

Inertial MEMS (micro electrical mechanical systems) sensors have woven their way into the fabric of modern society and technology. The automotive industry in particular continues to push the inertial MEMS technology [1], where inertial MEMS are often integrated into safety-critical systems, contributing to a global downward trend in road collisions and deaths since their inception [2]. This safety-critical factor means inertial MEMS sensors must undergo very stringent testing during development and qualification in order to prove their reliability.

Components are subjected to tough environmental conditions, inducing significant stresses and deformations [3, 4], which over the product lifetime can lead to electrical drift [5] and even mechanical failure [6]. Minimising this lifetime drift is essential for a reliable, long-lived, product, which is up to 15 years in the automotive industry [7]. From a packaging point of view, delamination or cracking between MEMS die, adhesive, and package interfaces, are common failure modes that lead to electrical drift [8, 6]. Fully understanding the nature of these failure modes in detail is fundamental in the pursuit of workable solutions. This involves knowing exactly what the failure mode is and whether it is, for example, a consequence of non-optimised processing, material and geometric fatigue limits, and therefore design-related limitations, or micro-level surface interface incompatibilities. The specific area of interest for this study is the cracking and delamination of MEMS dies bonded by a silver-filled epoxy to an over-moulded lead frame.

In the case of over-moulded packages, internal defects such as cracks cannot be fully explored without destructive testing. When confirming and examining suspected internal cracks, usually cross-section (CS) analysis is relied upon [9]. However, CS analysis has limitations, for example, only 2-dimensional views of the component are achievable, the quality of CS is fully dependant upon lab worker accuracy, and interfacial delamination is sometimes difficult to confirm, even with the high magnification of the scanning electron microscope (SEM).

A common method for testing adhesive strength is by performing an adhesive peel test. There are a number of adhesive peel methods in use [10, 11, 12, 13] and peel mechanics are well studied and understood [14, 15]. However, for each case the peel test is either component-specific or performed in a lab with pre-prepared samples. There is no literature defining a peel test which specifically looks at pre-manufactured over-moulded electronic packages and associated adhesive interactions.

This study sets out to implement such a peel test method, where the die pad is peeled away from the components bonded to its surface and the surrounding over-mould (OM) material. and methods of achieving quantitative data from the test and results will be investigated. It is believed a peel test will reveal new insights into crack formation and provide a clearer view of possible delamination. If a crack is present, the peel test will give a 3-dimensional view of the crack surface, through the adhesive thickness as well as across the interface area. It is also believed that important information regarding the surface interactions between the constituent materials will also be revealed.

2 Background

MEMS in Society

Inertial MEMS are a type of inertial sensor which are manufactured by microfabrication processes. They are micro-systems substantially composed of 3D semi-conducting silicon structures which deflect under inertial changes. As a result of these deflections, there are changes in measured capacitance values, which are then interpreted by the system as some form of motion.

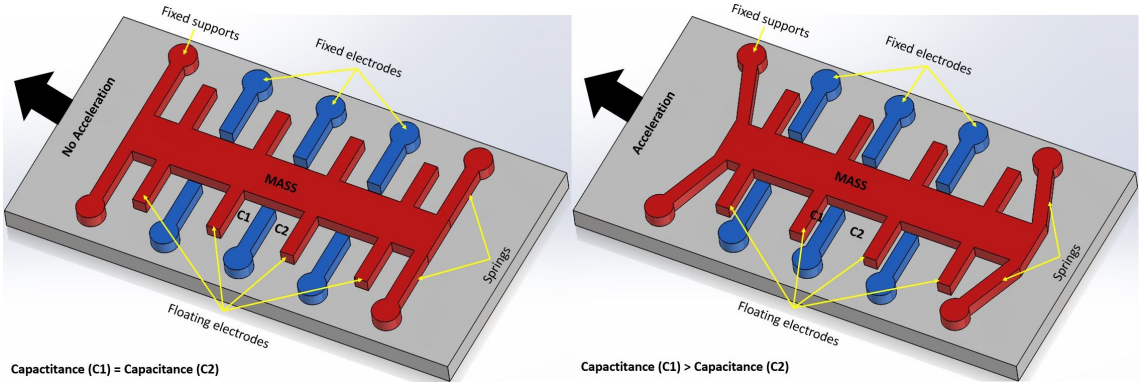

Figure 1: Working principle of a simple unidirectional capacitive spring/ mass accelerometer.

Figure 1 shows how the inertia of the silicon mass (red) affects the gap between the fixed electrodes and floating electrodes, hence creating a capacitance differential.

The inception of MEMS sensors has led to substantial downsizing of systems, giving MEMS a size and cost benefit over other inertial navigation methods [16]. The earliest developments of MEMS can be traced back to the 1950's [17] but inertial MEMS were first developed for commercial use in the 1990's for automotive crash detection [18, 19].

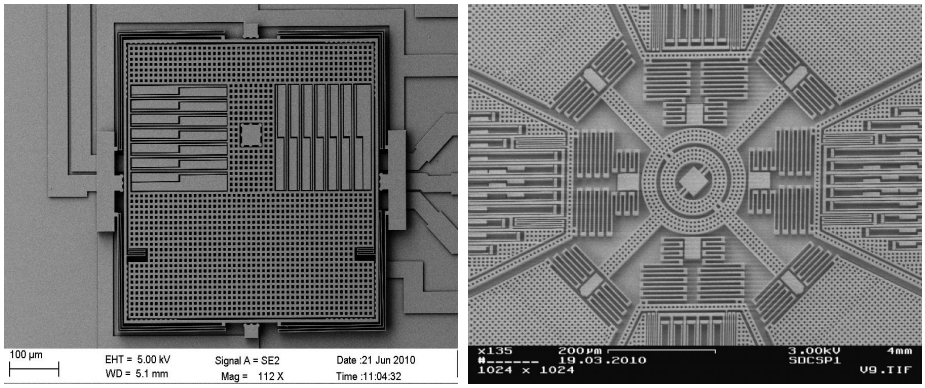

(a) 3-axis MEMS accelerometer.[20] (b) MEMS gyroscope [21]

Figure 2: SEM images of a 3-axis MEMS accelerometer and a MEMS gyroscope.

As can be seen in Figure 2 modern MEMS are very complex and intricate designs, this allows them to be extremely sensitive.

Inertial MEMS have traditionally been heavily utilised in the automotive and aviation industries, yet are now also commonly found in everyday consumer devices [22, 23], such as smart phones and sports watches. Although the global inertial MEMS market share for consumer electronics continues to grow, the automotive industry remains at the forefront of the technology [1, 24], where package space and cost are important design constraints, but arguably the most important constraint is reliability. As often is the case in the automotive industry inertial MEMS end up being integrated into safety-critical systems, for example, vehicle stability control (VSC), airbag deployment, and rollover detection [2, 25], where the sensor provides real time feedback to the control unit about the vehicle's motion; X,Y, and Z acceleration, as well as yaw, roll, and pitch rates.

Safety-critical systems are those characterised by the Automotive Safety Integrity Level (ASIL), outlined in ISO 26262 [26], as having a high severity where a failure could result in loss of life. The ASIL classifies risk based on the formula:

$$RISK = SEVERITY \times (EXPOSURE \times CONTROLLABILITY)$$

When there is a high severity the risk can only be minimised by minimising exposure and controllability which essentially define the probability of a failure occurring, this is where designing for reliability becomes crucial.

Although it is difficult to say exactly how MEMS devices have directly reduced road collisions and deaths, it can be said that they have enabled the development of some car safety systems [27] which has led to an overall decrease in road fatalities, as Kahane indicates in his report [28]. From 1993 to 2012 there was a 23% increase in lives saved, when comparing actual deaths vs potential deaths without safety systems in the United States, and an overall downward trend in actual fatalities [28, 2].

This safety trend is expected to continue with more and more safety systems being incorporated into modern vehicles. The proliferation of driver-assistance and autonomous vehicles will also require high performance inertial MEMS [29], which will mean global demand will naturally increase in the next few decades.

Package Technology

There is no standardised design for inertial MEMS packaging, with each sensor having its own bespoke package based upon its constituent MEMS elements. Therefore, packaging technology covers a broad range of designs. The designs can be categorised by the materials from which they are manufactured, metals, plastics and ceramics, and the method of connection to the system. The focus package of this study is frame level packaging, meaning a package based on a lead frame design, specifically a SOIC (small outline integrated circuit) design.

The packaging of inertial MEMS devices entails the complete assembly of the component. The packaging is what connects the MEMS elements to the outside world while at the same time protecting the MEMS integrity and sealing from the elements of nature. The packaging also defines internal connections and the placement of the

MEMS elements. For these reasons the packaging is arguably the most crucial part of the device development, requiring co-development with the system-level engineering [30] and is often the main obstruction in the development process [6]. This is because the packaging is what ensures the component remains reliable and stable in operation [6, 30], and takes up the largest material proportion of the complete device. The material and processing costs of the device are also largely made up by the packaging materials [31].

Package design presents many difficulties in trying to control and balance three main factors; electrical performance, mechanical robustness, and dynamic stability. Fundamentally the electrical performance and stability has to be good, as this is what the customers are predominantly seeking. To ensure stable electrical performance the mechanics of the device need to be robust, this comes with its own difficulties as there are numerous contrasting materials that need to be interfaced and withstand extreme environmental loads [6] such as differing coefficients of thermal expansion, and careful consideration of bonding interfaces and chemical compatibilities is required. In addition to challenging temperatures, automotive applications have very dynamic environments characterised by vibrations from the road, air and engine, therefore, the geometry and mass balance of the package should also be considered in order to prevent unwanted parasitic eigen modes. For these discussed reasons, inertial MEMS are a lot more difficult to package than conventional IC components [4].

Generally the SOIC type of packaging is made up by the following components:

- **Some form of lead-frame:** The lead-frame is the mechanical connection of the whole package to the PCB and acts as a platform onto which all the elements are attached, which requires good structural properties. As well as mechanical connection, it is also the medium of electrical connection of the internal elements to the outside system, this means the lead-frame must be made from a conductive material. SOIC lead-frames are generally around 1mil thick [32] and are formed by stamping, therefore the lead-frame material must also be ductile, with copper alloys being the common choice by displaying all of these required properties, and at more affordable prices than nickle-iron alloys for example [33, 32]. Lead-frames are made to have excellent surface finishes and are cleaned regularly in between process steps to prevent debris contamination, this is to create a suitable substrate for die attachment and plating [32]. Some surfaces of the lead-frame are also selectively-plated with inert metals, this is to prevent oxidation from inhibiting connectivity between bond wires and the copper alloy [34].

  Figure 3(a) is a nice example of a lead-frame used for a single component presented by W.-H. Li, note the wire bond pads have already been plated with silver, and Figure 3(b) shows some examples of frame-level lead-frames from the Shinko Industries website. Frame-level is how the frames are usually processed, it consists of an array of individual lead-frames stamped into a rectangular frame of one or multiple rows. This allows the manufacture and testing of greater quantities of components at the same time. Once all the assembly steps are complete the parts are formed and singulated.

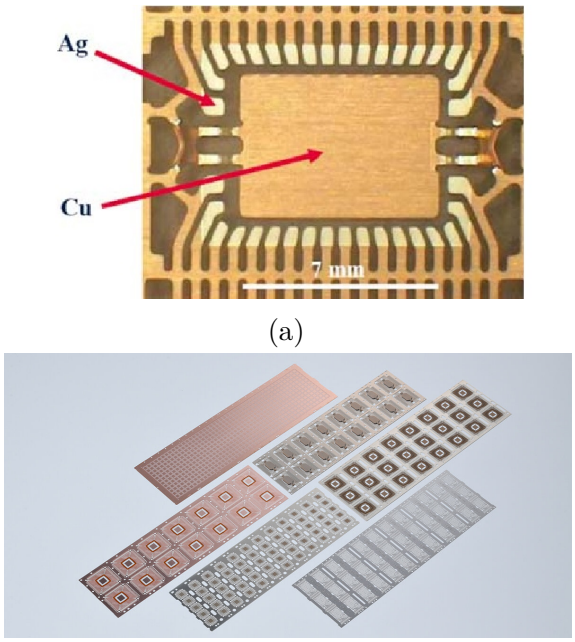

(a)

(b)

Figure 3: (a) Individual lead-frame [35] (b) Frame-level lead-frames [36]

- **Some sort of housing:** There are many different housing materials in use which has led to various packaging designs, but for SOICs the housing falls into one of two types, pre-moulded or over-moulded. The pre-moulded type housing is over-moulded onto a lead-frame into a cavity form, all the active components of the part are bonded inside this cavity, which is then filled with a protective medium, such as silicon gel, and then sealed with a lid, see Figure 4(a). The over-moulded housing is moulded onto the complete package after every component has been bonded to the lead frame, effectively enclosing and sealing everything from the elements see Figure 4(b). The materials commonly used for these two types of housings are application specific polymers; commonly used materials are liquid crystal polymers (LCP) and epoxies. These materials should be able to cope with changing temperatures with glass transition temperatures above the maximum operating temperature of the system, and withstand moisture penetration. They should also withstand the mechanical stresses exerted upon the package and limit the amount of stress transferred to the MEMS, also the housing material of over-moulded devices should not delamiante from the contained components; often adhesion promoters are used in the material to help prevent this.

- **Die attach materials:** Die attach (DA) materials essentially attach the MEMS dies and ASIC securely to the lead-frame or stacked on top of each other. There are various DA materials including, adhesives [39], films [39], sintering and soldering. However, for the purpose of this study the main focus will be adhesive-based DA, where commonly a silver-filled epoxy is used. The

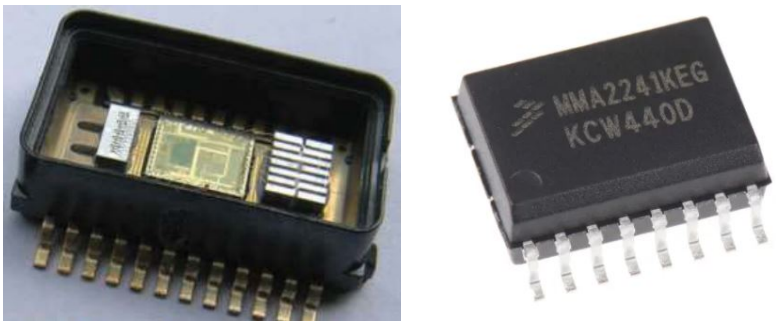

(a) (b)

Figure 4: (a) Pre-moulded cavity housing [37] (b) Over-moulded Housing [38]

adhesive is responsible for securely anchoring the dies to the substrate. It is important the integrity of this adhesion remains throughout the product lifetime in order to avoid drifting electrical outputs. These materials are often susceptible to cracking and delamination over lifetime, but the severity and occurrence of these should be kept at a minimum and not have any considerable effects on output of the MEMS. Difficulties in selecting the right adhesive are found when considering compatibility between substrate and adhesive and die, also interactivity of the adhesive with the overall package stresses should be carefully considered, for example, a relatively soft adhesive might absorb more stress and prevent inter-facial cracking but could introduce unwanted sensitivity in electrical output.

- **Bond wires:** These are generally very small diameter wires which are used to join electrical connections between MEMS dies, ASIC and lead frame. The wires themselves have little bearing on the overall package mechanics, however the integrity of the wire is important and often analysed for failure. Commonly used materials are gold, copper and aluminium, with two different attachment types, wedge bond, and ball bonding.

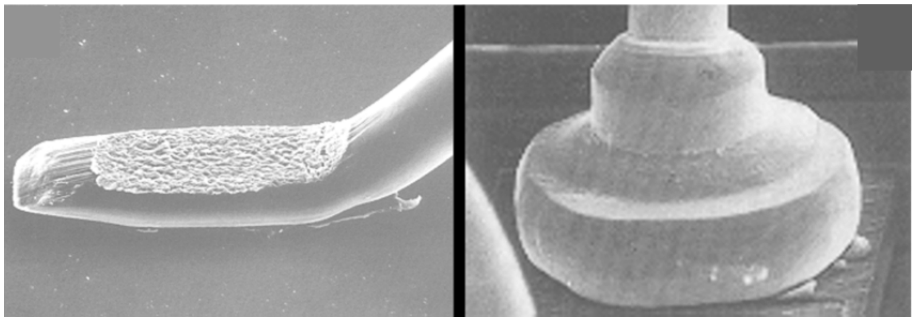

Figure 5: Comparison between wedge bond (left) and ball bond (right). [40]

The SEM images in Figure 5 taken from B. Mouawad's Phd thesis give a good visual comparison between wedge bonds and ball bonds.

Package Process Steps

The following section will briefly outline the basic process and assembly steps involved for over-moulded SOIC inertial MEMS packaging:

1. **Lead-frame forming:** The basis for the rest of the assembly is the lead-frame, which initially begins as a long reel of a specified lead-frame material. The material is then passed through a continuous flow assembly process and the desired 2D form of the leads and die pad are stamped into the material; the continuous flow stamping makes for rapid manufacture and is usually the desired manufacture technique for high volume production [41]. In some scenarios when at low volume or extra precision is required, especially when there is a high density of leads, sometimes chemical etching is used [41]. Some lead-frames are designed to have downset, this is where the die pad sits above or below the mid-plane of the lead-frame, the downset is bent into the frame after the initial stamping process. After the mechanical forming steps the lead-frame surface is treated, if required, to give the desired surface finish [42], followed by some form of cleaning process, often plasma cleaning. The cleaning ensures the surface is debris- and contaminant-free ready for plating. The areas that do not require plating are masked, and the areas that do require plating are electroplated. Finally, the lead-frames are cut to a specified length and sent to the assembly line.

2. **Dicing:** The MEMS and ASICs usually arrive at the assembly line in wafers which they require separation from. This separation process is dicing, where the dies are cut from their wafers.

3. **Die attach:** After another clean of the lead-frame surface die attach can begin. This is the process of fixing the MEMS and ASIC dies into their desired positions. The process takes place inside a machine which first dispenses the adhesive onto the lead-frame via syringe. The exact dispense patterns are designed to satisfy coverage and bond-line thickness (BLT) requirements and are often intellectual property but regularly patterns resemble star shapes, snowflakes, spirals, or dot matrices [43]. The pre-diced dies are then transferred and pressed into position on the frame. DA materials such as adhesives and films require curing in an oven [39], if there are multiple dies with different attachment methods, one will be attached and cured before the other is attached, as different attachment materials require different curing [39]. Sometimes there are also stacked MEMS [44], which will also require attaching after their substrate has been cured into place. Wait times in between these DA steps need to be carefully controlled in order to prevent too much process variability or moisture absorption into the components before curing.

4. **Wire bonding:** For wire bonding the frames are placed into a machine and heated. For ball bonding the metal wire is transferred through a capillary tube, a high-voltage charge is applied to the tip of the wire to melt it and create a ball, then the ball is pressed onto the wire bond pad and bonded via pressure

and ultra-sonic vibration. The wire is then fed to the next spot, similar to a sewing machine, and the ball bond is repeated. Wedge bonding is a similar process however instead of forming a ball, the wire tip is just forced onto the wire bond pad and bonded using ultra-sonic power. Usually ball bonding is more favourable for thin wires and wedge bonding is more favourable for thicker wires. Wire bond temperatures can affect some die attach adhesives, therefore wire bond temperatures should be considered during the adhesive selection process.

5. **Over-moulding:** Before over-moulding the lead-frame surface and components are cleaned again, ensuring there are no contaminants present which could prevent a good bond between the OM material and package. The moulding is performed either via transfer moulding or injection moulding. Both processes use pelleted pieces of OM material, however the difference between injection moulding and transfer moulding is the method by which the OM material is transported to the mould cavity. With injection moulding the pellets are first churned-up, heated to melting point and placed under pressure by a rotating screw, the liquid OM material is then forced under pressure through a runner system to each individual component and injected into the cavity; one effect of injection moulding is the presence of a circular injection point permanently set into the final product. Transfer moulding does not require a screw, but instead the OM material is heated and transferred into the cavities with brute force.

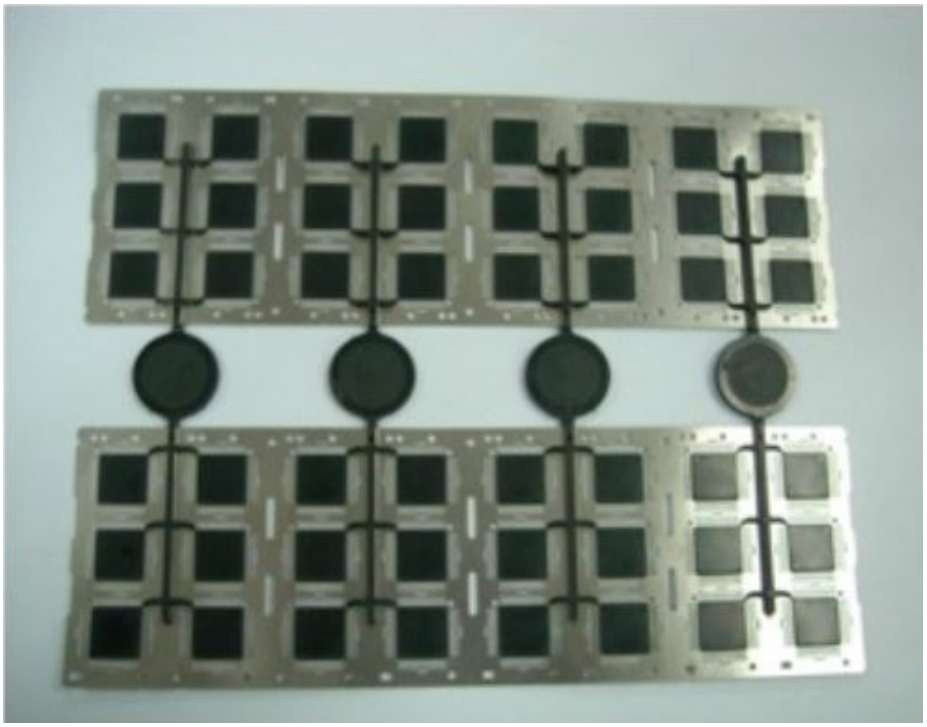

Figure 6: Example of transfer moulded lead-frame [45]

Figure 6 is an example of transfer moulded lead-frames, the four circular black discs are where the OM material pellets have been compressed; each with two runners on opposite sides which both then branch into three opposing pairs of cavities. In this example it can be seen that the lead-frame rows closest to the compressed discs are filled with OM material first, while the most distant cavities are the last to be filled. Also visible from the leftover material in the discs and the runners, an excess amount of OM material is used in order to prevent under-filling (aka short shot) and ensure every cavity is completely filled. Once the filling is complete the moulds will be held under pressure for a short period of time until the OM material solidifies and maintains its form.

6. **Post mould cure:** Immediately following the moulding process the frames are transferred to an oven where the OM material is be fully cured.

7. **De-flash:** After post mould cure, the lead frames can be tidied up by removing the flash (leftover unwanted material), this is often done by hand, but arguably a better approach is to first soften the flash by submersing the lead frames in a chemical bath and then using a water jet to remove it, this is nicely described on the Sun Surface Technology Co.,LTD website [46].

8. **Laser marking:** Laser marking is where identification markings are placed onto the surface of each component. This ensures every part has a unique reference that can be used for traceability reasons.

9. **Lead plating/ coating:** During this phase the exposed leads are plated or coated, the EEsemi [47] website gives a good description of this process. In plating, the leads are usually plated with tin, and with coating the leads are usually coated with solder material [47], this is important as it helps prevent the leads from oxidising and promotes good solderability.

10. **Trimming and forming:** The final steps of lead-frame manufacture finalise the shape of the component and singulate the components from the frame. If not already done, the leads are cut from the frame, and then formed into their final shape using a press tool; this is the form in which the components will be soldered to the PCB and the exact leg shape can affect the package eigen modes and therefore should be carefully considered during design. The parts are then trimmed from the lead-frame and calibrated.

11. **Calibration:** The calibration is a crucial step in the manufacture because, even though great effort is put into manufacturing identical parts, every component has minute differences [48, 49]. More importantly however is the effect of changes in temperature on electrical output [49, 50]. The automotive environment subjects the components to regularly varying temperatures with typical ranges from -40°C to 125°C, this places significant stresses on the package which are expressed in the sensor output. In order to ensure consistent and reliable operation, the device is calibrated over a temperature range [49, 50]. The calibration is performed by placing the component on a rotating table, which

itself has been calibrated to a high accuracy, and rotating the product in all axes subjecting it to gravitational forces [48, 49, 50]. When gravitational forces are not adequate for calibration the device is rotated with controlled accelerations and angular rates [48]. A common method for calibration is the six-position method defined by Aggarwal et al [51]. For temperature compensation the calibration is performed in an oven and repeated at various hot and cold temperatures as well as at room temperature.

Electrical Output

For automotive applications inertial MEMS provide vehicular motion feedback for acceleration along the three orthogonal principal axes, and angular rates about the three rotational axes. The coordinate system was devised by Gillespie in 1992 [52] and can be seen in Figure 7.

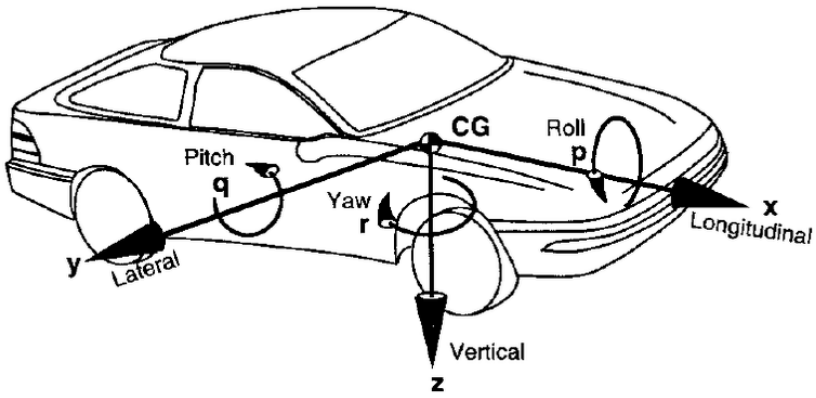

Figure 7: SAE Coordinate System [53].

Inertial MEMS packages house combinations of MEMS accelerometers and MEMS gyroscopes to achieve measurements from the axes required by the system. Table 1 describes the SAE coordinate system (Figure 7) and the required MEMS.

NAME	DESCRIPTION	MEMS REQUIREMENT
Longitudinal	Fore/aft acceleration along axis of driving direction (X).	X-Accelerometer or multi-axis acc
Lateral	Sideways acceleration perpendicular to road (Y).	Y-Accelerometer or multi-axis acc
Vertical	Up and down acceleration of vehicle (Z).	Z-Accelerometer or multi-axis acc
Roll	Rotation about driving direction (about X).	X-Gyroscope
Pitch	Rotation from front to rear of vehicle (about Y).	Y-Gyroscope
Yaw	Rotation controlling driving direction (about Z).	Z-Gyroscope

Table 1: MEMS requirement for six degrees of freedom.

To say inertial MEMS give feedback does not do justice to the vast amounts of data that can be measured from them, however the majority of these data points and how they are calculated are out of the scope of this study, instead the electrical output shall be examined from a package perspective. For inertial sensors the most

important parameter regarding accelerometer and gyroscope stability is zero-g offset [54, 55], which is affected by environmental changes such as moisture and temperature, as well as mechanical changes due to processing and changing stress states caused by cracking and delamination [56, 57]. In the case of this study the primary electrical output parameter discussed is accelerometer zero-g offset.

Zero-g offset is essentially the electrical output value in mg[1] given zero acceleration of the system. Hypothetically at zero acceleration the output should also be zero, however in reality this is only the design target and not actually achievable due to package mechanics and process errors, hence the term offset. During testing the inertial MEMS units are subjected to various temperature points where the zero-g offset measurements are taken. To relate the offset measurement to package mechanics zero-g offset is often used to calculate plots of temperature dependency (t-dep) and offset drift. T-dep is a simple plot of offset in mg vs each temperature point, see Figure 8, this plot is independently recorded after each test interval, for example, fresh parts[2], parts after preconditioning, parts after TC steps[3]. Offset drift is monitored during the component lifetime and is a plot of the change in offset at each test point, where the initial measurement is set to zero, this is done independently for each measurement temperature, see Figure 9.

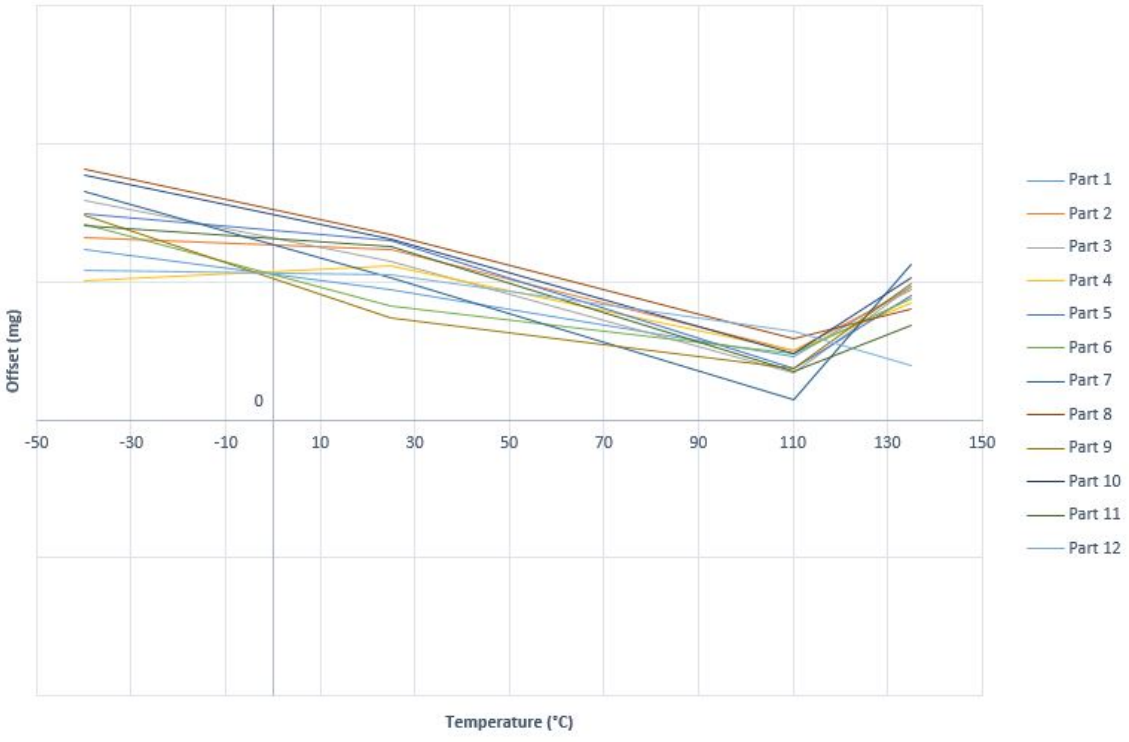

Figure 8: Example T-dep plot.

[1] $mg = Gravitational Acceleration/1000$

[2] Straight from assembly line without any preconditioning or TC

[3] For an explanation of the testing sequence and the abbreviation TC see subsection "Testing"

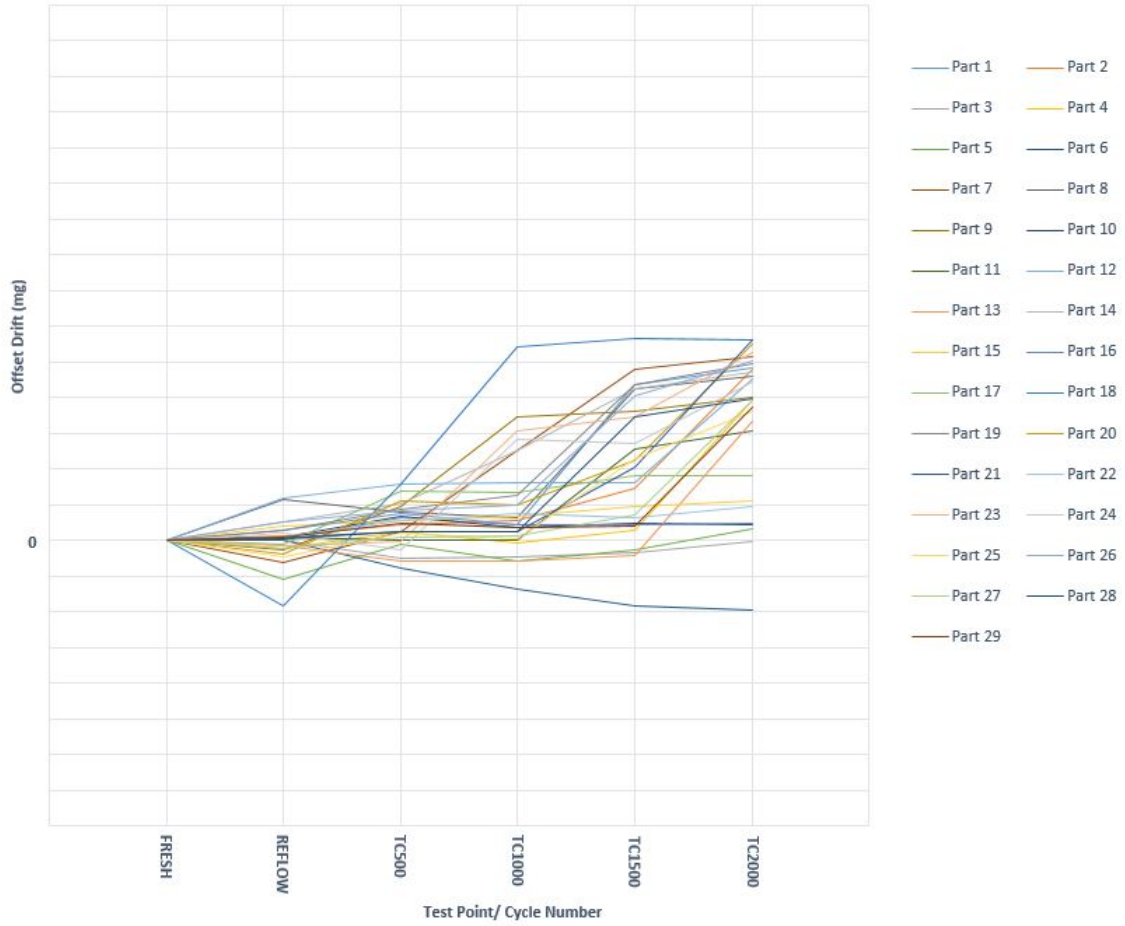

Figure 9: Example offset drift plot at -40°C.

Figure 8 shows how the highest offset is at -40°C and then decreases inversely with increasing temperature until 110°C where the offset begins to increase again. This increasing offset can be due to changes in package stress state, where, at this elevated temperature, the OM material and MEMS adhesives are approaching their Tg (glass transition temperature), changing in structure, and thus increasing their coefficients of thermal expansion (CTE). In Figure 9 it can be seen that Fresh samples are set to zero offset and for each successive test interval the offset is measured as drift from this zero point. As the testing progresses the amount of drift increases, which can be expected, but it is important to monitor this and keep it at a minimum through design and controlling manufacturing processes. Good components can clearly be seen from these results as lines which gradually increase in offset drift, and do not sharply diverge from the zero line. Bad parts are those displaying excessive drift or those which show sharp deviations in drift between test points, as this could indicate a change in package mechanics caused by cracking or delamination.

Testing

Being safety-critical components with a large focus on reliability, inertial MEMS are subject to rigorous testing and qualification processes. The Automotive Electronics Council (AEC) has devised a standard for all ICs named the AEC-Q100 [58], which specifies the appropriate qualification testing. Inertial MEMS sensors are an intricate mixture of package mechanics and micro-electronics which both contribute to the output signal, where poor electrical reliability is often the result of poor mechanical durability, for this reason the AEC-Q100 specifies multiple test groups, A-G, which cover mechanical integrity, electrical reliability and overall package durability tests [58]:

A Accelerated Environment Stress Tests

B Accelerated Lifetime Simulation Tests

C Package Assembly Integrity Tests

D Die Fabrication Reliability Tests

E Electrical Verification Tests

F Defect Screening Tests

G Cavity Package Integrity Tests

Group A, Accelerated Environment Stress Tests prove the overall durability of the MEMS package and ensure the components can survive the extreme conditions subjected on them by the environment, this includes temperature cycling (TC) and moisture effects on component lifetime performance. Usually within a vehicle the package will experience cold temperatures due to geographic location and time of year, and hot temperatures due to proximity to hot-running components, such as engines and brake units [59, 60]; often on cold days a large temperature change can occur in a short period of time, with adjacent hot-running components gradually getting up to operating temperature, therefore the operation environment of the components can be simplified as temperature cycling [61] and hence an accelerated TC test has been devised by the AEC to prove the mechanical durability of the component. Some automotive original equipment manufacturers (OEMs) demand up to 2000 cycles for IC qualification, with no failures, depending on the component operation temperature grade [58]. As TC testing places some of the most demanding mechanical conditions on the device over lifetime, it will be the basis of testing for the analysis presented in this study.

As outlined on page 11 of the AEC-Q100 [58] the testing can be summarised as per table 2. Automotive components which are integrated into harsh thermal environments are tested at Grade 0, see table 3, which are the most stringent test conditions, subjecting the components to 2000 cycles with temperature shocks from -55°C to +150°C. Prior to TC testing all parts undergo preconditioning, which is

TEST	GRADE	TEMPERATURE TEST RANGE	NUMBER OF CYCLES	ACCEPTANCE CRITERIA
Temperature Cycling	0	-55°C to +150°C	2000	0 Fails
	1	-55°C to +150°C	1000	0 Fails
	2	-55°C to +125°C	1000	0 Fails
	3	-55°C to +125°C	500	0 Fails

Table 2: Summary of TC testing requirements.

GRADE	AMBIENT OPERATING TEMPERATURE RANGE
0	-40°C to +150°C
1	-40°C to +125°C
2	-40°C to +105°C
3	-40°C to +85°C

Table 3: Part Operating Temperature Grades (as per Table 1 in AEC-Q100) [58].

also a requirement of the AEC-Q100, however exact preconditioning parameters are determined on an application specific basis.

For TC testing the following test sequence and analysis steps are performed:

1. **FRESH:** Fresh parts, parts which have come straight from the assembly line without any preconditioning or testing but often already calibrated, are analysed using various non-destructive imaging techniques such as, X-ray and CSAM[4]. If electrical data is required, zero-g offset will also be measured. These are baseline measurements to ensure the parts are in spec before being subjected to testing.

2. **PRECONDITIONING:** Preconditioning in general engineering practises simulates a break-in period, such that the tested components better represent components that are already in-situ in their working environments, for automotive MEMS sensors, this would be already soldered to a PCB and installed on a car. Before attaching the components to a PCB they are often transferred between factories and sometimes stored in warehouses, during this time the package will absorb moisture from the air. When being attached to a PCB the components undergo a solder reflow process, where temperatures are usually in excess of 215°C [62], this is well above the boiling point of water causing the moisture to immediately vaporise. These high temperatures and vaporisation place elevated stresses on the components, thus preconditioning is required for IC packages to test their robustness against this reflow process. Preconditioning consists of first soaking the components with moisture and then repeatedly subjecting them to solder reflow temperatures. The same imaging and electrical analysis is also carried out after this step.

3. **TC:** TC is performed on the components in predetermined intervals, such as every 500 cycles or every 1000 cycles. The process uses an environmental chamber which can quickly switch between sub-zero temperatures and temperatures above 100°C; commonly a two zone shock chamber is used, similar

[4]See section "Current Analysis Methods" for descriptions of X-ray and CSAM analysis

to that pictured in Figure 10. This chamber consists of two compartments, where a controlled platform transfers the parts between the two chambers. For general TC testing, one chamber is raised to the maximum temperature value specified in the test requirement, the other chamber is set to the corresponding minimum temperature, and the parts are switched between the two chambers at set intervals, generating a thermal shock. One cycle consists of two thermal shocks, one of the thermal shocks is generated by quickly transferring the parts from the hot chamber to the cold chamber and the other thermal shock is generated by the opposite operation (cold to hot). The intervals between thermal shocks are devised based on the time it takes for the components to reach equilibrium at each temperature. For Grade 0 automotive components the shock cycle temperature range is -55°C to 150°C. After each TC test interval the components are imaged and analysed electronically.

Figure 10: Two-zone thermal shock test chamber [63].

Package Mechanics and Cracking

During operation inertial MEMS packages will experience various mechanical loads from the environment, many transient loads come from vibrations from the road surface and other forces on the vehicle, as well as processing forces, but inertial MEMS packages are not load-bearing devices and therefore cyclic loading of this nature is not a great concern. More critically however, inertial MEMS packages are subjected to cyclic thermal loads from their environment, this is an area of great interest when considering device reliability and longevity.

The molecules of any material that is at a temperature above absolute zero[5] will have heat, a form of kinetic energy, this energy causes the molecules to vibrate, which results in separations between them. As the temperature increases the amount of heat within the material also increases, and more kinetic energy means the molecules will vibrate more vigorously, causing them to separate further apart. Thus, any material will increase in geometric dimension when heated, this phenomenon is known as thermal expansion. The amount of thermal expansion for any given temperature change varies from material to material due to differences in molecular structure, therefore the amount of thermal expansion for any given material is defined as a coefficient of thermal expansion (CTE). It is also important to note that a material's CTE value is dependent upon the temperature and state of that material, as the dimensions of the material do not change linearly with temperature.

MEMS packages contain materials within them of differing CTEs which leads to a conflict in geometric dimensions as temperature conditions deviate from steady-state [64, 3]. The conflict in the amounts of thermal expansion causes the materials to fight against one another, with constituent molecules battling for space to vibrate. As a result the materials find a compromise which causes deformation and deflection of the overall package. These deformations give rise to significant stresses on the internal structures of the package [3, 4].

MATERIAL	**CTE** ($\times 10^{-6}/^{\circ}C$)	
Copper	16.63	[65]
Mould Compound	3.9	[65]
Die-attach Adhesive	30 to 50	[66]
Silicon	3.0	[66]

Table 4: Typical values of CTE for package materials.

Table 4 displays some typical values for CTE of general package materials. Common constituents of IC packages are copper and silicon, which have significantly different CTE values. Copper is typically around $16\times10^{-6}/^{\circ}C$ in the ambient operating temperature range (see Table 3), but can vary a little depending on the particular alloy type. Silicon generally has a CTE value of 2.5-3.5$\times10^{-6}/^{\circ}C$ in the same temperature range, but given its isotropic nature, the CTE of silicon varies

[5] Absolute zero is the theoretical minimum temperature in the universe, defined as 0K. K is the symbol for the unit of temperature devised by William Thomson, 1st Baron Kelvin, which is equivalent to an increment of degrees Celsius plus approximately 273°.

linearly with temperature [67]. Interfaced around and between these two materials are complex material compounds such as epoxies, which make up a substantial percentage of the package. These materials exhibit a very broad range of different CTEs based on filler type and quantity as well as resin type. The shape and distribution of fillers can also affect the directional thermal expansion of the component, for example, this is often the case for fibre-filled compounds, where the mould-flow dictates the fibre orientation within the component, and because thermal expansion along the length of the fibers is less than thermal expansion across the fibres the resulting expansion is not uniform.

Deformation of MEMS packages not only introduces stresses between the components but also has a knock-on effect on the electrical output [5]; short-term changes in the stress-state of the package, mostly from thermal changes, can be compensated by the system [50] often through aforementioned[6] calibration techniques [48, 49]; however, long term stress effects can lead to electrical drift over lifetime [5] due to changing packaging mechanics. A problematic source of lifetime drift is inter-facial adhesive cracking, cohesive cracking, and delamination [68]. Often at material interfaces within IC packages, abnormalities such as voids are present [68], these can be sources of high stress concentrations under deformation and are starting points for crack propagation [69]. In addition to abnormalities, IC packages are generally made up from very square components, with sharp corner interfaces. These types of geometries also introduce high stress concentrations [70]. When the stresses in these areas exceed a certain level the crack will propagate across the interface [68], this is described by well established and understood fracture mechanics [71, 72].

Although cracking can occur as early as the processing stage, or during preconditioning, inertial MEMS fatigue cycle requirements are often 2000 cycles [58], where the components undergo plastic deformation in a cyclic manner, therefore failures can be described by the low-cycle fatigue model [73, 74]. L. F. Coffin and S. S. Manson defined the Coffin-Manson relation equation 1 which describes this behaviour.

$$\frac{\Delta\varepsilon_p}{2} = \varepsilon'_f \left(2N\right)^c \tag{1}$$

Where:

- $\frac{\Delta\varepsilon_p}{2}$ is the plastic strain amplitude.
- ε'_f is the fatigue ductility coefficient[7].
- $2N$ is the number of reversals to failure, where N is the number of cycles.
- c is the fatigue ductility exponent.

Typically with die-attach adhesives there are three types of cracking mechanism, these are nicely visualised in Figure 11 from a report by S. Bazhenov [75]. Figure 11(a) shows cohesive cracking through the adhesive itself, Figure 11(b) shows delamination,

[6] See section "Electrical Output"
[7] Strain intercept at $2N = 1$

characterised by layer separation, where the adhesive layer has debonded from the die or substrate layer, and Figure 11(c) shows cracking which has propagated across the adhesion interface. Mechanisms (b) and (c) are different in the way the adhesive interacts with the adhesion surface, in (b) there is complete debonding which indicates a failure of adhesion to the surface, which can be due to chemical incompatibility or contamination of the substrate surface for example. Whereas (c) is a failure of the adhesive material at the adhesion interface but there is still adhesion between the two layers.

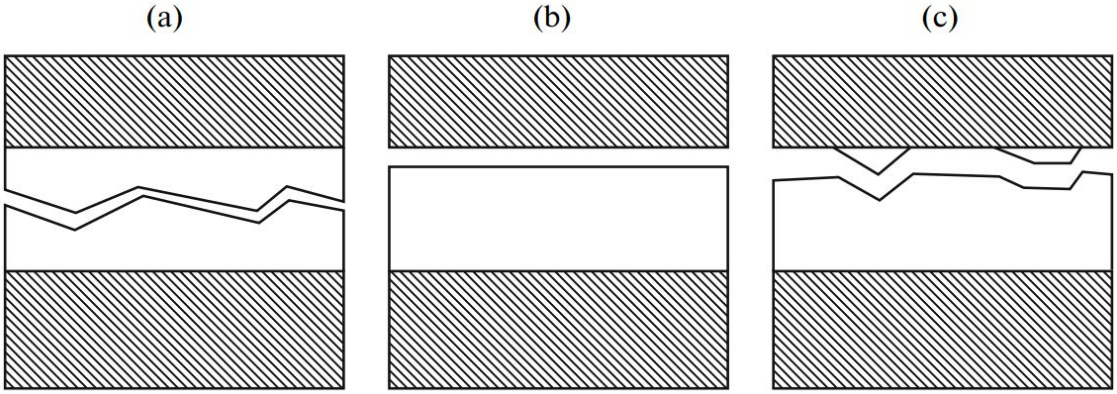

Figure 11: Typical failure mechanisms associated with adhesion layers [75].

Usually mechanisms (b) and (c) are initiated from the highly stressed areas at the outer corners of the die and along one of the interfaces with the adhesive; either the die-adhesive interface or substrate-adhesive interface. As cycling continues, the crack propagates from this initial corner across the interface area. Figure 12 displays a series of CSAM[8] images of an ASIC die at different TC testing intervals; the upper and lower images are the same except for the filter used. The ASIC and adhesive area of the upper images are visualised by a square of a lighter shade of grey and the die pad is the surrounding slightly darker shade of grey. At test interval 1 a small abnormality can be seen in the bottom right hand corner, characterised by a white-ish area in the upper images and a yellow area in the lower images. At each successive test interval these white-ish and yellow areas progressively increase in spread, which indicates some form of propagation from either a crack or delamination.

Mechanism (a) usually occurs purely due to low-cycle fatigue described by Coffin-Manson [73, 74], the initiation point is a defect or pre-existing crack. Often in die-attach adhesives the cohesive cracking initiates from an inter-facial crack, then propagates through the adhesive layer until it reaches the second interface. After the crack has propagated through the thickness of the adhesive it then continues to propagate along the second interface as per mechanism (c). This cohesive behaviour can be clearly seen in the cross section displayed in Figure 13. Also in the CSAM images of Figure 12 at test intervals 4 and 5 darker shade areas appear just above

[8]See section "Current Analysis Methods"

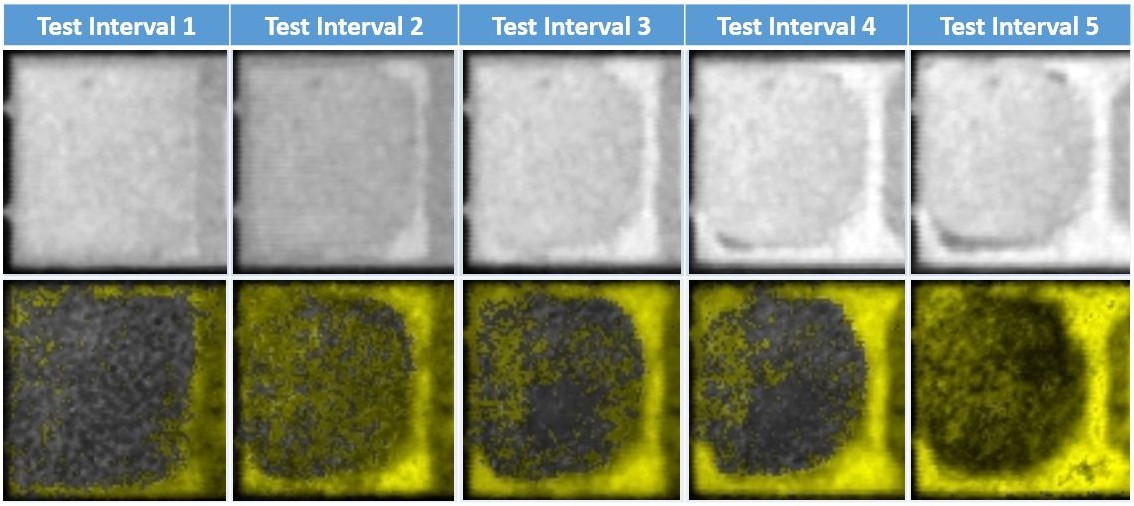

Figure 12: CSAM images of crack propagation at various intervals of TC testing.

the white-ish cracking/ delamination areas, this is also indicative of where a cohesive crack has propagated to the opposite adhesive interface.

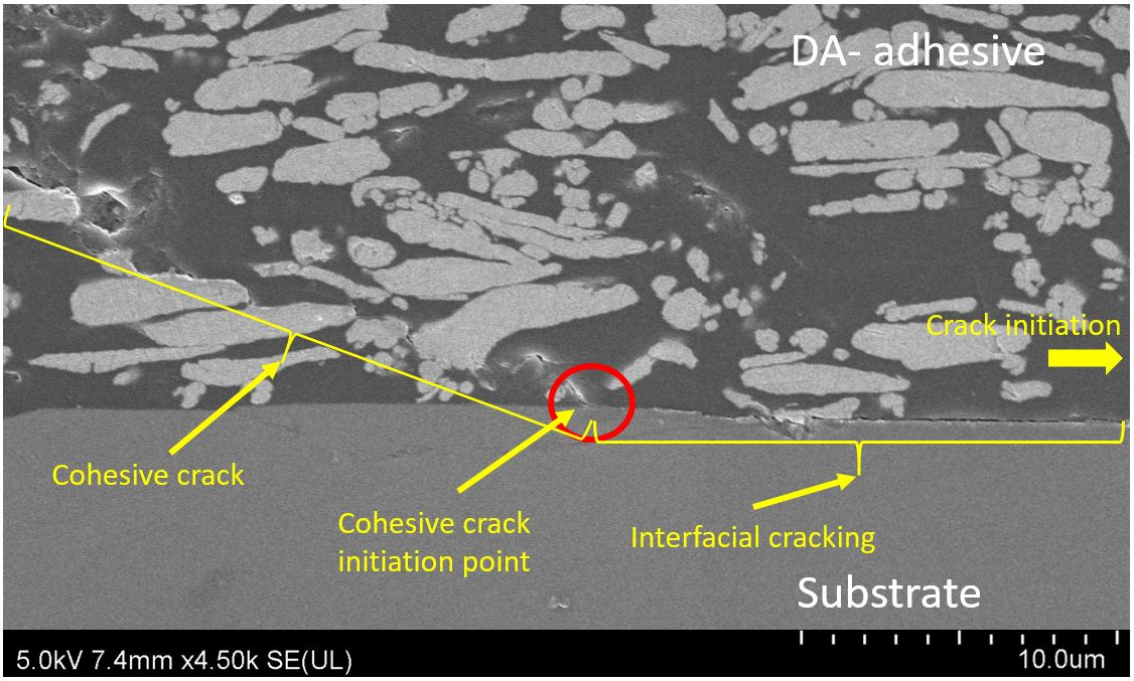

Figure 13: Cross section displaying cohesive crack behaviour in silver-filled epoxy DA material.

Current Analysis Methods

A number of non-destructive testing (NDT) methods exist for electronics package crack analysis [76], including X-ray and various acoustic microscopy methods, such as confocul scanning acoustic microscopy (CSAM). These methods, described below, are useful for looking inside the over-moulded housing without having to destroy the component, this means these methods are generally used for monitoring the components during testing. Often X-rays are taken once during testing to screen for processing defects, and CSAMs are taken at each test interval to check for potential cracks and delamination, or other abnormalities occurring due to test conditions. Post testing analysis is often carried out through cross-sectioning at pre-determined locations where defects might lie, or where various geometries can be measured, and imaging using microscopes.

- **X-ray:** X-ray imaging is achieved by exposing the sample to electromagnetic radiation from an X-ray tube. The X-rays generated penetrate the sample, where different materials absorb different amounts of X-rays. Behind the sample is usually a detector or camera of some kind, which is exposed to the X-rays after the sample. The absorption pattern is interpreted by the system, which outputs an image of various contrasts based on the absorption [76], see Figure 14.

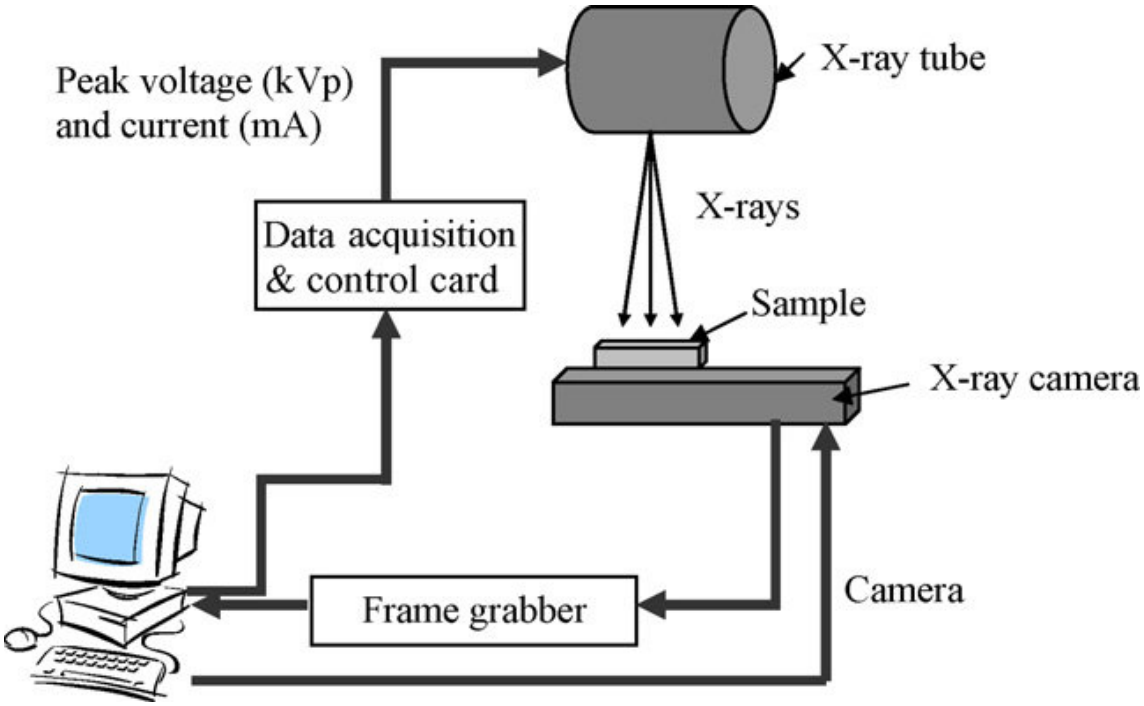

Figure 14: Diagram of X-ray equipment [77]

Importantly for IC packages, housing materials, like plastics and epoxies, absorb very few X-rays in contrast to metals, which absorb a much greater percentage

of what they're exposed to, this contrast allows for good X-ray imaging of IC packages. Figure 15 displays a couple of examples of 2D X-ray images, this is when the sample is imaged from only one view point. Figure 15(a) shows a component with two dies attached, notice how the polymer housing can barely be seen, but the metal lead-frame is quite clearly visible. The epoxy adhesive is also visible around the dies, this is likely due to the filler content being highly X-ray absorbing. The thickness of the materials is also an important factor in X-ray absorption, thicker cross sections of the same material will appear darker in the image. In the case of very thin ASIC dies, X-rays mostly penetrate through, however their outline and position in the component can be seen from the contrast created from a metal-filled DA adhesive; where the adhesive spews outside the perimeter of the die, creating a fillet, the adhesive cross section becomes thicker, creating a darker contrast in the image.

Computed tomography (CT) scanning can also be carried out, which follows the same principle as 2D X-rays however, instead of an image being created from just one view point, the sample is rotated and multiple images are taken from set angles, which are then combined together to create a 3D image. This is useful for more detailed images, and for building 3D maps of the component.

X-rays are useful for checking the assembly of the package and for screening for process defects, such as wire sway and voiding. In Figure 15(a) the bond wires are clearly visible and any sway introduced during processing can be spotted, excessive sway could introduce stray capacitance, or in a worse case cause a short-circuit, which will affect the electrical output. In Figure 15(b) voids can be seen, which could also introduce stray capacitance. Voids are typically formed by trapped air bubbles, or due to material shrinkage, indicating a non-optimised manufacturing process.

Due to the fact package cracks are extremely small, X-rays are often unable to produce good images of the defect, however useful information relating package cracking can be obtained, such as, DA adhesive coverage, adhesive fillet shape, and adhesive voids.

- **CSAM:** CSAM stands for confocul scanning acoustic microscopy, which means instead of using light to obtain an image of an object, ultrasound is used. This imaging method is useful as the contents of opaque materials cannot be seen using light, and sound has a higher penetration depth. The CSAM creates images of internal components by measuring the acoustic impedances of the constituent package materials. A transducer is positioned over a component and focused at a particular level, the focus is set by measuring the time of flight of the sound wave. After the focus has been found the transducer moves to a starting position, then scanning begins, where the transducer is swept back and fourth across the sample surface.

  Figure 16 demonstrates how the time of flight, x-axis, corresponds to the reflection signals of the constituent components. In this image the lowest time of light corresponds to the reflection signal from the top surface of the package.

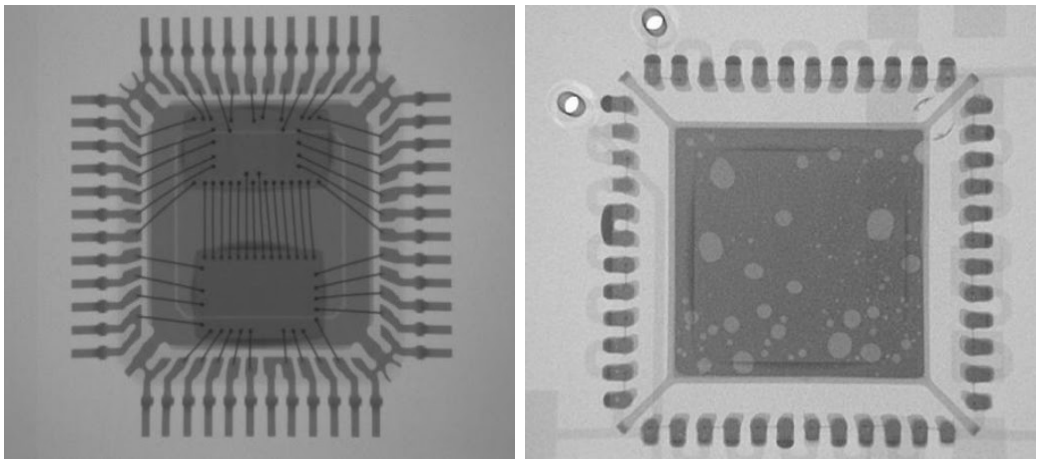

(a) (b)

Figure 15: Example images achieved from 2D X-ray: (a) Component with two dies [78]. (b) Component with visible voids [79]

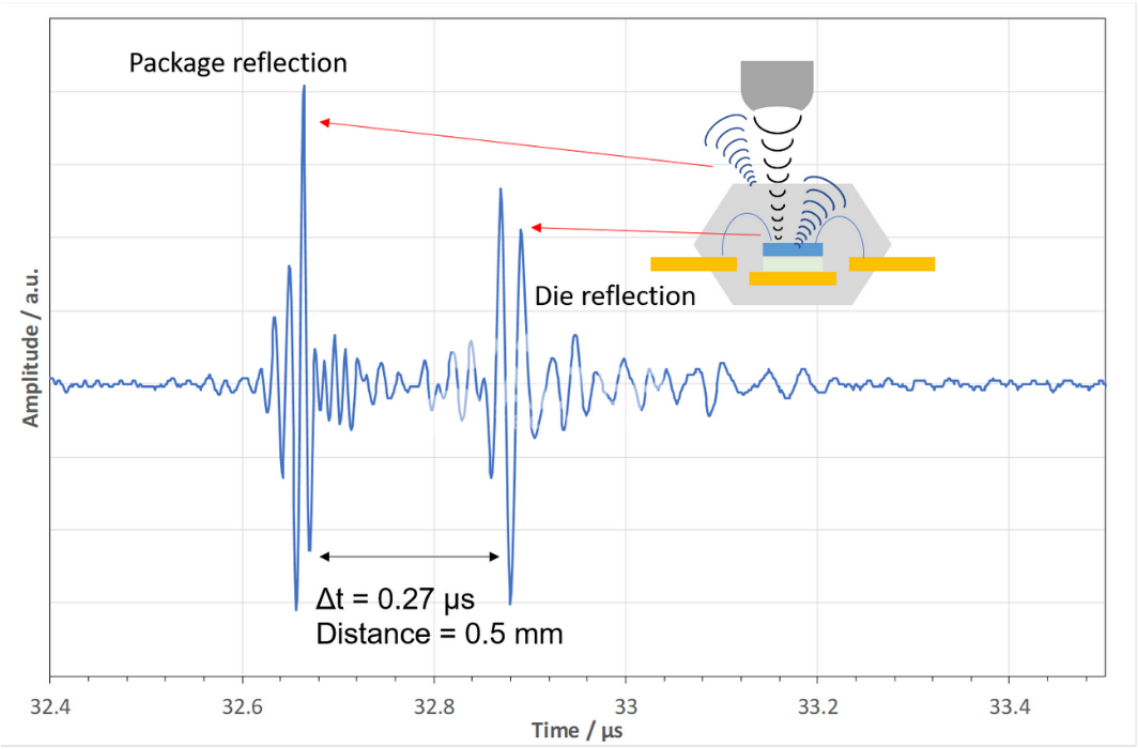

Figure 16: Focusing a CSAM [80].

The sound waves are transmitted which penetrate into the sample, where some are reflected, some scattered, and others absorbed. The reflected waves are then compared with the transmitted waves and material impedances are then calculated [76]. These impedances allow the creation of visual images. An example of how different material interfaces and gaps affect the reflection

of the sound waves can be seen in Figure 17. To obtain good images of the various areas in an IC package, multiple scans are required, where the transducer is focused at different depths, and constituent parts and materials are distinguished in images by colour contrast. Cracks, delamination, voids and other abnormalities, are very easily indicated with CSAM imaging.

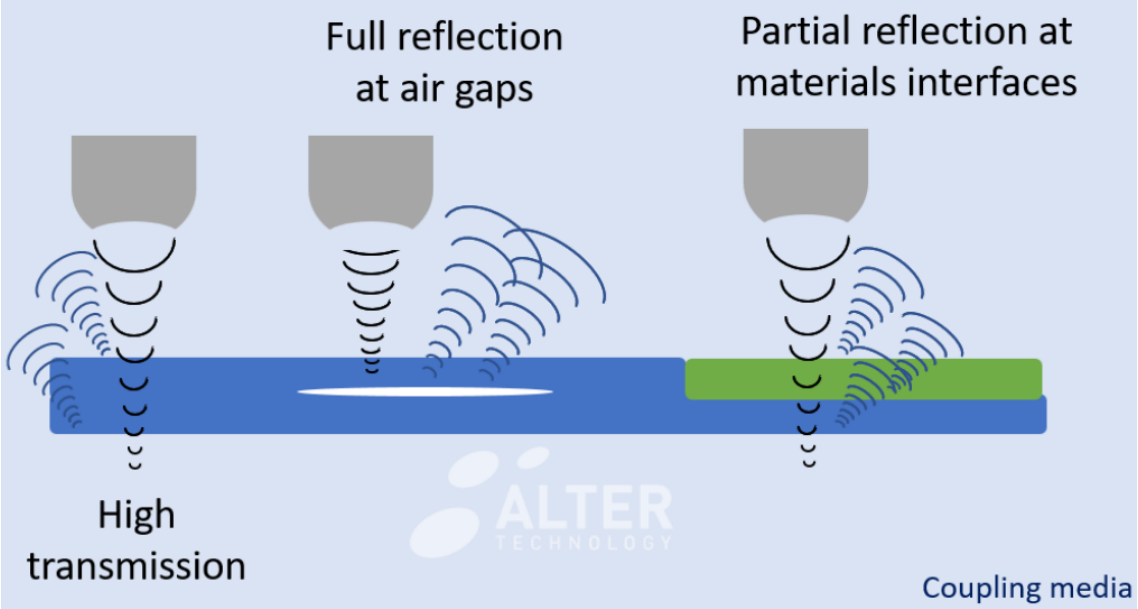

Figure 17: Effect of gaps and material interfaces in CSAM imaging [80].

CSAM is a very important tool during inertial MEMS qualification as it allows the components to be monitored throughout the testing process, which means failures can be reported and analysed more quickly. However, CSAM can only indicate and give a limited amount of information with regards to a defect, where phenomena such as cracks, delamination, and voiding are indistinguishable in CSAM images if they occur at the same depth or at the same material interface, therefore indicated defects later need to be confirmed through destructive testing methods.

- **Cross-Section Analysis:** To achieve a more detailed view of defects within the components destructive testing methods are required. Heavily relied upon in electronics packaging industries for crack analysis is cross-section (CS) analysis [9] (often referred to as cross-cut analysis). A CS view is achieved by selecting a plane that is required to be seen and removing material up to that plane. There are various methods of removing the material, such as cutting, milling, and wet or dry etching, however the most commonly used method for IC packages is grinding. Typically, for well defined and detailed CSs, the sample is first encapsulated in an epoxy button. This is a mixture of resin and hardener which is moulded over the sample in a cylindrical form, then left to cure. The over-moulded button allows for better control over the sample when grinding,

and it also allows for a highly polished surface finish to be achieved; which is optimal for imaging. Usually, the grinding stage of the CS is broken down into several increments with successively finer grit paper, this helps control the speed and accuracy of the result. The majority of the material is removed using a coarse paper, then a few finer grits are used to get close to the required CS depth, and finally the finest grit paper is used to finish; a finer grit gives a smoother surface finish without large gashes. Even after grinding with fine grit paper the surface remains relatively rough, hence the requirement for polishing, which is performed when the correct CS depth is reached. Cross-sectioning is typically an iterative and time-consuming process, where image quality is limited by operator skill. An example polished CS is imaged in Figure 18, note scratches remain on the surface, likely leftover from the coarse grinding paper stages and too deep to be polished out, which could effect the level of information obtainable from the image.

Highly detailed CSs are achievable, especially when over-moulded into an epoxy button and sufficiently polished; often as fine as 1μm, which can then be inspected under a microscope, where the CS can be examined for defects and important geometries can be measured. However, only a two-dimensional view is produced by CSs, which does not give a full perspective of defects, such as cracks, which propagate in three dimensions. Surface interaction information cannot be obtained from CSs either, especially surface finish and possible presence of surface contamination. Also, whether two layers are adhered to one another or just touching is impossible to see with CS analysis.

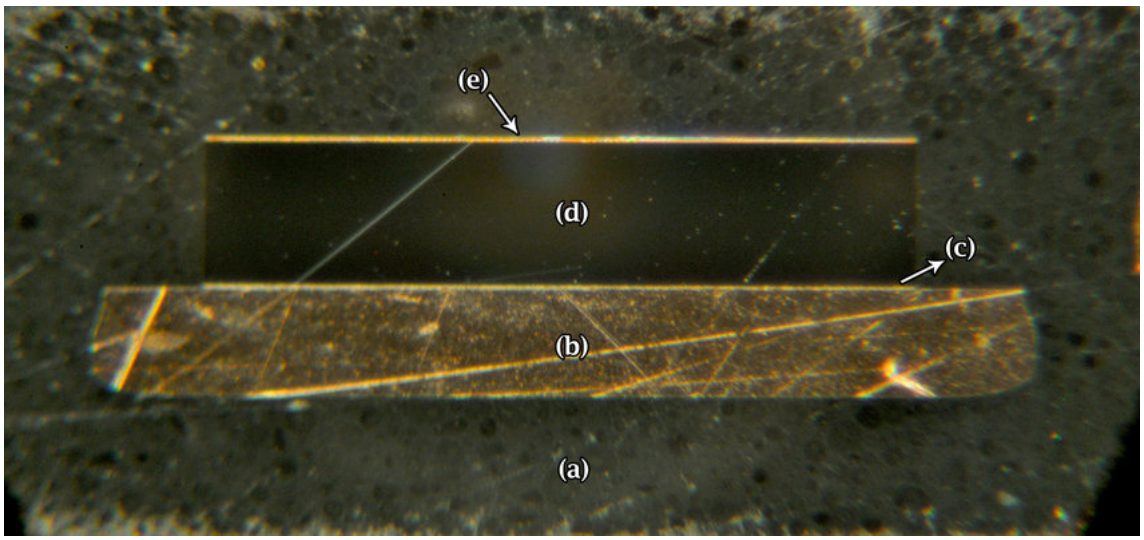

Figure 18: Cross section of a SOIC package. (a) OM Material, (b) Die Pad, (c) DA adhesive, (d) Die, (e) IC metalization layers. Image captured by optical microscope [81].

- **Microscope Imaging:** Typically two types of microscope are used for imaging the CSs, these are optical microscopes and scanning electron microscopes (SEM).

Optical microscopes use light for imaging a sample, however package materials have highly varying reflectance which can make seeing certain details quite difficult. In the case of DA cracking, the die pad substrate is a highly reflective metallic component, as well as the silver filler in the DA material, but the epoxy component of the DA material is dull, therefore optimum exposure adjustments are difficult to obtain, making very thin-line cracks impossible to see. For good quality images of high magnification, usually a SEM is used. Instead of reflecting light off of the sample, a SEM sends fast moving beam of electrons to the sample, positioned in a vacuum chamber, which scans over the surface, generating various signals which are transformed into an electron micrograph, which can be a highly magnified. Before placing a sample into a SEM it often requires coating with conductive gold, especially when the sample is predominantly composed of non-conductive material, this process is called sputtering and prevents the sample surface from charging and distorting when being bombarded by electrons. Usually DA cracks can be seen in SEM images of cross sections, unless very fine, however no information is obtainable as to the level of adhesion between the DA and the die or die pad, which necessitates a need for an alternative analysis method.

Peel Testing

This study proposes to implement a novel "Peel Test" method for overmoulded lead frame-based IC packages, which can be used instead of CS analysis for crack and delamination investigations. The destructive test will be specially devised for checking the adhesion strength of DA materials, as well as surface characteristics of the adhesive and bond surfaces, for correlation with crack and delamination occurrence.

A peel test is a method by which two bonded surfaces are pulled apart by peeling; there are several different peel test setups, T-peel, 90° Peel, and 180° Peel, which can be seen in Figure 19, are generally used. T-peel describes a method where two bonded flexible adherends are arranged into a t-shaped sample, and pulled apart, whereas 90° Peel and 180° Peel are where a flexible adherend is bonded directly to a substrate, and then pulled off whilst the substrate remains fixed, at 90° or 180° respectively. In order to quantify the peel force, usually peel forces are recorded during the test, either by plotting the load vs extension curve for the whole test, or alternatively by just recording the maximum load.

Peel tests are common testing methods for adhesion characterisation [10, 11, 12, 13], and the mechanics of such tests are well studied and modelled [14, 15]. 90° peel tests appear the most common form of peel test in use for electronic chips due to the multi-layer makeup of the components, where each layer consists of a contrasting material. Studies carried out in [10, 11] are examples of where 90° peel tests are used. [10] investigates the effect of cure state on the adhesion strength of an anisotropic conductive adhesive film and characterises the adhesion by performing a 90° peel test. This study also demonstrates how the fracture surfaces post-peeling can be inspected under SEM and important information which can be gained from them; in this case,

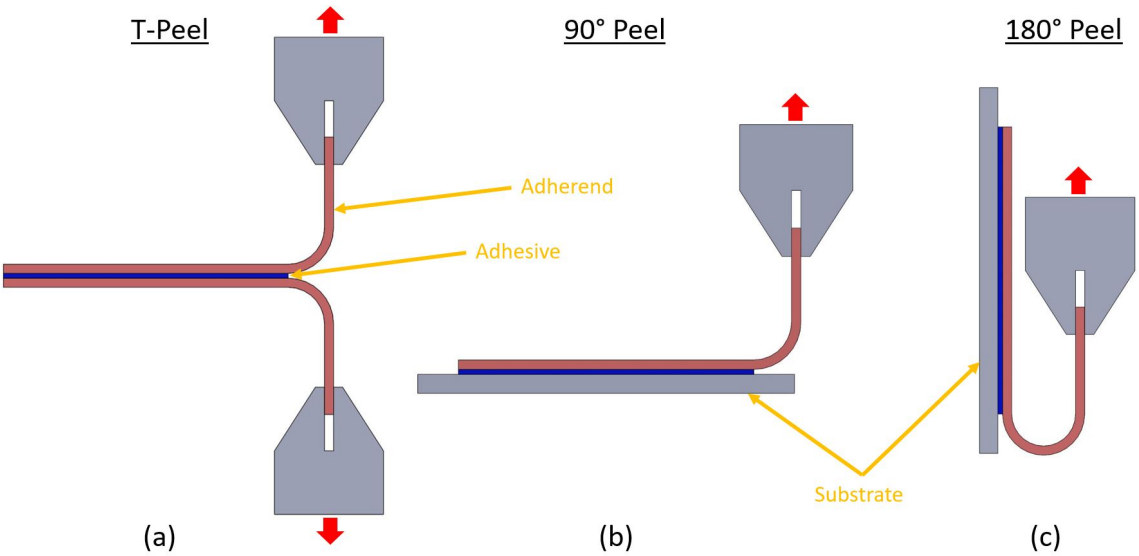

Figure 19: Peel test methods (a) T-Peel, (b) 90° Peel, (c) 180° Peel.

as well as fracture morphology, the cure state of the film could be determined; Figure 20 is a nice image, highlighting the possibility to image the crack morphology under a SEM after peel testing. [11] is another example of a 90° peel test being performed on chip-in-flex packages. In this case the peel test was used to correlate the adhesion strength of an adhesive film with whether it had been plasma treated on one side, both sides, or not at all. [13] models a peel test similar to the T-peel test imaged in Figure 19(a), however in this case two bonded materials are forced apart using a wedge at the adhesive interface, instead of being pulled apart; this example does not include a physical test.

[12] sets out to develop a quantitative peel test method in a similar fashion to this study, which highlights important factors which need to be controlled during peel testing such as, peel rate, peel angle, magnitude of peel force, duration of peel force, and wait time before peel, however wait time between application and peel is irrelevant for cured DA adhesives. The study found these factors would contribute to the peel test result, necessitating control measures to keep them consistent and ensure the results are repeatable. The study successfully defines a quantitative peel test method, however it approaches the topic from purely an ideal lab-based scenario with pre-prepared samples; the study also acknowledges that the method is not suitable for small-scale devices such as inertial MEMS, the main reason being the tape used was too large (19mm width) for micro-fabricated components.

A common characteristic of all the peel test examples provided is the pre-prepared nature of the samples, designed specifically to be peel tested in a lab with the correct equipment. In contrast, the main difficulty with the peel test method to be investigated herein is how the method requires being implemented on a sample which has not been specifically designed for peel testing. In pre-prepared samples connections to test machines can be catered for, however the subject of this study does not have any mechanism for connecting to a test machine.

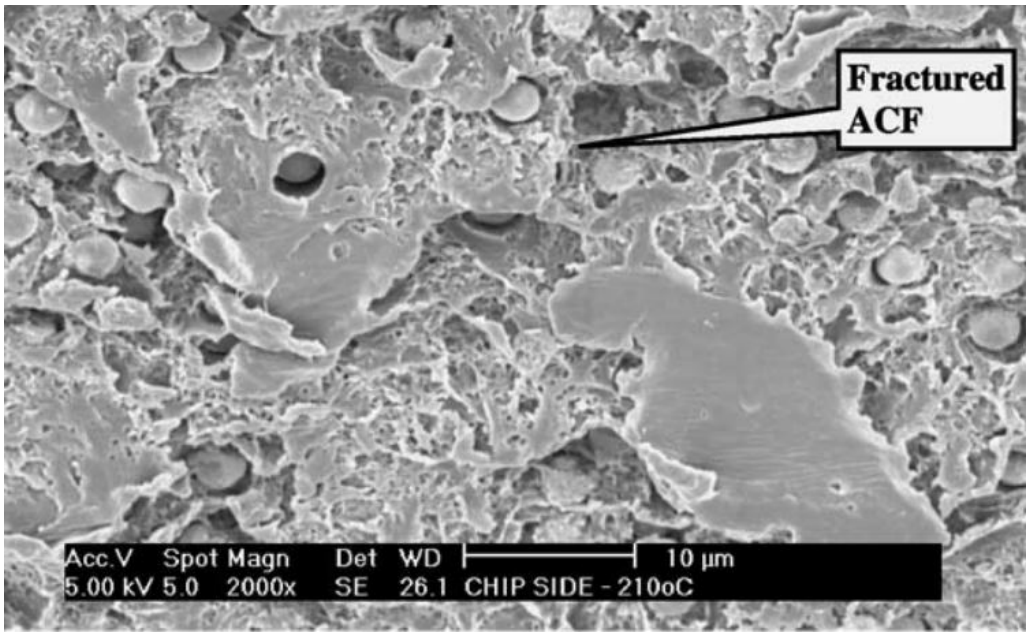

Figure 20: Crack morphology imaging capability [10].

There are no published examples available of a peel test being carried out specifically on an overmoulded package, where the components of interest are surrounded with OM compound, therefore there is a requirement for this study, which investigates such a method and explores ways of overcoming encapsulation by mould material and ways of applying a controlled and repeatable peel test to the small components. It is also important to be able to perform the peel test on samples which have already been ramped-up to high volume and have undergone their respective high volume manufacture methods, to allow analysis support for process qualification, and ensure the analysis is done on products which are fully representative of what is delivered to the final customer.

The subject devices of this study are completely over-moulded inertial MEMS assemblies, ready for application to a system PCB. The samples will have undergone TC testing and selected for peel testing with varying levels of adhesive cracking. A 90° peel test will be implemented, where the die pad is peeled away from the die bonded to its surface and the encapsulating mould compound, followed by analysis of the fracture surfaces. It is expected that the mould compound adhesion to the dies will be sufficient enough such that a failure will occur within the DA adhesive, where pre-cracked layers will separate cleanly, leaving behind a preserved fracture surface from TC testing. A clear 3D view of the cohesive fracture surfaces is expected to be visible, as well as surface characteristics of inter-facial cracking. Delaminated surfaces are expected to be made visually distinguishable from cracked surfaces, where the delaminated areas on the die pad or die are clean of residual DA adhesive. Another area of interest is the interaction between the mould compound and the die pad surface, evidence of the adhesion quality should also be visible.

3 Methodology

Contained in this chapter is a description of the methods used and decisions made whilst conducting the study herein. It should be noted that all testing was carried out in a pre-equipped laboratory and resources were limited to those that were already available upon the commencement of the study, unless easily and quickly obtainable.

Specimen Design

The subjects of this study are overmoulded SOIC packages with an ASIC and stacked MEMS accelerometer. The design can be represented by a package comprised of the following components:

- Copper lead frame with plated wire bond pads.
- ASIC die, bonded to the lead frame with a silver-filled epoxy adhesive.
- MEMS accelerometer die, stacked on top of the ASIC and bonded by a die attachment film.
- Gold bond wires, connecting MEMS to ASIC and ASIC to the leads.
- Epoxy OM material housing.

The complete assembly of the design is depicted by CAD models in Figure 21, and individual components are labelled in the cross-sectional images shown in Figure 22.

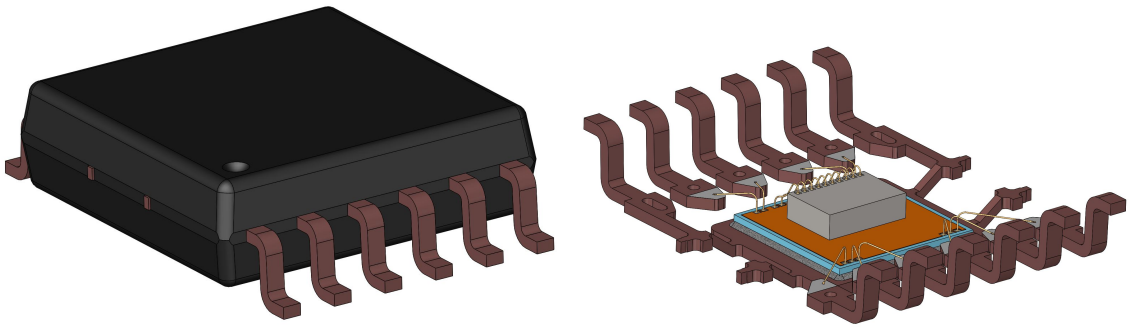

(a) (b)

Figure 21: CAD model representation of subjects being tested herein (a) Complete assembly with overmoulded housing (b) Inverted bald frame representation without housing.

For analysis, the particular interfaces of interest are the bond surfaces between the ASIC die and ASIC adhesive, as well as between the lead-frame and ASIC adhesive. This can be seen clearly in Figure 22(b). First of all, the DA adhesive is dispensed onto the lead-frame, and then the ASIC die is pressed into the adhesive, which spreads the DA material across the ASIC and lead-frame surfaces and causes a fillet

to form around the edge of the ASIC; this is the triangular feature at the ASIC boundary depicted in Figure 22(b), which can be used to determine the adhesive coverage quality.

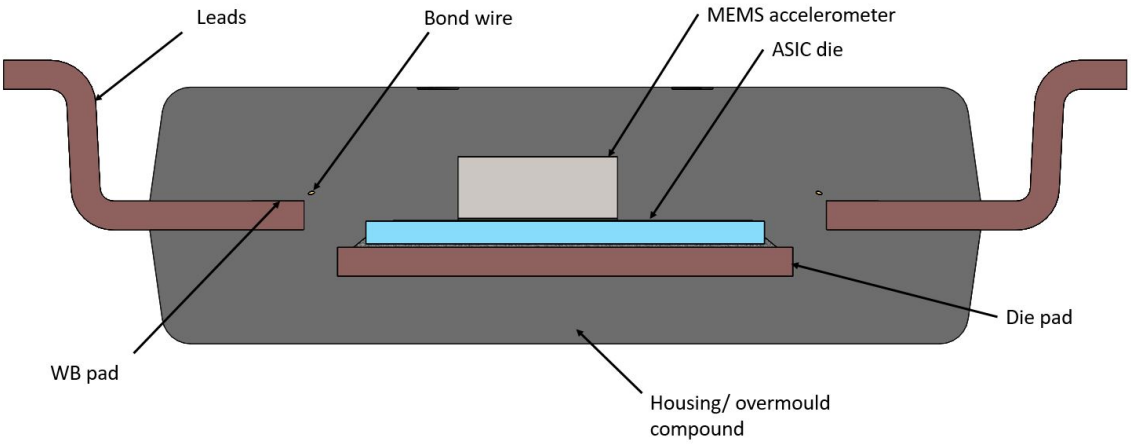

(a)

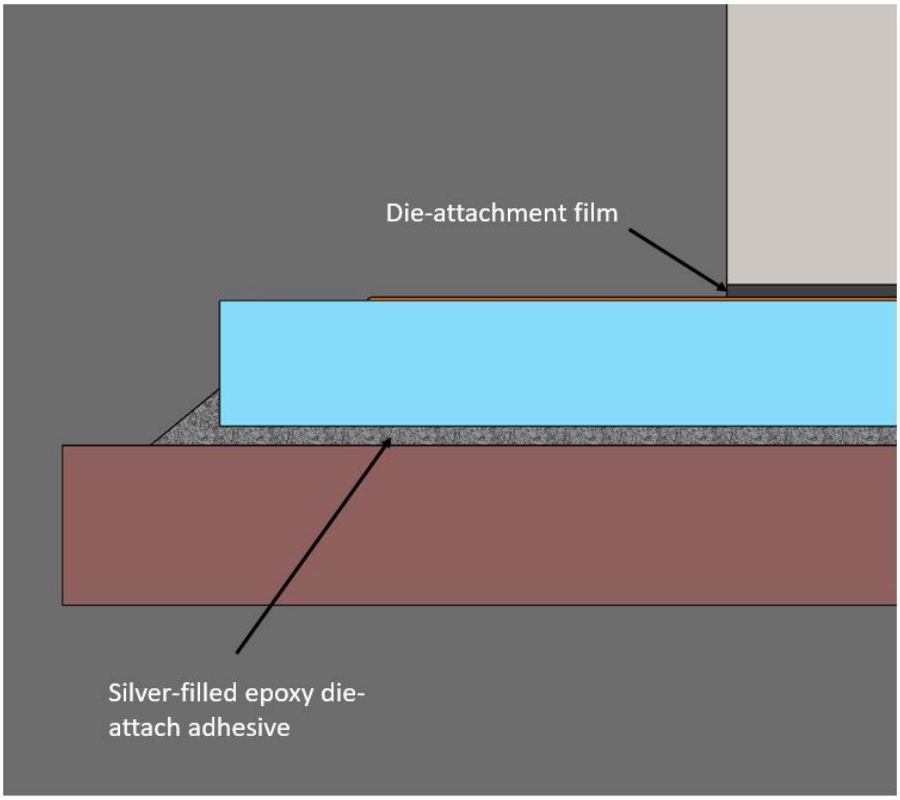

(b)

Figure 22: CAD model cross-sections (a) Full view of cross-section (b) Magnified view of bonded interfaces.

Accessing Die Pad (De-capping)

One of the main difficulties in performing a peel test on an overmoulded package is accessing the target components for peeling due to encapsulation by mould compound. There are a multitude of de-capsulation methods that have been developed for use across electronics industries as failure analysis often requires accessing encapsulated components [82, 83, 84, 85, 86]. These methods include:

- **Mechanical de-capsulation:** Mechanically removing material which can be performed by milling, grinding, cutting, or blasting with gas or water. Milling and blasting can be performed selectively on targeted areas of the housing, however grinding and cutting usually remove material from entire surfaces. The extent of the material removal can be easily controlled with these methods as machine settings are adjustable, however they are limited by the fact they remove material vertically from the application surface and are not selective of component materials, this means mould material underneath components such as bond wires cannot be removed unless the bond wire itself is removed or possibly damaged in some way.

- **Chemical de-capsulation:** Chemically removing material by selectively etching away by dripping acid onto the material surface. This method is known as wet etching and often used for failure analysis as mould compound can be removed without damaging bond wires and other components. The dripping amount can be controlled and due to the way liquids spread out when they land on a surface, material underneath bond wires can also be removed without post processing. This is a slow and messy process and the depth of the etch cannot easily be controlled.

- **Laser Ablation:** Similar to mechanically removing material, however a laser is used which utilises heat and light energy to irradiate the specimen surface and evaporate the material. This can be performed selectively and to a high accuracy, however exact locations of encapsulated components are required in the programming in order to avoid damaging them during ablation. A laser ablation machine can be very costly and again cannot remove vertically hidden areas of material.

In order to perform a peel test of the samples in this study, access to the backside of the die pad was required as per Figure 23. Between the die pad and extremity of the housing is only mould compound, therefore there were no obstructing components present which meant the material removal process would be simplified, however several important factors needed to be controlled to promote the repeatability of the test. As the die pad peel forces would require measuring during the test, controlling the vertical extent of the material removal was essential, this is to ensure the die pad thickness remains consistent between specimens and prevents varying thicknesses from skewing the results. The surface finish of the revealed die pad and surrounding OM material was also important to consider as this could potentially affect the

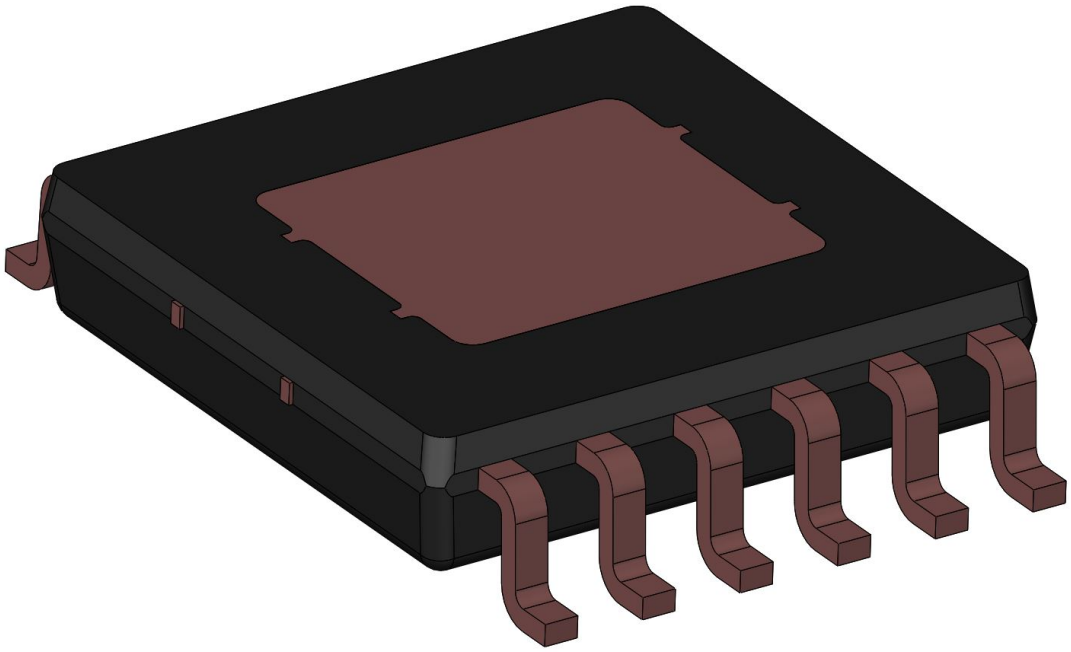

Figure 23: Backside of die pad exposed, OM material ground away, see Figure 21(a) for original specimen pre-grinding

peel application. Eight de-capsulation methods were individually considered for this study:

1. Grinding by hand

Grinding the backside of the package until the die pad is revealed. Processed by hand, using a grinding machine and varying the coarseness of the grit paper to control the speed, accuracy, and finish of the grind.

+ **Pros** Simple and low cost method.

– **Cons** Difficult to maintain level grind and depth accuracy.

2. Grinding with use of a jig

Grinding the backside of the package until the die pad is revealed. Sample mounted in a jig with a dial which can be accurately set to a predetermined height, ensuring consistent depth and flatness of grind between samples. Speed and surface finish can be controlled by varying the coarseness of the grit paper.

+ **Pros** Potential to accurately control grind depth, and improved repeatability over hand grinding.

– **Cons** Costs and time associated with jig design and procurement.

3. Mechanical/ heat de-capsulation

Heat mould compound of sample to above Tg using heat gun or blow torch, then clamp die-side half of sample and remove backside of sample OM material using hand-held tools.

+ **Pros** Low cost.

– **Cons** Heating of package could damage adhesive integrity and worsen cracks, rendering the results unreliable. Poor repeatability, low control and excessively destructive.

4. Machine etching (manual)

Remove material gradually by milling with a rotary hand-held power tool.

+ **Pros** Easily sourced power tool and reasonably low cost.

– **Cons** Accuracy dependant upon operator's steadiness, with low repeatability, low accuracy and poor surface finish.

5. Machine etching (automated)

Remove material gradually with a programmable milling machine, where the machining paths can be controlled such that depth is consistent between samples.

+ **Pros** Improved repeatability over manual milling and a slight improvement of surface finish. Depth can be controlled.

– **Cons** Programmable milling will require outsourcing if there is no in-house capability, and machine path accuracy is dependant upon programming and similarity of sample to CAD reference models.

6. Laser ablation

Selectively etch away material up to die pad backside using a laser.

+ **Pros** Controllable with high accuracy and repeatability, as well as good surface finish. Can be programmed to remove material from die pad sides to improve ease of peel.

– **Cons** Expensive machinery and would require outsourcing if there is no in-house capability.

7. Wet etching

Selectively drip a strong acid onto the backside of the sample until die pad is revealed.

+ **Pros** Common failure analysis process, therefore equipment is readily available.

– **Cons** Difficult to control depth of etching and therefore low repeatability.

8. Slicing

Slice component to die pad backside using a cross-section cutting machine.

+ **Pros** Can control depth of cut with good repeatability.

− **Cons** Expensive equipment and unfeasible if there is no in-house capability.

For the selection of an appropriate de-capsulation method for this study a systematic approach was taken with the help of a decision matrix; Table 5. In a decision matrix the candidates are scored either -1, 0, or 1 against various decision categories. The numbering -1, 0, and 1 can be interpreted as, negative factor, indifferent factor, and positive factor respectively. Each method was scored either -1, 0, or 1 for each of the following categories:

> **Current availability -** Whether the method apparatus was already available in the lab.

-1 = not available, 0 = mostly available, 1 = already available and established.

> **Feasibility to obtain -** Whether the apparatus could have been easily obtained, without excessive cost or lead times.

-1 = not feasible, 0 = quickly obtainable at low cost, 1 = already available.

> **Accuracy -** The accuracy of the material removal process.

-1 = little or no control, 0 = some control, 1 = high level of control.

> **Finish -** The quality of the surface finish after material removal.

-1 = poor finish, 0 = satisfactory finish, 1 = good finish.

> **Repeatability -** The consistency of results from sample to sample.

-1 = completely unrepeatable, 0 = some repeatability, 1 = good repeatability with comparable results between samples.

> **Throughput -** The speed at which the process could be completed.

-1 = slow, 0 = medium throughput but manual, 1 = fast and automated.

As can be seen from the decision matrix in Table 5 the highest total score and hence the choice for de-capsulation was for grinding by hand, highlighted in orange. Hand grinding was an already established de-capsulation method in the lab, which gave it an immediate advantage over other methods. Some apparatus was not available in the lab and the possibility of acquiring such equipment was infeasible in the time frame and budget of this study. This left only a few realistic possibilities, grinding by hand, mechanical de-capsulation, machine etching 1, and wet etching. The grinding by hand method was a convincingly better choice than the other three

Method	Current Availability	Feasibility to Obtain	Accuracy	Finish	Repeatability	Throughput	Total
Grinding by hand	1	1	0	1	0	0	**3**
Grinding with a jig	-1	0	1	1	1	0	**2**
Mechanical de-capsulation	0	1	-1	-1	-1	-1	**-3**
Machine etching 1	0	1	-1	-1	-1	-1	**-3**
Machine etching 2	-1	0	0	1	1	1	**2**
Laser ablation	-1	-1	1	1	1	1	**2**
Wet etching	1	1	0	0	0	-1	**1**
Slicing	-1	-1	0	1	1	1	**1**

Table 5: Decision matrix for deciding appropriate de-capsulation method.

realistic options, where mechanical de-capsulation and machine etching 1 would be far too inaccurate for the purposes of this study, and wet etching is a much slower process.

Grinding by hand is not the most accurate method, however, a satisfactory level of accuracy and repeatability was achieved through careful control of the grinding paper roughness, and in addition to this, as the development of the peel test progressed, the accuracy of de-capsulation became less significant to the overall results [9].

Firstly, the leads were cut from the package, the sides of the package would need to be grasped at various stages of the peel process and removing the leads ensured this would be possible. A P800 grinding paper was fixed onto the grinding wheel and moistened with water, then the grinding wheel was turned on and set to rotate at 200rpm. Whilst the grinding wheel was rotating a constant flow of water was used to ensure the grinding paper remained moistened. The component was positioned die pad backside down and grasped from the tie bar ends by a set of grip pliers. The grip pliers were used to maintain a firm and steady hold of the package, see Figure 25, to ensure the grinding is as level as possible and prevent fingers from being caught by the grinding paper, as the height of the component is small and hence difficult to clutch with gloved-hands. The component was lowered onto the grinding paper and material gradually removed. After every 5 seconds of grinding the part was removed from the paper and the ground surface checked to see the progress of the grind, followed by turning the part $180°C$ about the Z axis, after which the grinding was repeated. The reason for turning was to try and even out any levelling errors caused by the ergonomics of positioning the pliers and part onto the grinding paper.

[9] See "Peeling Method" and "Discussion" for more on this.

A diagram of the apparatus used for the grinding can be seen in Figure 24.

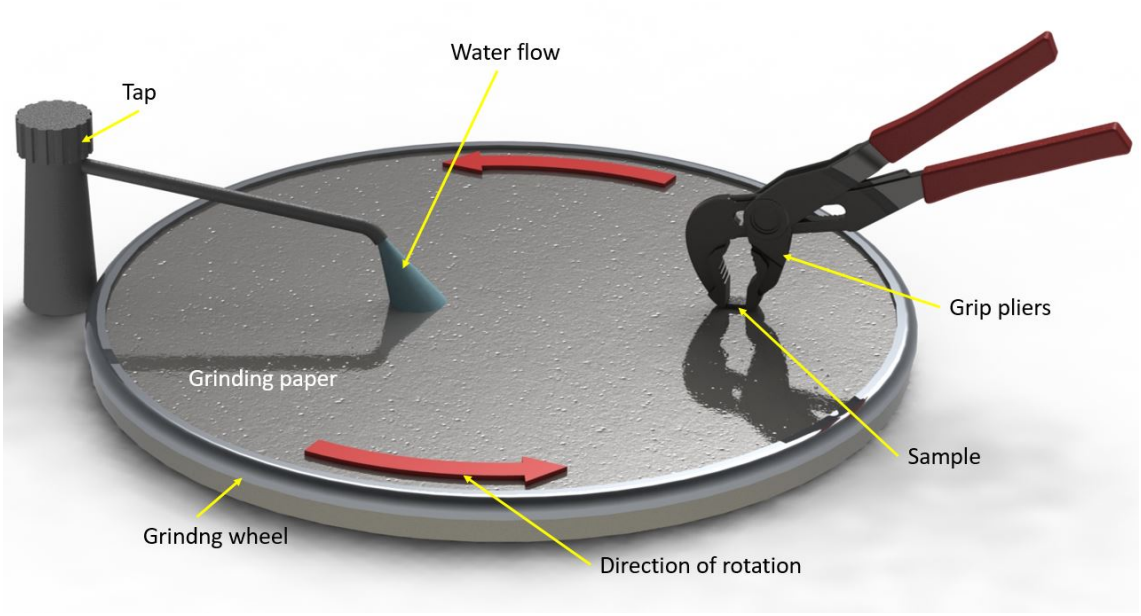

Figure 24: Diagram of the grinding setup.

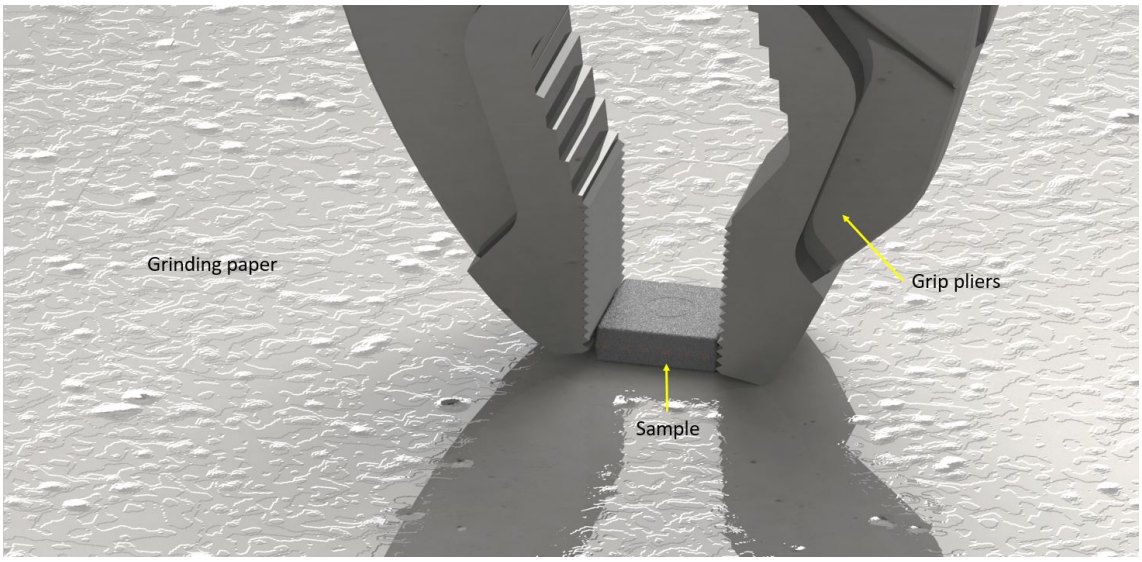

Figure 25: Grasping of component from tie bar sides with grip pliers.

This grinding process was repeated until the die pad started to become faintly visible from the backside of the component. At this point, there is still a thin layer of mould compound on the die pad surface, and the die pad area may not be 100% visible. This was the perfect moment to switch to a finer grinding paper, P1200, and the grinding was repeated until the complete die pad was visible.

This method is a systematic approach at de-capsulation by grinding where the procedure remains consistent for each part, improving the repeatability of the peel test.

For reasons described in the subsection "Peeling Method" it was also decided to grind up to the die pad from the tie bar edge, as per Figure 26. This was performed via the same process as the die pad backside grinding with the component held from the top and bottom surfaces and pitched onto the tie bar edge. In this case P400 paper was used instead of P800, which was to speed up the grinding process as there was a larger depth of overmould compound to be removed. The grinding was stopped as soon as the whole edge of the die pad was completely revealed, this includes the removal of the fillets at the corners of the die pad.

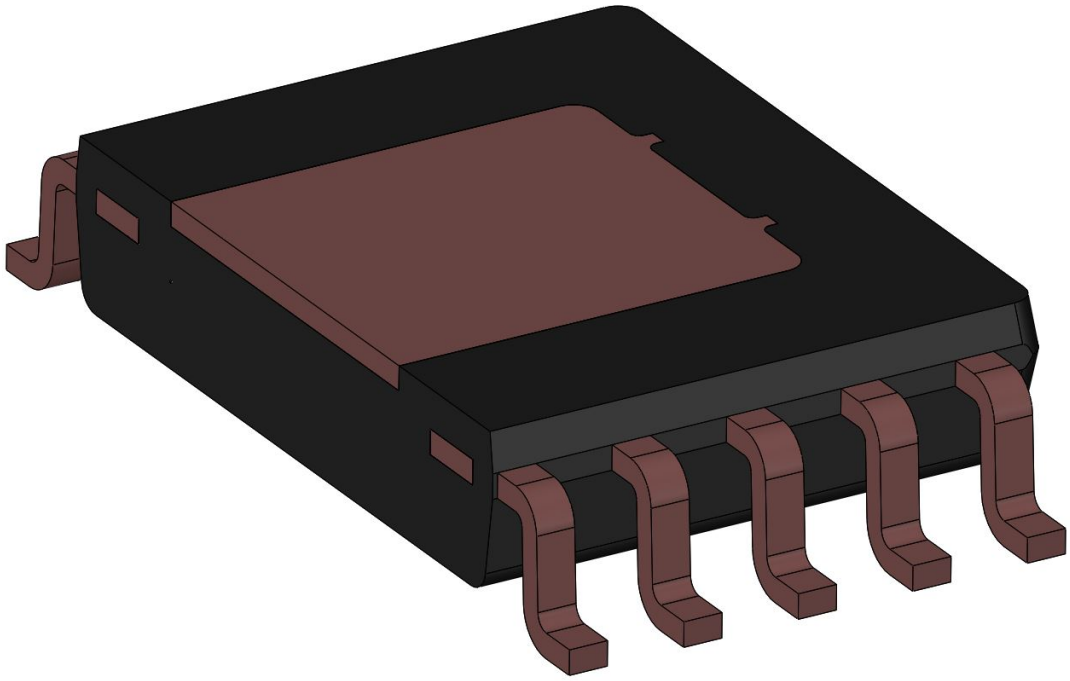

Figure 26: Component also ground up to die pad from tie bar edge.

Peeling Method

The main focus of this study was defining a peel test which could be performed on an end of line manufactured product. The peel tests were performed on inertial MEMS devices which had been ground until the die pad backside was revealed and the peel was to be initiated at the edge of the die pad, which would be peeled away from the bonded components and OM compound.

Quantifiable Peel Test

The initial aim was to somehow quantify the peel forces required to separate the die pad from the OM cavity and MEMS dies, this meant the die pad would need to be attached to a load cell and the peel rate would need to be controlled. Readily available in the lab was a single axis test machine with controllable speed, this machine is used for de-capping MEMS elements for analysis. The test machine, pictured in Figure 27(a), was equipped with a force gauge, and hence selected for performing the peel test. The force gauge outputted the load experienced through the chain to the screen and the maximum value was stored. It was decided this maximum load value could be used for quantifying the peel force.

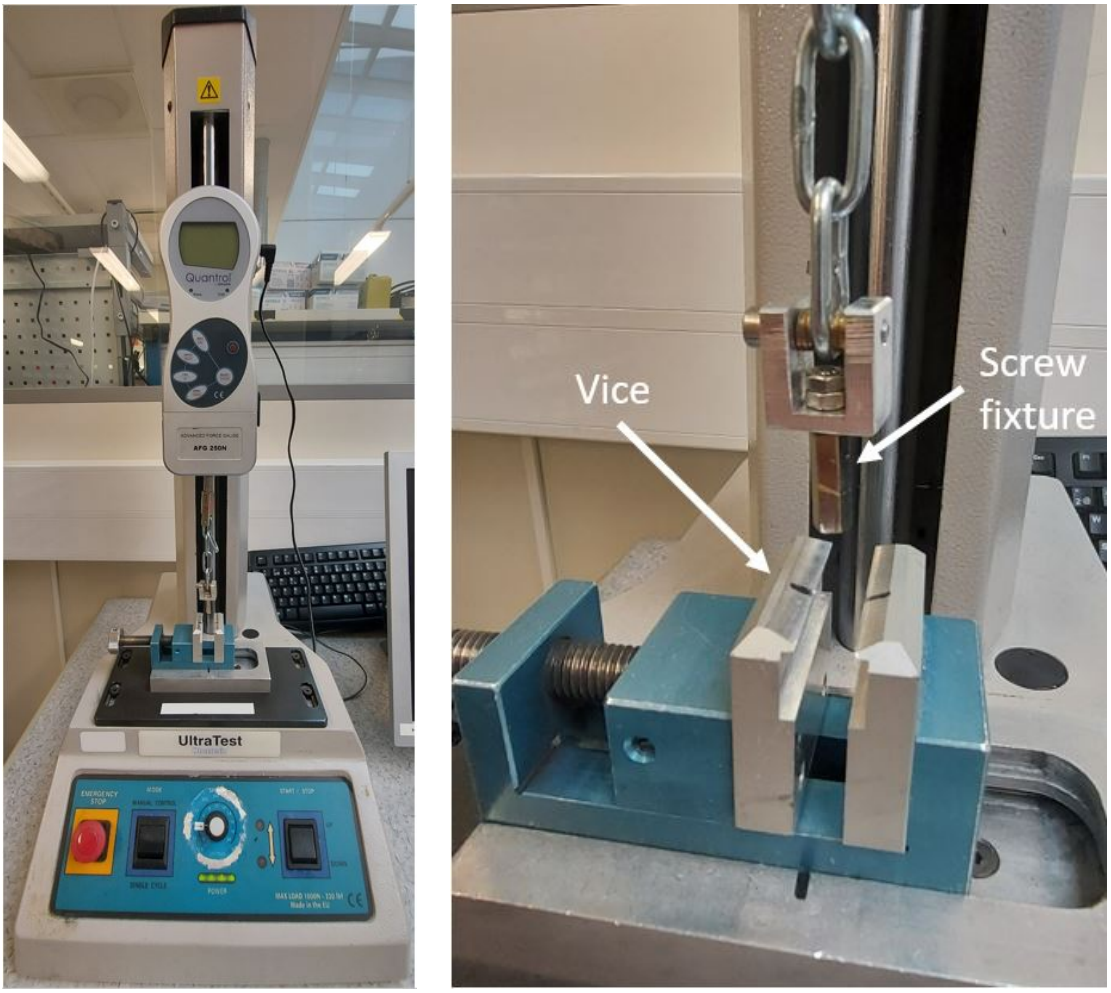

(a) (b)

Figure 27: (a) Single axis test machine (b) Test fixture.

The small nature of the die pad meant attachment of the sample to the test machine was limited to gluing, as there were no other surfaces for establishing a mechanical connection. A screw was glued to the die pad backside, however the screw head area was too large to fit within the confines of the die pad, therefore the

edges of the screw head were ground to size. To generate more of a peel on the die pad rather than vertically pulling the die pad from the sample, the screw was ground more on one side and set as close to one edge of the die pad as possible. Figure 28 is a depiction of what this set up looked like. Seen in Figure 27(b) are the fixtures used for fixing the samples to the machine, the sample was first screwed into the screw fixture and then clamped into the vice such that the screw and chain were colinear. The slack was removed from the chain and the peel was initiated at 50mm/min.

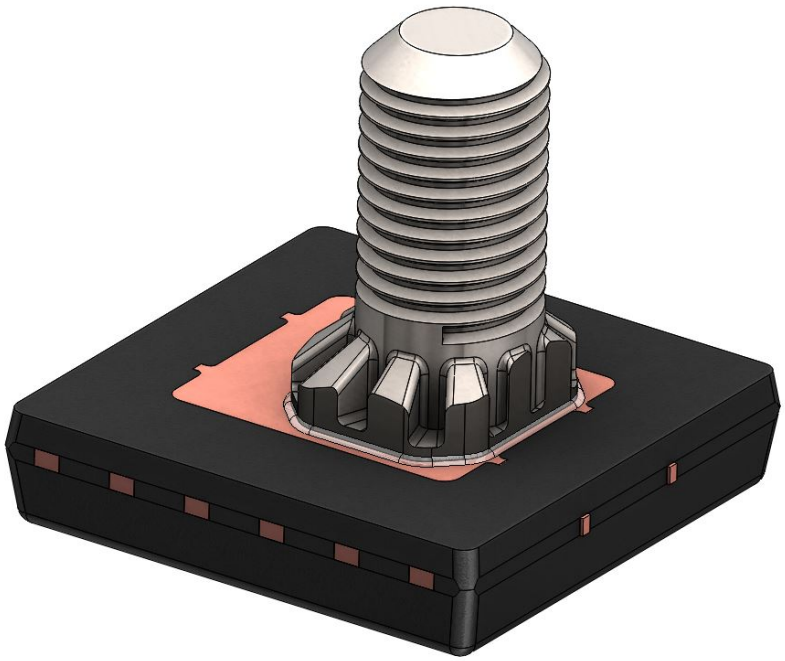

Figure 28: Ground screw glued on top of die pad backside.

Initial trials of this method were unsuccessful because the bond between the screw and die pad broke before the glue. Four different off-the-shelf glues were trialled, two epoxy/hardener mixtures, 3M^{TM} Scotch-Weld^{TM} DP410 and LOCTITE® Power Epoxy, and two rapid-curing cyanoacrylates, Bison Super Glue Gel and LOCTITE® Super Glue. None of which yielded positive results. An early hypothesis was that the OM compound resisted the peel due to the compound penetrating into the edges of the die pad. In practice, the cutting process of the die pad does not leave a straight edge, instead a curved profile which can be seen in Figure 29. Also the tie bars were embedded in the OM material, and still connected to the die pad. To try and alleviate this resistance to peeling the sample was ground up to the die pad edge from the peel side, removing the tie bars, as can be seen in Figure 30. The sample was ground until the fillets at the die pad corners were removed.

This alteration proved a little more successful, where some of the peel tests yielded positive results with maximum load values, but ultimately, out of the samples trialled, positive results were rare and unrepeatable and therefore this method was deemed a failure, prompting a change of approach.

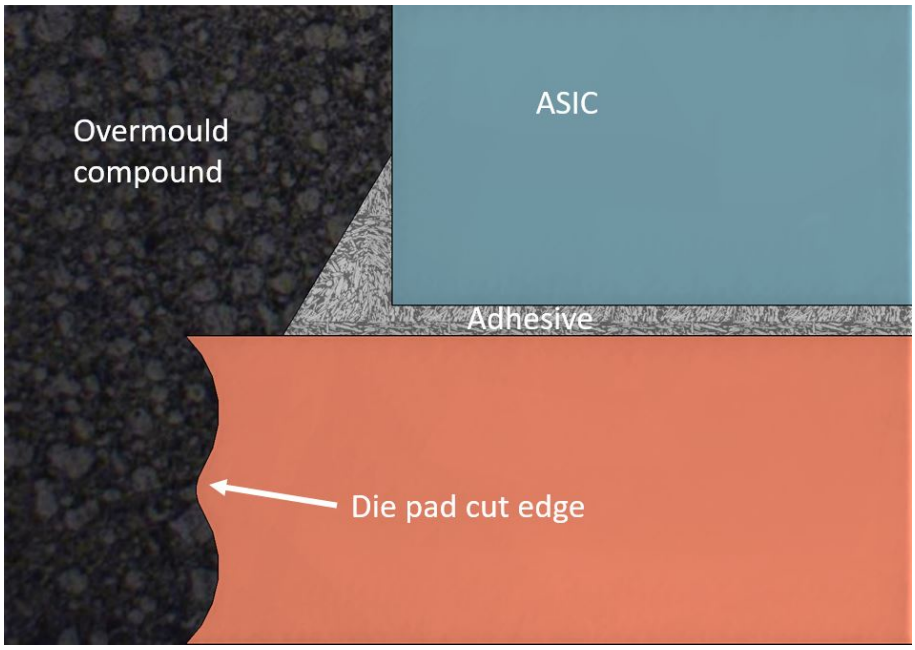

Figure 29: Cut die pad allows OM compound penetration into the edges.

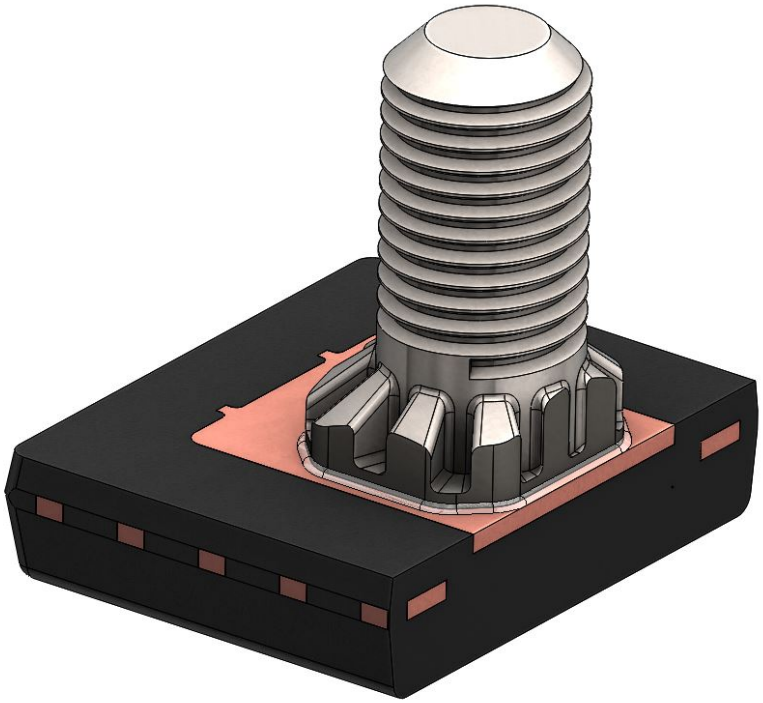

Figure 30: Ground screw glued on top of die pad backside with sample ground to die pad from tie bar edge.

Manual/ Knife Peel

Being unable to consistently perform peels by bonding to the die pad backside surface, and with no other way of peeling from the backside, it was decided to try and initiate the peel from the die pad edge; where the sample had been ground. The die pad thickness was in the order of 250 microns making attachment very difficult, therefore attempting to quantify the peel forces was considered unfeasible, and instead the focus was shifted onto correlating peel surface images with CSAM images and electrical results.

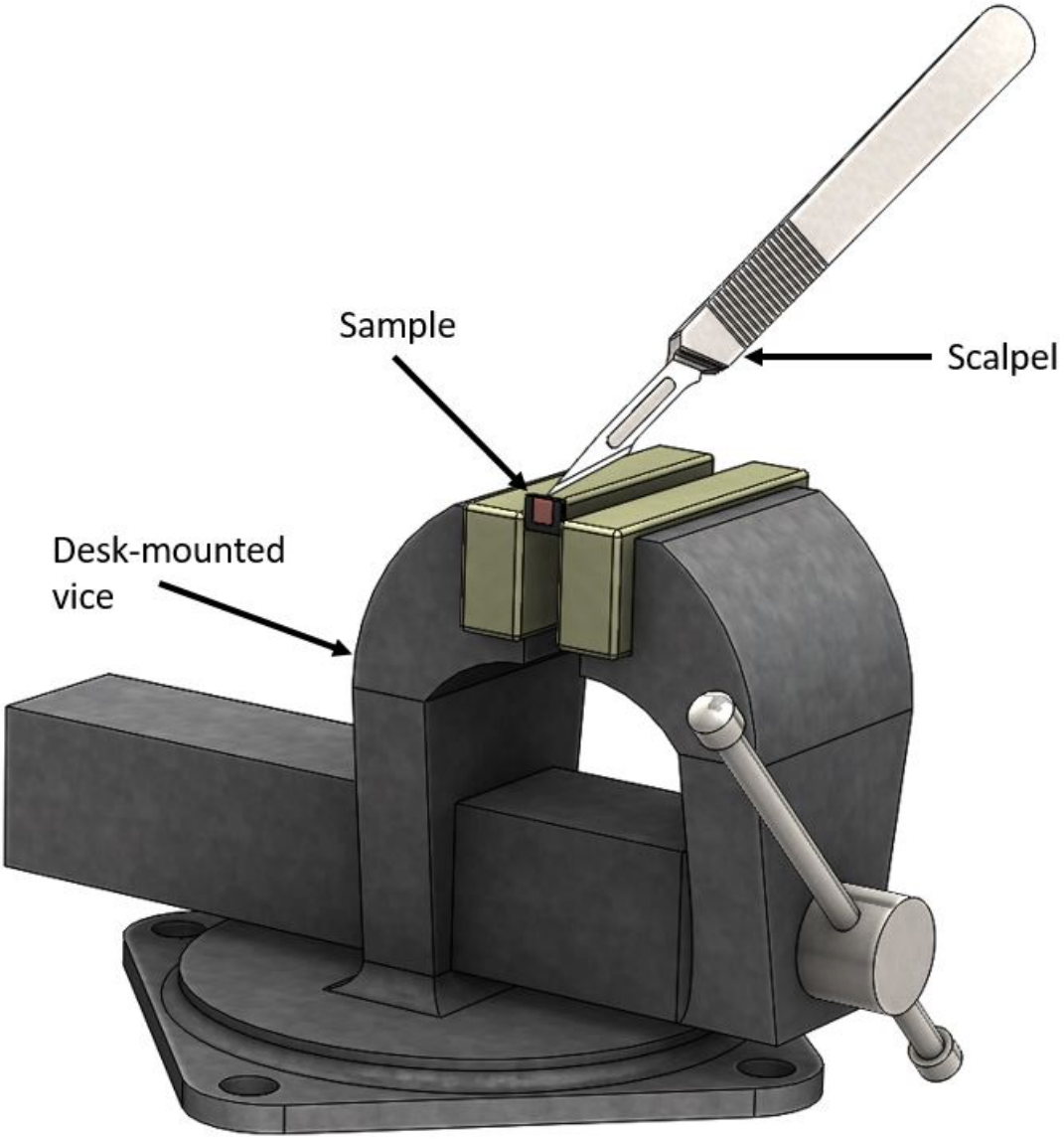

Figure 31: Peel test apparatus.

Without the need for quantifiable peel forces, the peels could be performed manually, without repeatable control, hence the die pad was prised open by hand,

using a finely bladed knife, or scalpel. Initial trials were performed on samples which had not been ground up to the die pad edge, however this was a time consuming process and resulted in messy samples as the die pad was effectively dug-out of the OM compound. For this reason, grinding up to the die pad edge was continued to give better access for the knife, and cleaner peels could be performed.

The revised peeling method could be performed quickly, however the samples needed fixing in place and magnification was required to help with precise positioning of the scalpel blade. This was achieved by clamping the samples from the lead edges into a vice, and looking through an articulating arm binocular microscope when performing the peels. The setup, minus binoculars, can be seen in Figure 31.

After the sample had been secured in the vice, the point of the knife blade was pressed-in to the centre point of the interface between die pad and OM compound, by pressing-in the knife, more grip was achieved for the next phase of knife movement. The knife was then tilted 45° to the surface on which the blade is pressed, and with a careful application of force, the knife was pulled parallel to the vice clamping plane, as per the orange arrow in Figure 32, whilst ensuring the knife remained firmly pressed-in to die pad edge. The peel force was applied until the die pad had completely separated from the OM compound surface, similarly to Figure 33.

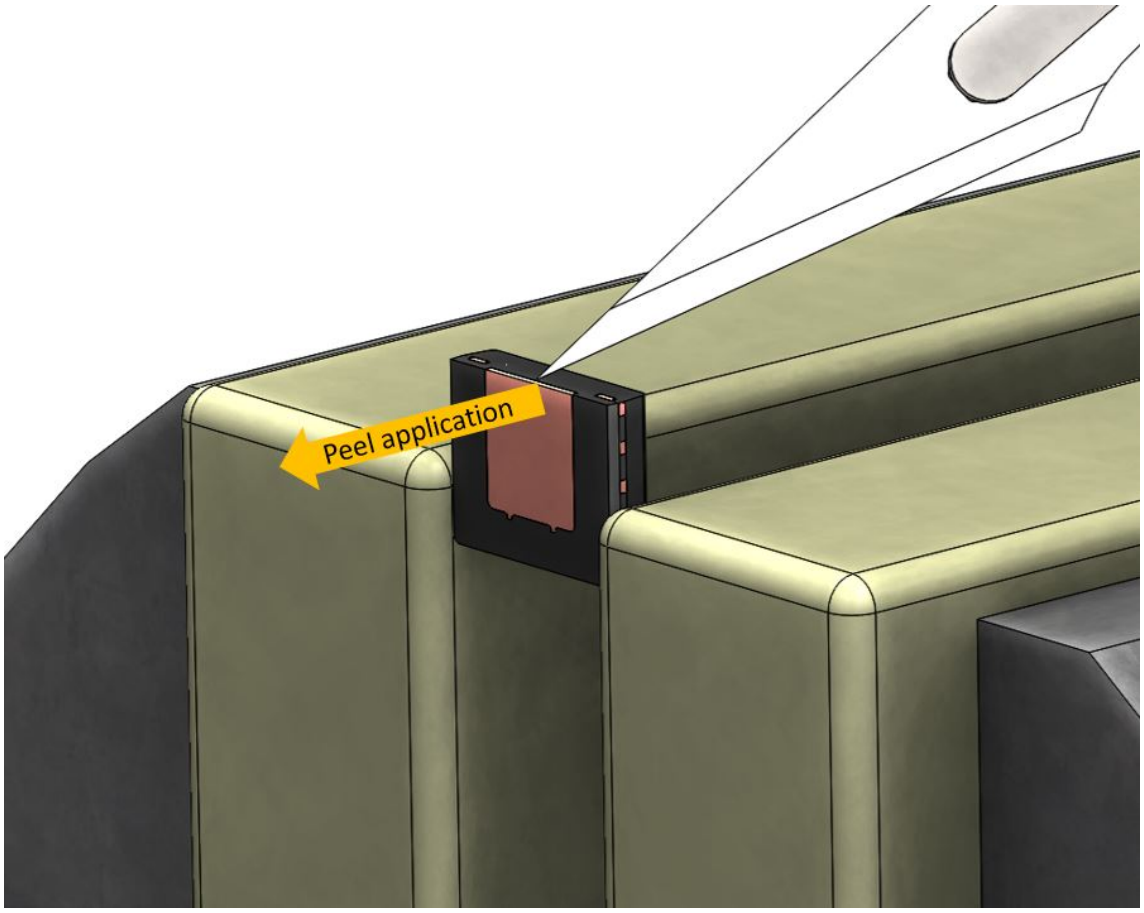

Figure 32: Knife position at die pad and OM compound interface.

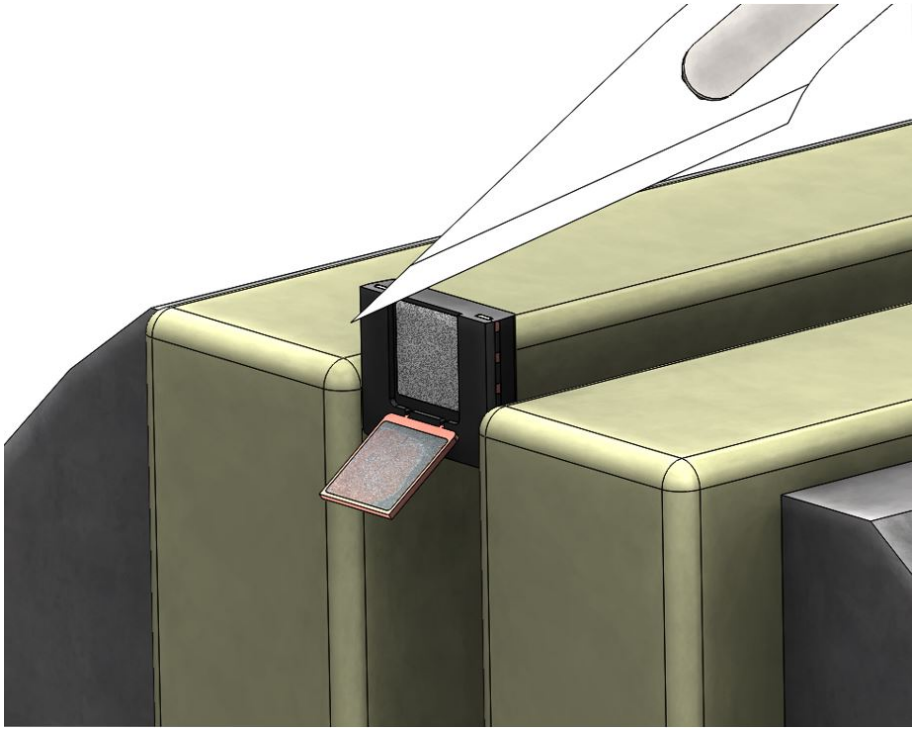

Figure 33: Peeled sample.

Once the die pad had been separated from the OM compound, the samples were removed from the vice and the die pad was carefully folded until 180° from its unpeeled position, as per Figure 34.

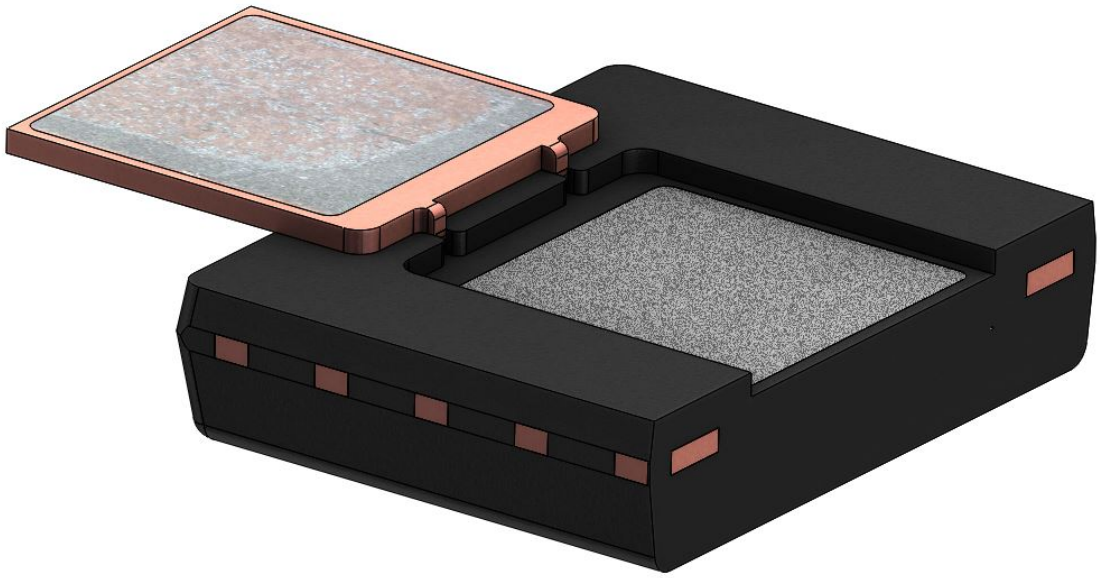

Figure 34: Fully peeled test sample, ready for imaging.

Post Peel Analysis

After the peels were completed, both the peeled die pad and remaining cavity on the OM compound side were imaged with an optical microscope. The images taken under optical microscope were studied and used to define particular areas of interest, which were then imaged using a SEM. Before imaging with the SEM, all samples were sputtered with gold and grounded to prevent charge building up on the imaged surfaces. Images were analysed using ImageJ software, where the surface areas of cracks and other abnormalities were quantified. This process was achieved by first selecting the ASIC area, Figure 35(a), and then selecting the crack area using the polygon selection tool, Figure 35(b). These selections returned estimated areas as the number of pixels within the yellow boundaries and the percentage of ASIC area cracked could be calculated by dividing (b) by (a), as per the example in Table 6. In this example the estimated crack area was around 25.7% of the ASIC area, this value can be compared to the delamination specification and a pass or fail can be scored. The reason for selecting the ASIC area as a reference is because this area is relatively consistent sample to sample, which means crack percentages can be compared sample to sample.

Area Measured	Area in Pixels	Percentage of ASIC Area
ASIC (Figure 35a)	502928	100%
Crack (Figure 35b)	129132	25.68%

Table 6: Calculations of crack areas example.

Electrical Correlation Study Set Up

For the peel test results to provide useful information, relationships need to be established between the visual results and the results from other analysis methods. All samples selected for peel testing already had a TC test history of 1000 to 3000 cycles associated with them, this means all samples already had CSAM images available after each test interval at the beginning of this study, and the non-dummy samples also had respective electrical measurements available. With all the given information available a correlation study was set up.

Selected frame-level components, from five batches of the same BOM (bill of materials), which consisted of +2000 parts in total per batch, were subjected to TC testing. The components had electrical testing and CSAM imaging performed after final assembly, preconditioning, TC500, TC1000, TC1500, and TC2000. Varying amounts of offset drift occurred over lifetime between batches. Three individual components from each batch were selected as being representative of the batch-level electrical performance, totalling 15 parts, peel tests were performed on all 15 parts and subsequently observations were carried out of the peeled surfaces to determine any correlations between the samples, analysis results and batches.

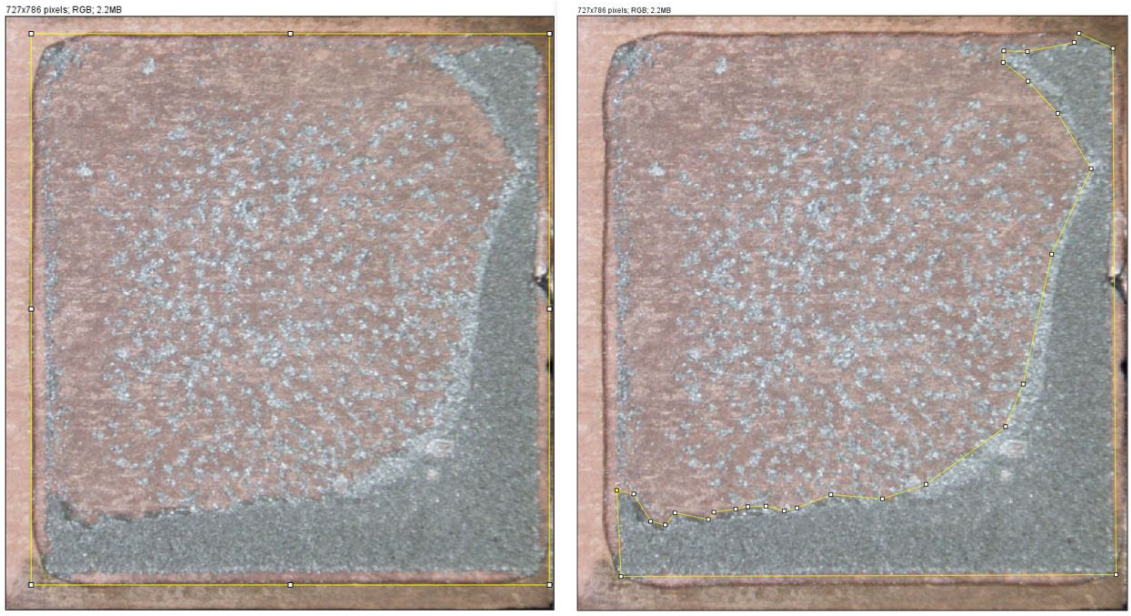

(a) (b)

Figure 35: Measuring, (a) ASIC area (b) crack area, with ImageJ.

4 Results

This chapter contains an overview of the results obtained during this study, a summary of the types of information obtained from peeled samples tested to TC2000, and some analysis techniques to help quantify the results. The analysis of the presented peel method was split into three main focus areas, which are presented herein in the following order.

Firstly, the peel method itself and the resulting sample to sample peel quality. These observations of the peel mechanics were important in assessing the reproducibility and success of the peels. Secondly, a more detailed look at the peeled surfaces using microscope techniques. Observations of the peel surfaces, at both macro and micro scale, were critical for obtaining useful information from the peel tests, and hence the foundations of analysis for the entire study. Finally, the results of the correlation study, which contains results and analysis that seek to link electrical output, CSAM images, and peel images, for failure analysis and process qualification.

Initial Peel Observations

Effect of not grinding up to die pad edge:

The first-off samples to be peeled had only been ground up to the die pad backside, this made getting good leverage with the knife difficult which produced messy samples. Figure 36 displays the damage to the OM housing and die pad edge as a result. It was also observed that cutting through the tie bars was required before the die pad would successfully peel, worsening the cleanness of the results.

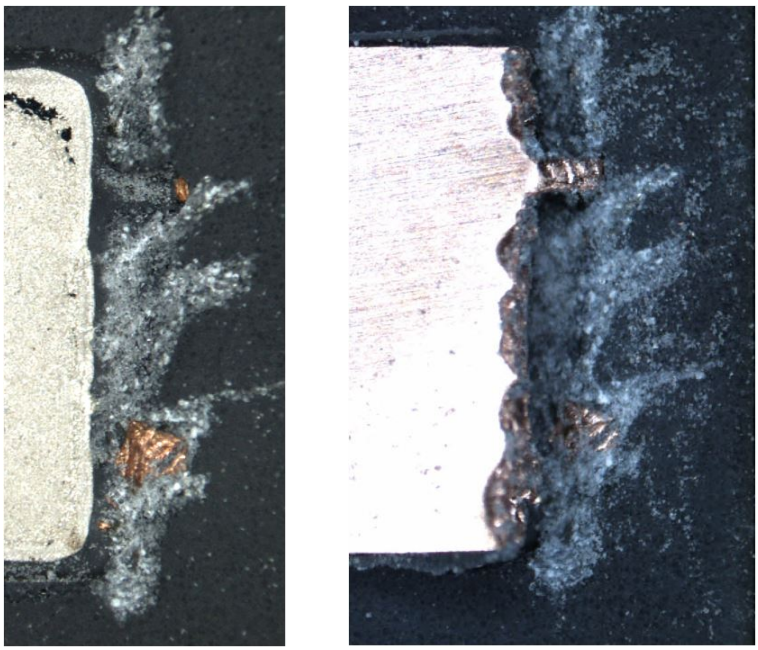

(a) (b)

Figure 36: (a) Damage to mould-side of peel, (b) Damage to die pad after peel.

Successful Peels:

A successful peel was considered a peel where the die pad was cleanly separated from the OM with a popping action, without bending, and without damage to the MEMS dies. The knife was embedded in the edge of the die pad and the peel motion caused the die pad to pop from the OM, leaving behind purely adhesive inter-facial artefacts. Figure 37 is an example of a successful peel post peel. Typically after peel application and die pad pop, the angle of the die pad to the OM was in the region of 5-15°, after this point the knife would lose traction within the die pad edge and the peel force application would come to a stop.

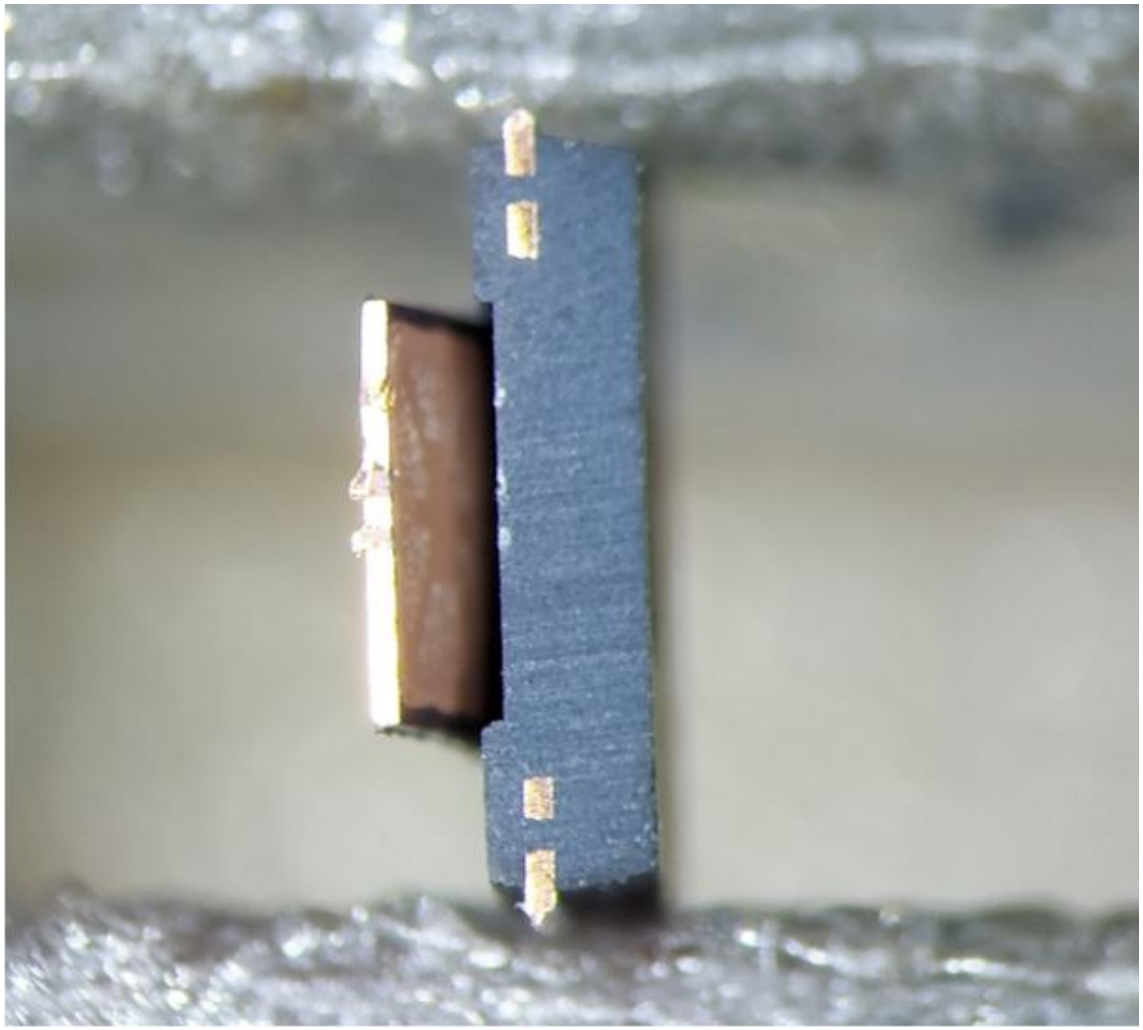

Figure 37: Typical successful peel result.

Figure 38 is a closeup view of the die pad edge post peel. The copper smears are witness points of the knife blade, in this example there are three witness points, which essentially means it took three attempts to position the knife blade and apply the peel force before the die pad popped. The number of attempts before a successful

peel was typically 1 to 5. Figure 37 also display these witness marks in the OM material, where the knife attempted to get purchase at the die pad/ OM interface.

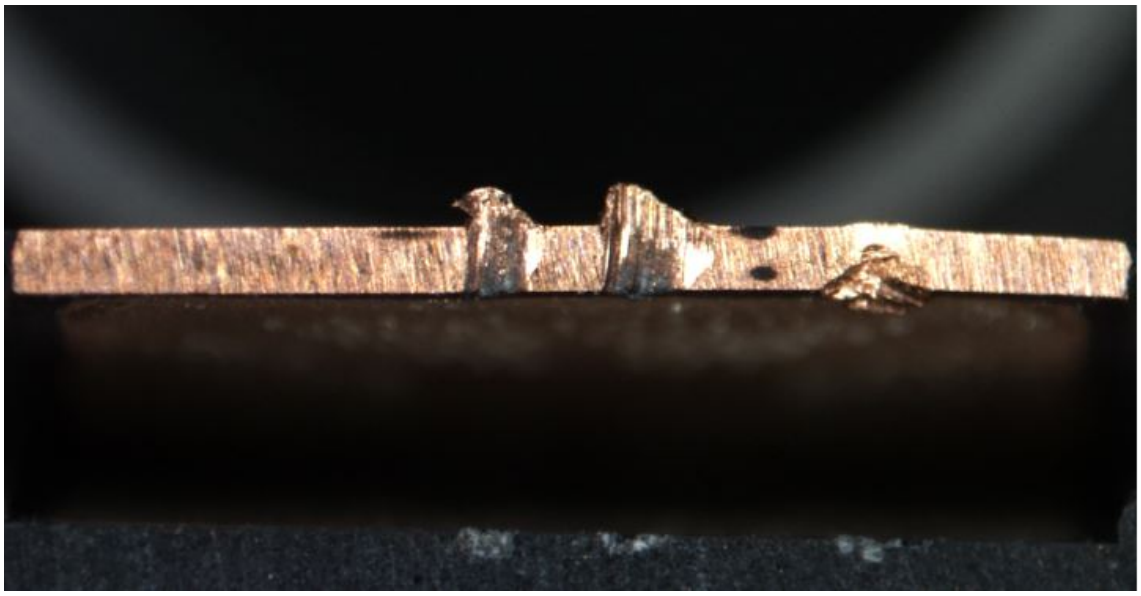

Figure 38: Post-peel die pad edge with knife witness marks.

Completing a 180° peel, ready for imaging, required the remaining bend of the die pad to be done by hand. After peeling, the only medium of attachment keeping the die pad attached to the sample was the tie bars, which were embedded in the OM, and due to the tiny nature of these, the remaining bend had to be done delicately. Typically the die pad was positioned 180° to the OM successfully, however some parts resulted in separation of the die pad from the OM. For example, if the bend was performed more than once there was a greater likelihood of the die pad completely detaching from the sample. Purely for convenience it was desired that the die pad remained attached to its sample, but this did not affect the imaging results.

Another initial observation, common to all peeled samples, was that the die pad edges perpendicular to the peel edge removed OM material from the sample during the peel. This could be seen to the naked eye as a thin strip of OM material stuck to the die pad edge, but it could be clearly seen under a microscope, as seen in Figure 39.

After peeling, samples were scored as either successful or unsuccessful. An unsuccessful peel was considered a peel where the die pad did not cleanly pop from the sample, instead the die pad bent, or was in some way deformed by the peel, or damage was inflicted upon the MEMS. These peels were often scrapped due to lack of information obtainable from damaged samples. Out of the 90 peels recorded for this study, after the peel method had been established, 6 of them were considered unsuccessful, with varying amounts of information obtainable from them, this resulted in a peel test failure rate of around 6.7%.

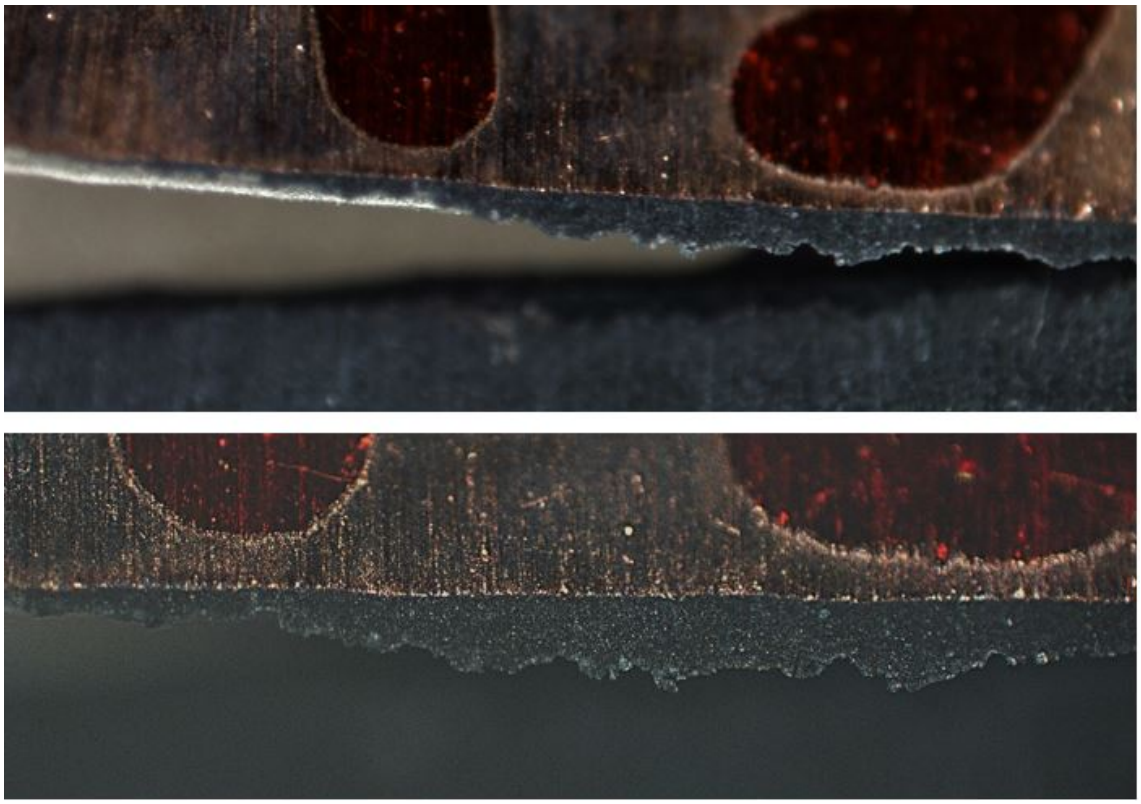

Figure 39: Magnification of die pad edge after peeling.

Damages to Samples:

Throughout the testing, various observations of damage to the samples were made. Some were considered minor and others were severe enough to result in scrapped samples. This subsection documents typical examples of damage which occurred during peeling.

The most common types of damage observed were left by the knife during peeling, some examples of these were witness marks at the edge of the die pad as per Figure 38, which did not affect the visual results of the peeled surface.

However, scratches from the knife often occurred on the inspected peel surface. These artefacts were the result of a lack of control over the knife motion during the peel. Due to the process of peel application, after the die pad popped from the sample, the knife would slip. This was the peel application force causing the knife to continue along its trajectory until it could be reacted to and stopped, but due to the relatively instant nature of the die pad pop, it was difficult to prevent these scratches from occurring. Usually the scratches emanated perpendicularly from the peel location and followed a straight or curved trajectory across the peeled surface, examples of such scratches can be seen in Figure 40.

These scratches were mainly superficial and very easy to distinguish from other artefacts, this meant they would not have any significant impact on the overall results of the tests.

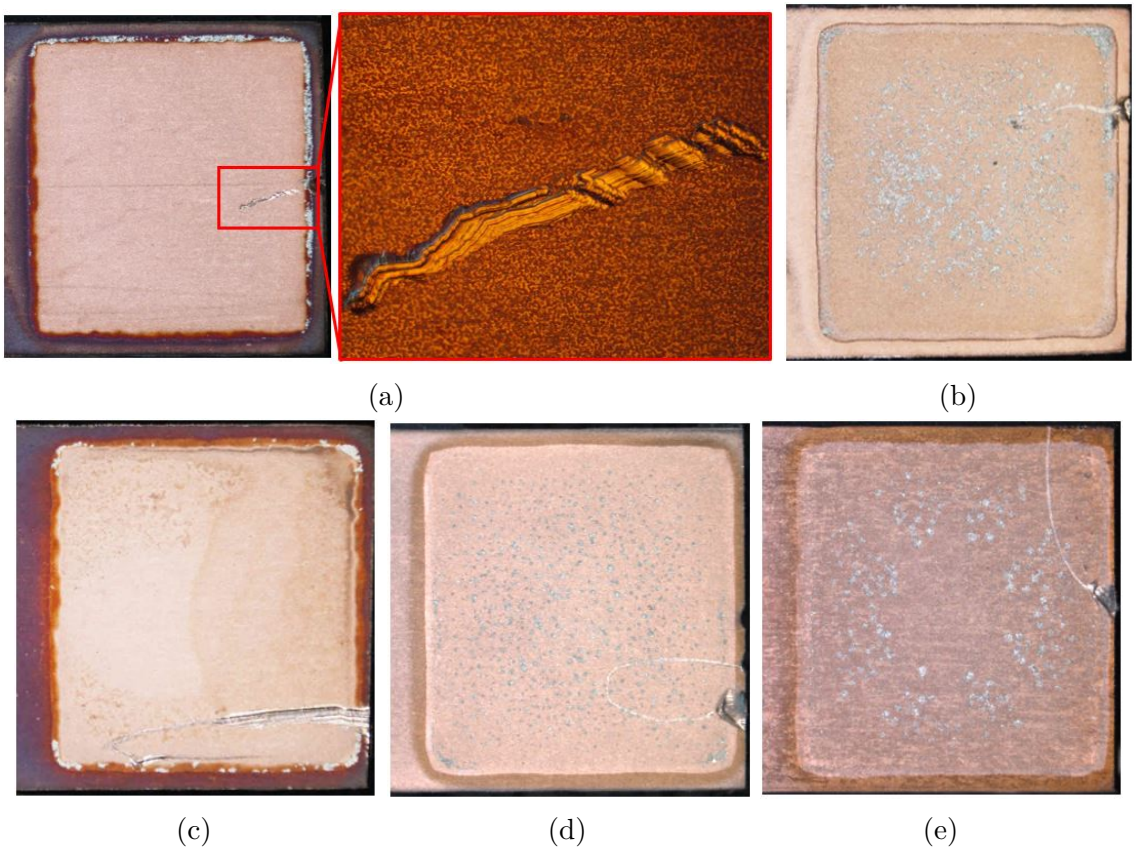

Figure 40: (a) (b) (c) (d) (e) All examples of typical post peel scratch artefacts.

Some samples proved difficult and did not peel cleanly, meaning the peel application did not result in a pop, but instead the die pad would begin to curl and bend from the initiation point. Excessive bending led to distortion of the peel surface, resulting in poor images under the microscope, and also damage to the ASIC die. These artefacts usually caused too much disruption to the peel image for strong crack correlations to be made and were scrapped.

Figure 41 gives two examples of die pads which have been excessively bent and distorted during the peel application.

Figure 42(a) and (b) show a comparison between a die pad which has been bent during the peel and a clean peel, respectively. A striping pattern can be seen in Figure 42(a) on the ASIC peel surface, caused by the intermittent peel due to the bending of the die pad. The striping pattern could potentially lead to misleading results, although this kind of artefact is usually distinguishable from the sample related artefacts.

The least common but most destructive form of sample damage was ASIC die fracture, which was usually due to a difficult peel and lack of knife control. Often when the die pad bent instead of popping, the knife would then slip and slice through the ASIC die, this resulted in a part of the die remaining on the die pad, which completely obscured the surface from imaging in this area, this was totally undesirable. Figure 43 displays an example of this occurring.

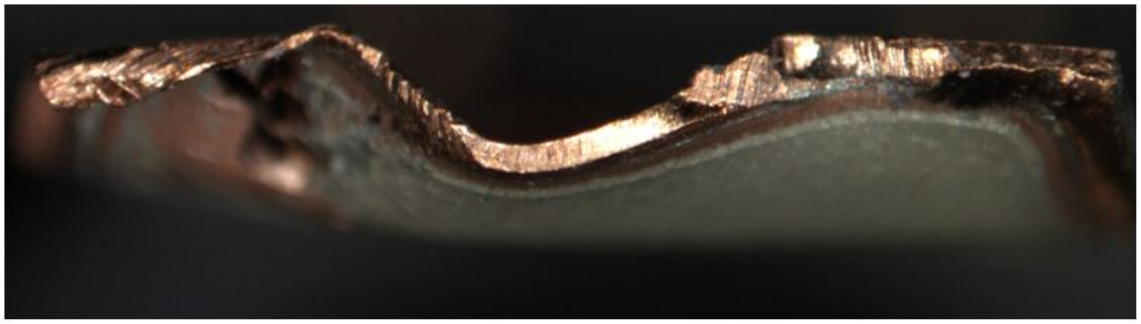

(a)

(b)

Figure 41: (a) End view of a die pad distorted by the peel application (b) Side view of bent die pad.

(a) (b)

Figure 42: (a) Sample with bent die pad (b) Clean peel.

(a) (b)

Figure 43: (a) Broken die on die pad (b) Broken die on OM side.

Difficulties:

Several difficulties were encountered during the peel testing. The first of which was a die pad which had been ground too thin or ground uneven. This would be due to the lack of control during the backside grinding process, and often due to difficulty keeping the sample level. A too thin or uneven thickness die pad would often result in the bending of the die pad during the peel. Figure 44 is an example of where the sample was ground uneven, resulting in one side of the die pad being thinner than the other side. This led to the die pad locally deforming where the knife was placed to initiate the peel. The damage to the top right corner in Figure 44 would mask any observations of potential cracking or delamination.

The main difficulty observed with this peel test method was the positioning of the knife blade. The die pad thickness was around 10mils, which meant the knife blade had to be positioned with high accuracy and surgical steadiness. One issue that arose was the knife tip of a fresh blade would soon chip, leaving a blunter edge for peeling. The problem with this is the blunter edge made accurate knife positioning even more difficult. Figure 45 is a magnified image of a fresh blade being positioned for peeling, it can be seen here that the tip has chipped, blunting the blade.

On top of knife blunting, the malleability of the die pad material also made getting an accurate and firm grip from the embedded knife difficult. The knife would be dug-in to the die pad edge at OM interface, but on occasion the copper deformed and the knife slipped from the sample before the peel commenced. Figure 46 shows the typical positioning of the knife blade upon peel commencement and the deformation of the die pad at the witness point.

Figure 44: Peeled die pad with bent corner due to uneven grinding.

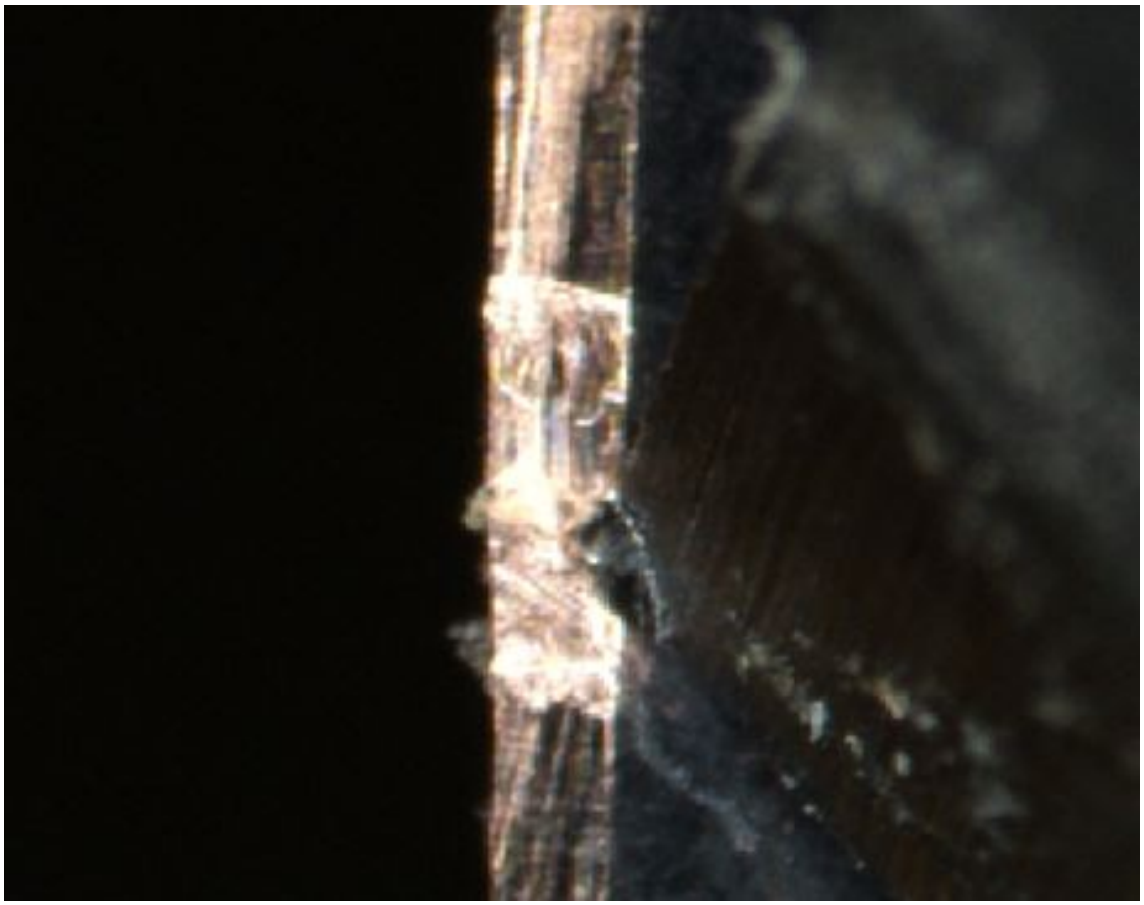

Figure 45: Chipping of fresh blade tip.

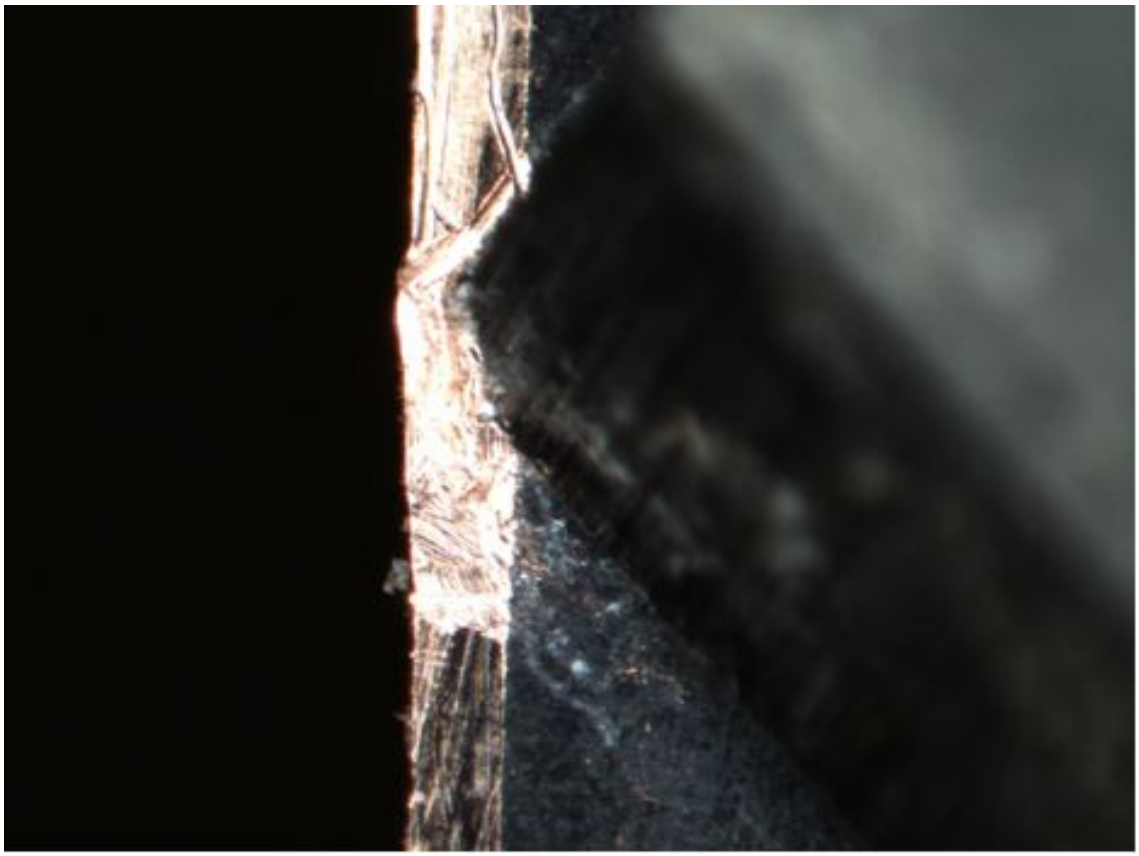

Figure 46: Magnified view of knife insertion and die pad deformation.

Under The Microscope

One of the most intriguing aspects of this study is what can be ascertained by studying the peeled surfaces of the samples. This section presents a collection of typical imaging findings and results with the optical microscope and the SEM.

Peeled Surfaces at a Glance

Ordinarily after the peel test two surfaces are left for imaging, the die pad side and the OM side. These are shown in Figure 47 and Figure 48 respectively. Before examining these peels in detail it is important to understand the constituent areas of the peeled surfaces to be examined. On the die pad peel the main areas are:

ASIC area: The square-shaped section, surrounded by a dashed yellow line. The ASIC area is of great interest as this is where the adhesive lies, which bonds the ASIC to the lead frame, and is the main focus of these peel tests.

Die pad die side: The die pad surface on which the ASIC is bonded and fills the entire frame of the images. Surface characteristics and patterns are of interest here.

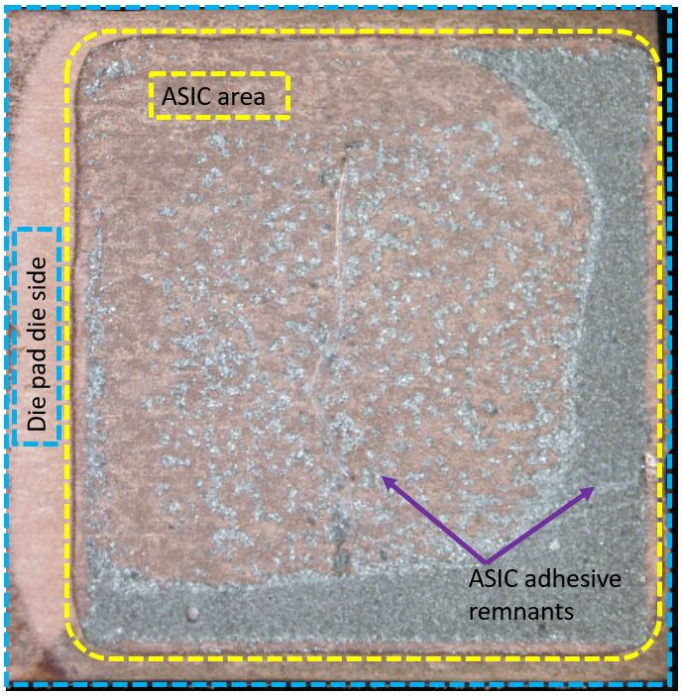

Figure 47: Main surface constituents on the die pad side of the peel.

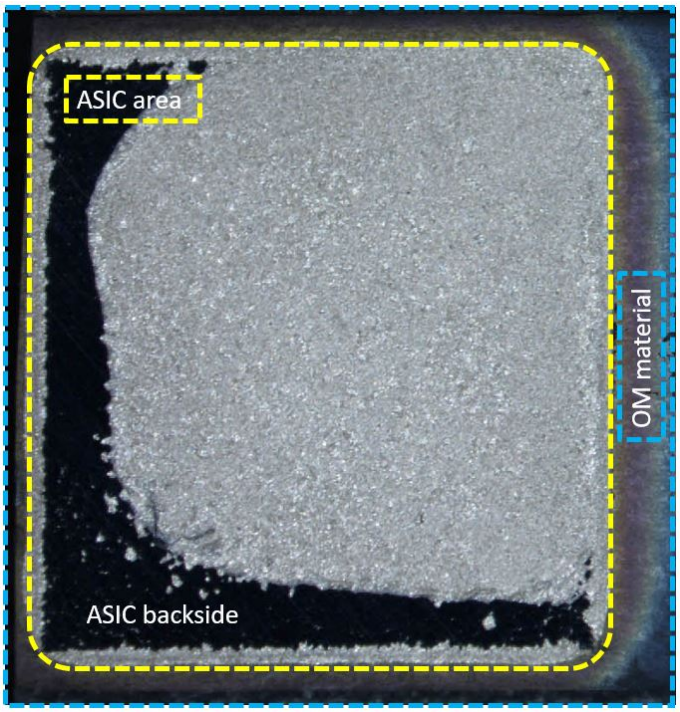

Figure 48: Main surface constituents on the over mould side of the peel.

ASIC adhesive remnants: Leftover adhesive on the die pad. Leftover adhesive gives important clues as to the position and size of cracks/ delamination.

On the OM side peel essentially the mirror image of the die side peel can be seen, the main areas for observation are:

ASIC area: Again this is the square-shaped area where the ASIC adhesive lies.

OM Material: The overmoulded housing which surrounds the entire package. The mirror image of the die pad die side surface.

ASIC backside: The dark areas in the ASIC area are the backside of the ASIC die. This a reflective silicon material, hence the darkness. This area is not visible in all images, but indicative of an ASIC interface crack.

More Detailed Observations

When observing the peeled halves of the samples it quickly became apparent that there was a lot of information to assimilate. Without too much detail, the main observations of various samples are presented here and possible causes are speculated, while further detail and speculation of the meanings behind the visible artefacts are left for the discussion section of this thesis.

Figure 49 is a labelled example of a peeled die pad imaged by a microscope, the descriptions of the labels are contained in Table 7. As can be seen in the image, there are a myriad of stand-out features. The first features to stand out are the remnants of ASIC adhesive in the ASIC area, C is a crack in the adhesive at the ASIC interface, this corresponds exactly to the crack seen in the CSAM image of the sample, see Figure 50, area of dark contrast. This clearly confirms the presence of the crack, and also confirms the cracks position. At the crack location the adhesive has essentially disconnected from the ASIC, this means during the peel test there would have been no resistance to peel in this area, and the crack surface will have substantially remained intact. At the perimeter of C the adhesive becomes a lighter colour, this is likely because the crack propagates through the adhesive thickness and hence the surface is no longer smooth and more reflective due to the exposed silver flakes.

In the remaining ASIC area are other adhesive remnants, F is indicative of void positions within the adhesive. Voids are a well known phenomena, which can be easily seen in X-ray images, in this case the peel has caused the adhesive bulk to detach from the lead frame surface, but where there is a gap in the adhesive, such as voids or cracking, the lead frame side of the adhesive remains attached.

I is evidence of silver-rich adhesive remnants on the die pad, it is not completely clear whether this is a consequence of cracking in the adhesive or is due to adhesion characteristics and cohesive cracking due to the peel test, in the CSAM image in Figure 50 there is a faint area of lighter contrast which corresponds to the "I" area which could support the former hypothesis.

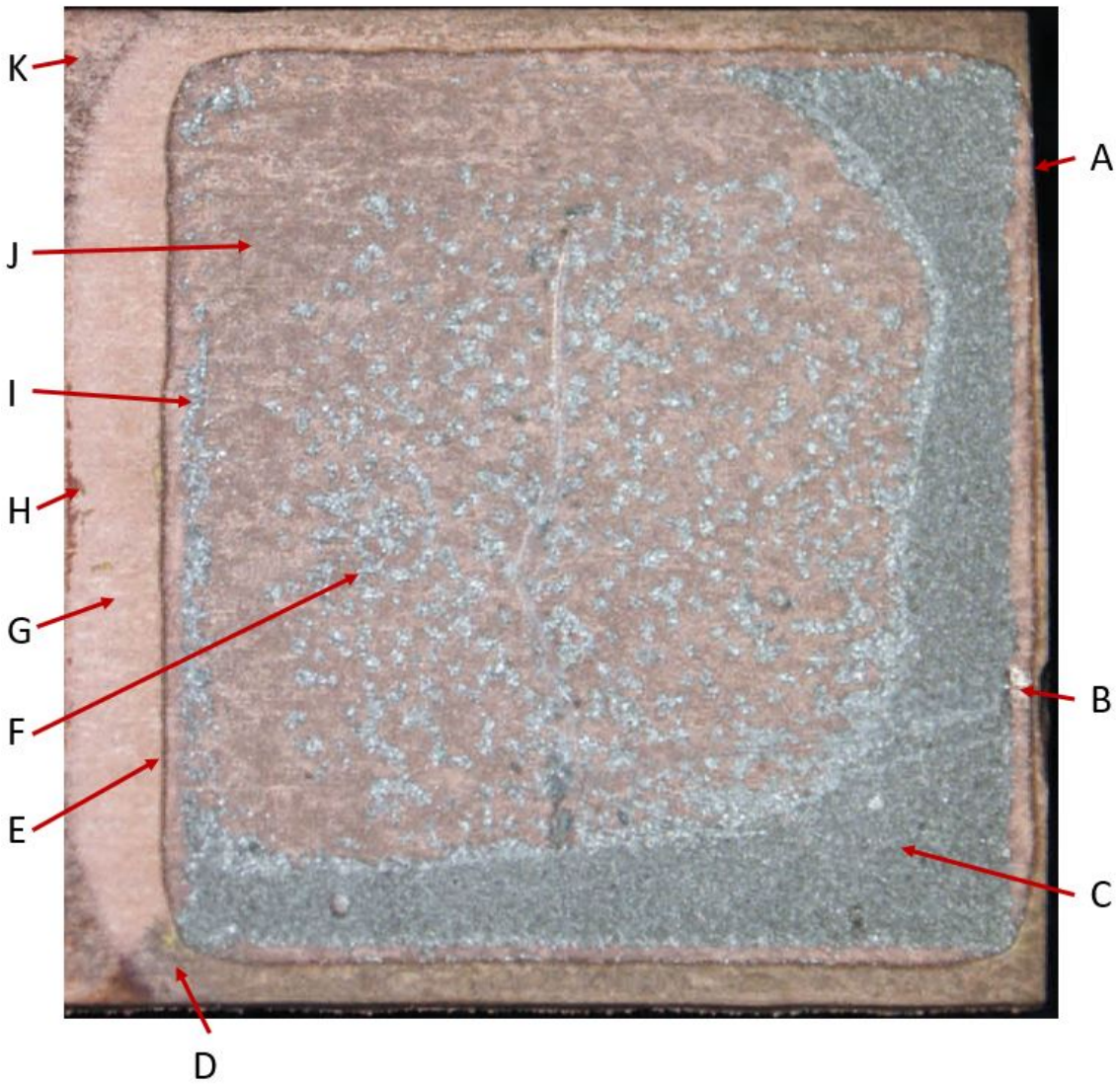

Figure 49: Labelled image of a typical peeled die side.

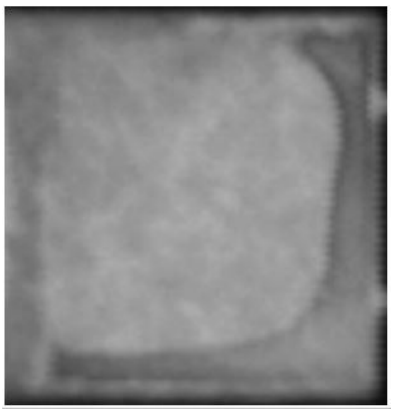

Figure 50: CSAM of sample in Figure 49

LABEL	DESCRIPTION
A	Sample ground to die pad edge
B	Peel initiation point
C	Crack at ASIC interface
D	Crack at lead frame interface
E	Adhesive fillet perimeter
F	Voids
G	Clean die pad
H	Discolouration
I	Silver-filled adhesive remnants
J	Adhesive resin remnants
K	OM residue on die pad

Table 7: Legend for Figure 49

Finally, in the ASIC area, as indicated by J, there is a darker patchy pattern left on the die pad surface. When comparing with G, which appears to be a clean die pad surface, there clearly seems to be some residue remaining attached to the frame. Due to the dark nature of this residue it is suspected to be thin layers of adhesive resin*[10], with no silver present. This would be an indicator that the adhesive had good chemical adhesion to the die pad and did not just delaminate during the peel test.

At the perimeter of the ASIC is a dark line, it is suspected that this dark line is the perimeter of the adhesive fillet*, rather than the perimeter of the ASIC itself due to the curved nature of the corners. The nature of this dark line will be investigated further under the SEM. This marks the boundary of what is ASIC adhesive surface and what is the die pad to OM surface.

Outside of the ASIC area are other interesting artefacts left on the die pad. At D, is a darkened area below the ASIC, which appears to be a witness area of cracking between the lead frame and the OM material, one clue which supports this is the triangular feature which sits towards the left hand side of this darkened area corresponds with an area of lighter contrast in the CSAM image (Figure 50). Lighter contrast under the ASIC area in CSAM images is usually an indication of cracking or delamination at the lead frame interface.

G is an area which appears to be clean copper, with no residue present, at least which can be seen with the optical microscope at this magnification. The clean area seems to extend from the edge of the ASIC and somewhat follow the curvature of the adhesive fillet, this suggests the clean area could be caused by the outgassing* of the epoxy adhesive. Epoxy adhesives are known for expressing various organic gases during their cure [87]. A similarly shaped pattern can also be seen at E in Figure 51. These gases may have prevented proper adhesion of OM material to the lead frame, hence the lack of any residue present*.

Another interesting feature left on the lead frame is K, an area of the die pad which still has some OM material attached*, this is likely the result of the peel event, similarly another patch of OM material is present in the bottom left corner of the image as well. This K area appears to overlap with the suspected crack area D and is bounded by the clean die pad area G, resulting in an intriguing darker patch in the shape of a triangle. It is possible that cracking at D within the G area, where there is very little or no OM adhesion to the die pad, leaves behind a light OM residue. But when the crack at D propagates beyond the G area into the bottom K area, there is a heavier residue left on the die pad. This is likely due to the greater OM adhesion at K. These kind of observations are good indications of how the materials interact with one another, and will be analysed further with the SEM.

Finally H shows some discolouration on the part, the source of this is unclear.

Moving on to Figure 51, which is the OM side of the peel, similar observations can be made, albeit less information is available from this half of the sample.

Label A shows the bulk of the ASIC adhesive appears to remain attached to the ASIC on the OM half after the peel. A similar void pattern can be faintly seen in

[10]* denotes a purely speculative suggestion which does not attempt to fully explain the phenomena, but merely suggest a possibility.

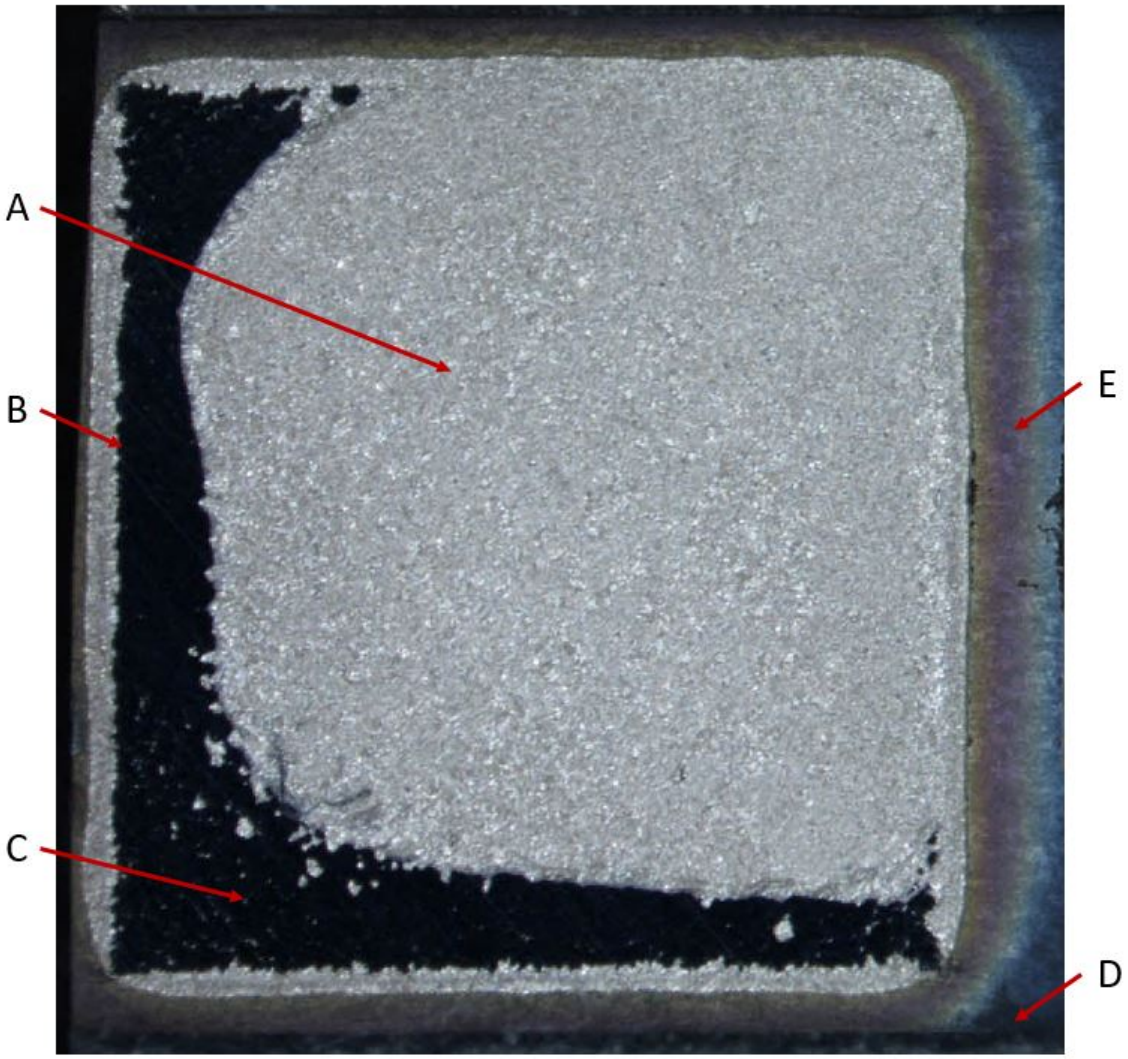

Figure 51: Labelled image of a typical peeled OM side.

LABEL	DESCRIPTION
A	ASIC adhesive
B	Crack at ASIC interface
C	ASIC backside
D	Crack at lead frame interface
E	Coloured pattern on OM material

Table 8: Legend for Figure 51.

this area as well. B also indicates a crack at the ASIC interface, which is essentially the mirror image of the crack in Figure 49. In this crack location there is also the backside of the ASIC present, indicated by C.

At D is an area of darker shade, which corresponds to the die pad interface cracking seen in Figure 49(D), this will be further analysed with the SEM. Finally, E indicates the mirror image of the clean die pad area seen in Figure 49(G), however on the OM half this displays an interesting colour pattern. It is possible this can be explained through structural colouration. Structural colouration is the effect of transparent thin films interfering with the light being reflected and refracted through them, where varying thicknesses lead to varying wavelengths, hence colour, of light being reflected. If there is a thin film residue left on the OM material, perhaps from epoxy bleed-out, the varying thickness of it would lead to different wavelengths of light being reflected. The thicker the film the larger the wavelengths reflected, which results in a reddish colour, and the thinner the film the smaller the wavelengths reflected, which results in a blueish colour. The colour pattern at E goes from reddish to blueish as it moves away from the ASIC area, this would be consistent with a thin film decreasing in thickness, if the hypothesis is correct.

Close ups

The peeled surfaces presented in Figure 49 and Figure 51 were examined with a SEM. The SEM examination primarily focused on the artefacts seen, labelled C-K, and labelled A-E, respectively in each figure. This section presents the SEM images with some description of the image findings.

1. ASIC adhesive crack

First of all the crack surface was examined with the SEM. Images of the crack from both the die pad side and OM side of the peel can be seen in Figure 52. Figures 52(a) and (b) are two different magnifications of the ASIC adhesive material left behind on the die pad surface in the location of the crack. This material remained adhered to the die pad during the peel, which suggests detachment from the rest of the adhesive prior to peeling, i.e cracking. These images give a 3D impression of the crack, displaying the cohesive nature at the edges, and the surface interface cracking at the top. On the top surface of this residual material is a relatively smooth surface of a darker shade, which is likely a film of adhesive resin which settled on the smooth ASIC backside surface, this is also part of the crack surface. The silver flakes in the adhesive are clearly seen in the cohesive region, through the thickness of the adhesive. Interestingly, on the die pad the micro-pores do not appear to be empty but instead filled with a dark substance, which is most likely to be adhesive resin, which supports the hypothesis that resin-rich residue is left on the die pad surface under the ASIC. This would have been residue left by the peel event.

Figures 52(c) and (d) are two different magnifications of the hole left by the crack on the OM side of the peel. The ASIC backside can be clearly seen, identified by the almost perfectly smooth surface, which confirms the observations seen under the optical microscope in this area. These are also good 3D images of the cohesive crack

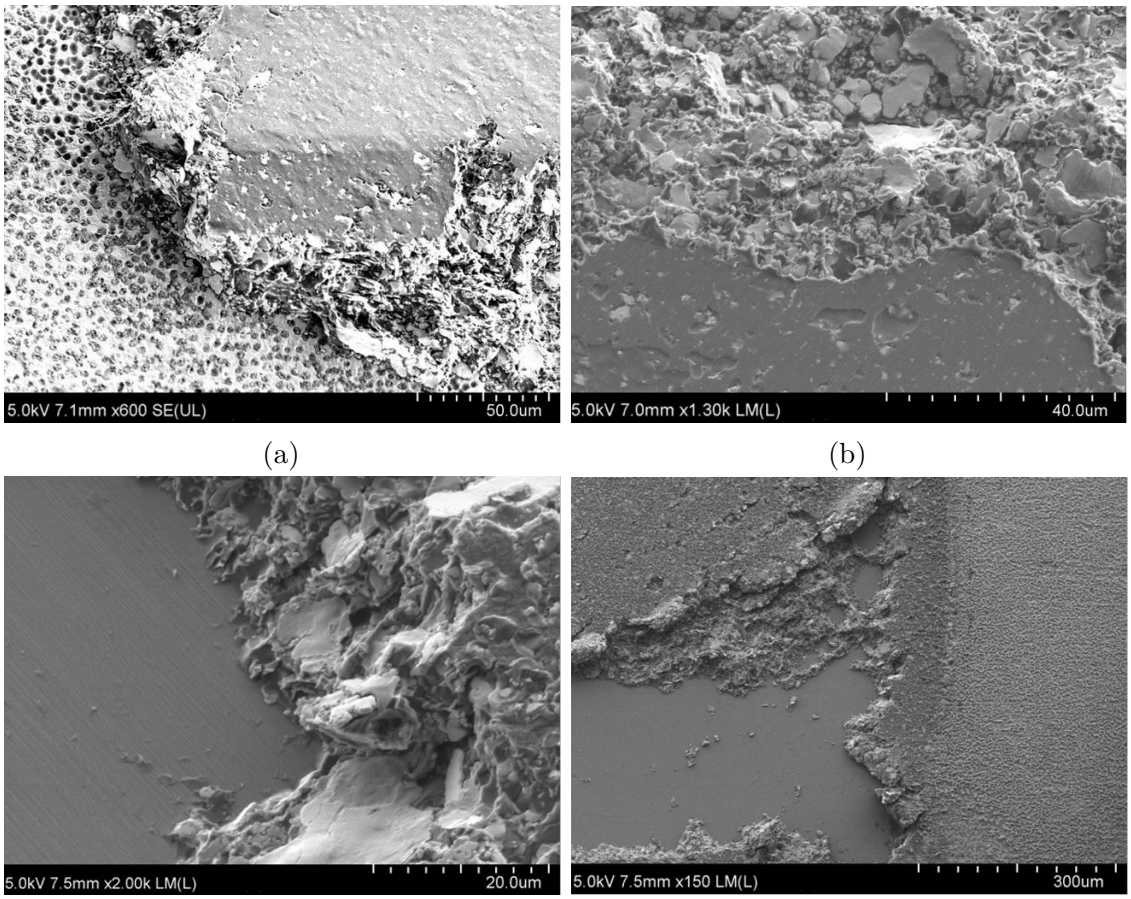

Figure 52: (a) & (b) Die pad side peel, cohesive crack, (c) & (d) OM side peel, cohesive crack

region and the crack pattern is clearly visible. In the top part of the crack in Figure 52(d) there appears to be a cohesive region of the cracked adhesive which seems to show the crack propagated from the ASIC backside surface, through the adhesive thickness, towards the die pad surface.

2. Crack/ delamination at at the die pad surface

Figure 53 contains two images of the crack visible on the die pad surface. Figure 53(a) displays clearly the micro-porosity of the die pad, which appears to be in two distinguishable sections. The top left section is in the clean die pad area, and the bottom right section is in the die pad surface crack area. The micro-pores in the clean area appear very dark in colour, however seem empty, but the micro-pores in the crack area seem to be filled with OM material, which can be recognised by the roughness in the pores.

Figure 53(b) is taken from the crack area at higher magnification. The OM material in the pores can now be more clearly seen, along with pores which appear empty and are also dark in contrast. The area where the micro-pores are filled with

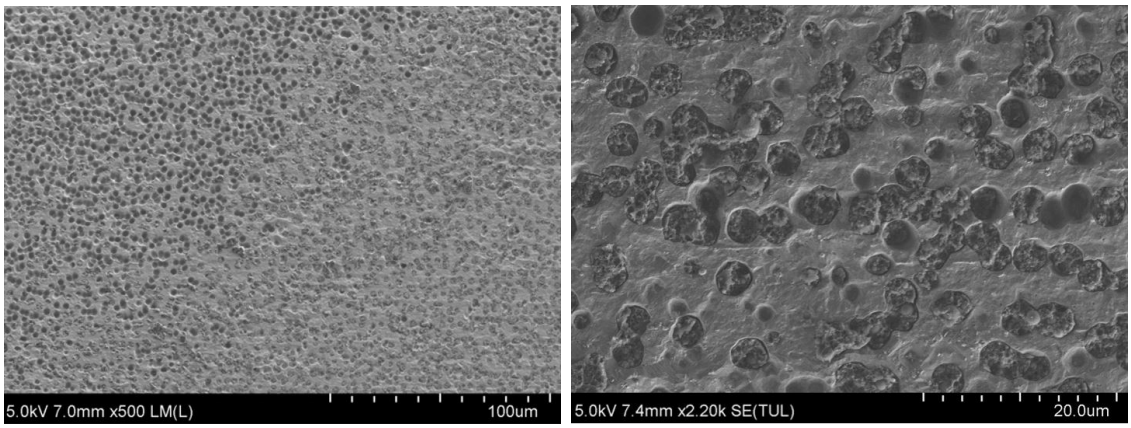

(a) (b)

Figure 53: (a) Die pad interface crack surface vs clean die pad, (b) Higher magnification of die pad interface crack

Om material is the crack surface. The area between the pores is completely clean of OM material which suggests the crack propagated along the die pad surface, and when it reached the pores, it cracked cohesively through the OM material in the pores at the same level. This explains why after the peel there is OM residue remaining on the die pad as the OM material in the pores is detached from the main OM body. This also shows there was at least some adhesion between the die pad and OM in this area before cracking, and the OM did not completely delaminate from the die pad. The area where the micro-pores are empty is likely the result of poor adhesion and occurred during the peel event rather than the cracking.

3. Clean die pad area

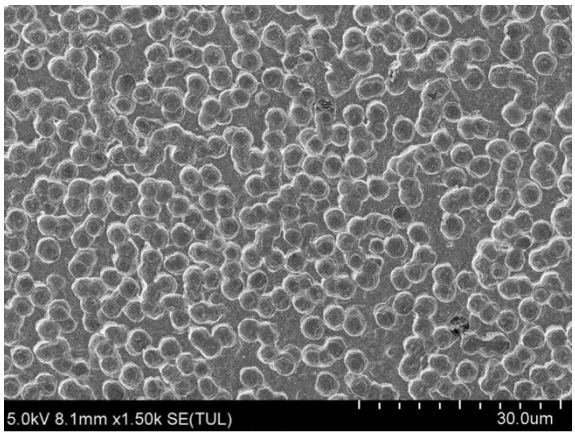

Figure 54: Clean lead frame area

Figure 54 displays the area on the die pad which looked clean under the optical microscope. The image clearly shows the micro-porosity of the die pad, and on the

whole the pores appear empty; at least nothing can be clearly seen within them, bar a few pores with OM material in them. This confirms the die pad is mostly clear of OM material in this area, which suggests there was a lack of adhesion between the OM material and die pad in this area. No clear evidence can be seen of any other residue in the pores which might hinder adhesion.

4. OM material residue on die pad surface

The two images in Figure 55 display areas of the die pad which have OM residue left on the surface. Figure 55(a) shows the boundary between K and G, (see Figure 49). On the right side of the image, empty micro-pores and clean die pad can be seen, and on the left side there are remnants of OM material in the micro-pores as well as on the die pad surface. This is distinguishable with the crack area presented in Figure 53 because there is still OM material on the die pad surface between the pores, which suggests this residue is not a consequence of cracking but evidence of good adhesion to the die pad.

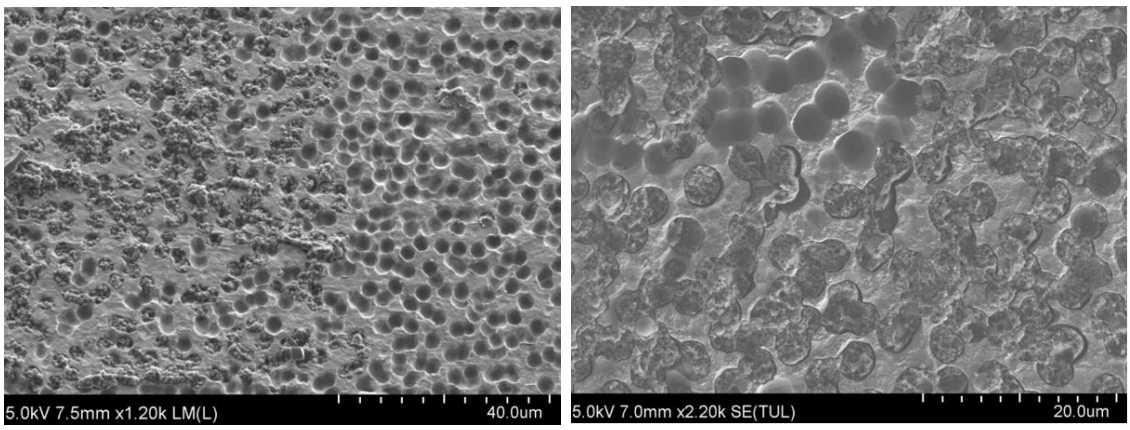

(a) (b)

Figure 55: (a) OM material on lead frame surface (b) Higher magnification of OM material on lead frame surface

5. OM surface observations

Figure 56 displays four images of the OM surface after peeling. In all of the images lots of spherical shaped globules are present on the OM surface, these are caused by the micro-porosity of the die pad and have remained intact after peeling. Figure 56(a) and (b) are taken from the boundary between the die pad surface crack area and clean die pad area. In the crack area (bottom left half) there are no globules present but instead the micro-pore areas display the cracked surface of each globule, where the crack on the die pad surface has propagated. It is interesting to note the contrast of the severed globules is a lot darker than the OM surface between them, this may be due to the clean separation from the die pad, leaving a smooth surface.

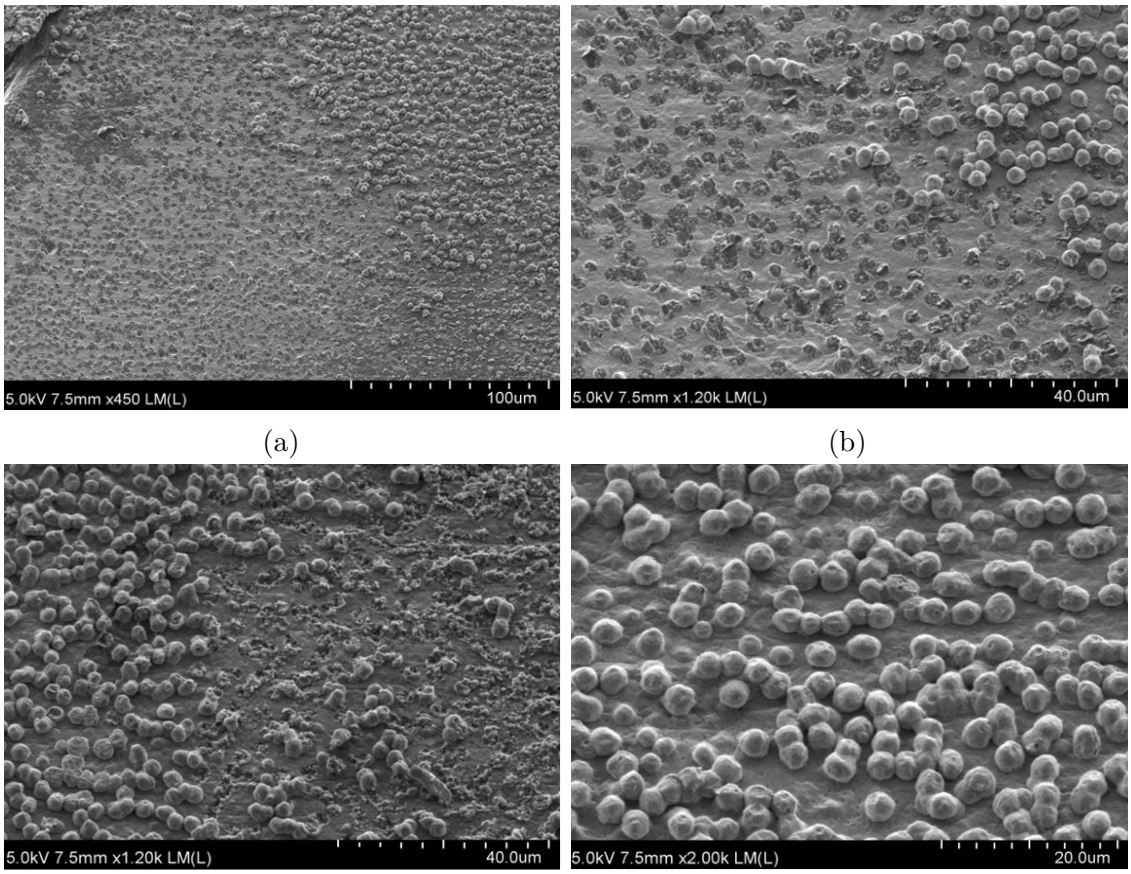

(a) (b)

(c) (d)

Figure 56: OM side peel: (a) & (b) die pad interface crack area (c) Clean die pad area vs OM material left on die pad (d) Clean die pad area

Figure 56(c) displays an area of the OM surface where OM material was left on the peeled die pad surface. This is the globule-free area, where instead of clearly defined micro-pore shaped fractures, there are uneven and irregular patches of fractures OM, again distinguishing a TC-induced crack from a peel-induced crack.

Finally Figure 56(d) is magnified image of the globules in the area of the OM side peel where there appears to be a colour pattern. It is not clear from the image if there is any layer of organic material from outgassing or bleed-out present which is causing the colouration and lack of adhesion to the die pad, however there is a light contrast on the globule surfaces giving them a slight sheen, which might could be a fine layer of something, but by no means conclusive.

6. ASIC adhesive perimeter

Figure 57 displays two different magnifications of the thin line surrounding the ASIC. These images conform the dark line is in fact remnants of ASIC adhesive, and it is likely this is the very tip of the adhesive fillet. It is possible that during the peel the adhesion strength of the adhesive at the thin tip of the fillet was sufficient enough to

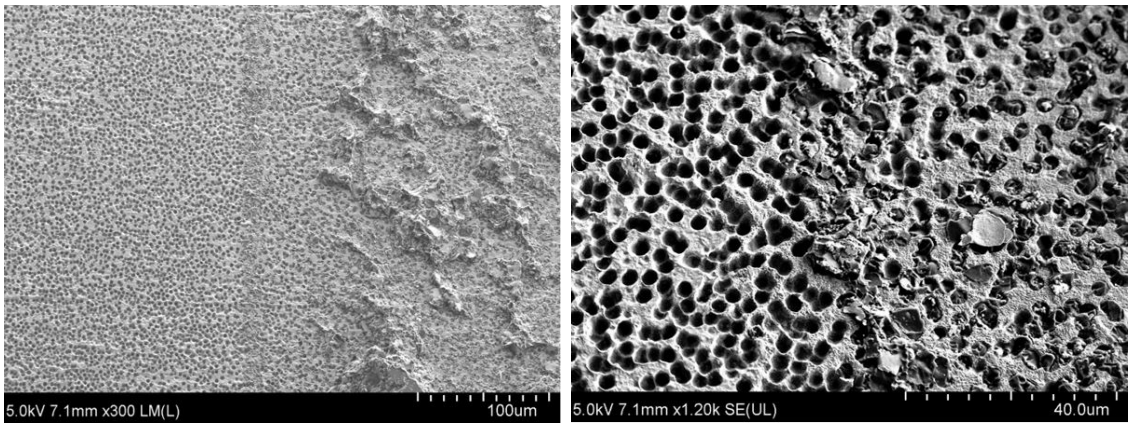

(a) (b)

Figure 57: (a) ASIC adhesive perimeter (b) ASIC adhesive perimeter with higher magnification

maintain adhesion while the bulk of the fillet separated from the tip during the peel.

More peel examples and other findings

This section presents a range of images from more peeled samples with artefacts which differ from those already presented.

The sample in Figure 58 displays dark patches in the corners of the ASIC area. Exactly what has caused this is unclear. This sample had an unusually low amount of adhesive coverage under the ASIC, which did not fully reach the corners, meaning the zones with dark patches may not contain adhesive, which may have left the corners exposed and consequently led to tarnishing, and hence the discolouration. Another possibility is the corner areas may have been filled with resin-rich adhesive, without the silver flakes. Resin-rich areas of adhesive are significantly weaker than the composite bulk, which would possibly lead to cohesive cracking of the resin, and the dark areas seen in Figure 58 could be the remnants of the resin-rich adhesive still attached to the die pad after the peel.

Figure 59 displays three samples with discolouration on the die pad. The discolouration appears to emanate from the ASIC area in sample (a), it is also possible this is the same case for (b) and (c), however the discolouration has covered the entire die pad area making it a little unclear. The slight orange hue around the ASIC is a common feature in many of the peels performed, across various different builds of samples. It is unclear what exactly is causing the orange hue, but it is possible that it is staining from outgassing of the ASIC adhesive, or alternatively oxidation of the surface where outgassing has taken place. There is also the possibility that the discolouration in (b) and (c) is due to oxidation of the die pad during the processing.

Figure 60 displays a sample with a large area of die pad interface crack. The crack is visible from the slightly darker contrast patches, in the top right corner, down the left edge of the ASIC, and from the large crack surface along the bottom edge of the ASIC which propagates away from the ASIC area towards the die pad

Figure 58: Poor adhesive coverage has led to discolouration of the lead frame at the ASIC corner areas.

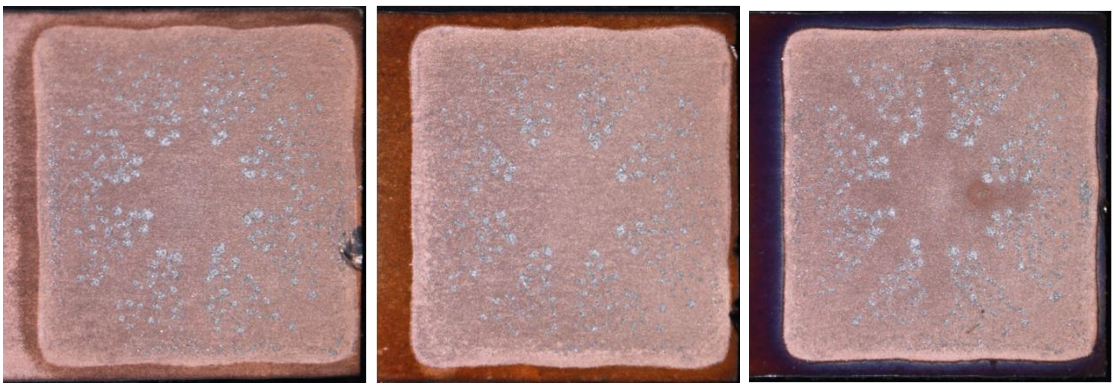

(a) (b) (c)

Figure 59: (a), (b) & (c) Various amounts of discolouration on die pad emanating from ASIC area.

edge. Slightly inbound of this crack at the bottom of the ASIC area is a line of adhesive, this indicates the adhesive began to crack cohesively. Again there is an orange hue visible around the ASIC and adhesive perimeter.

Figure 61 shows a die pad surface covered with blotches, which appear to cover the whole area, including the area under the ASIC. This phenomenon somewhat

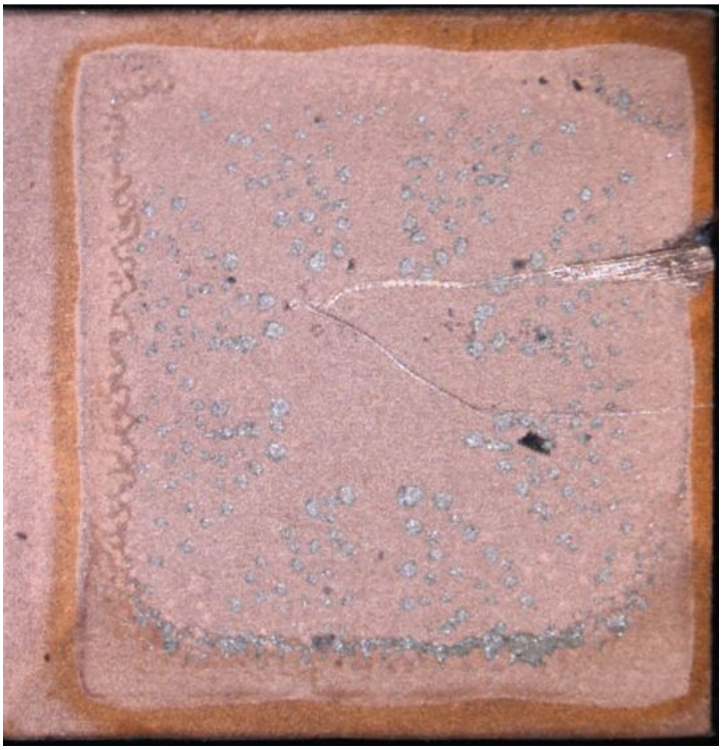

Figure 60: Large crack at die pad interface at ASIC lower edge.

obscures the die pad from being fully examined, masking interesting artefacts and details. SEM images confirm the micro-pores in the die pad contain lots of leftover OM material, but this does not explain why the blotchiness is also present in the ASIC area, assuming there would be no OM material here. This sort of finding was not very common and specific to just two different builds which had lead frames from the same batch. It is possible the lead frame surface has contributed to this phenomenon, where the blotchiness under the ASIC is due to resin-rich adhesive remaining in the die pad pores in specific areas. Another possibility is that the lead frame was already beginning to oxidise before manufacture. However, it is not entirely clear what the cause of this is.

Lastly, Figure 62 displays two images of the die pad area under the ASIC. In this sample the ASIC and adhesive have completely delaminated from the die pad surface. The higher magnification in Figure 62(b) confirms this with the visually empty micro-pores. This observation is important because it reveals an adhesion issue between the adhesive and the substrate rather than a durability issue. It can also be seen that the ASIC area is clean and pale in colour, whereas the surrounding die pad area is discoloured, which again could be due to a combination of outgassing and oxidation.

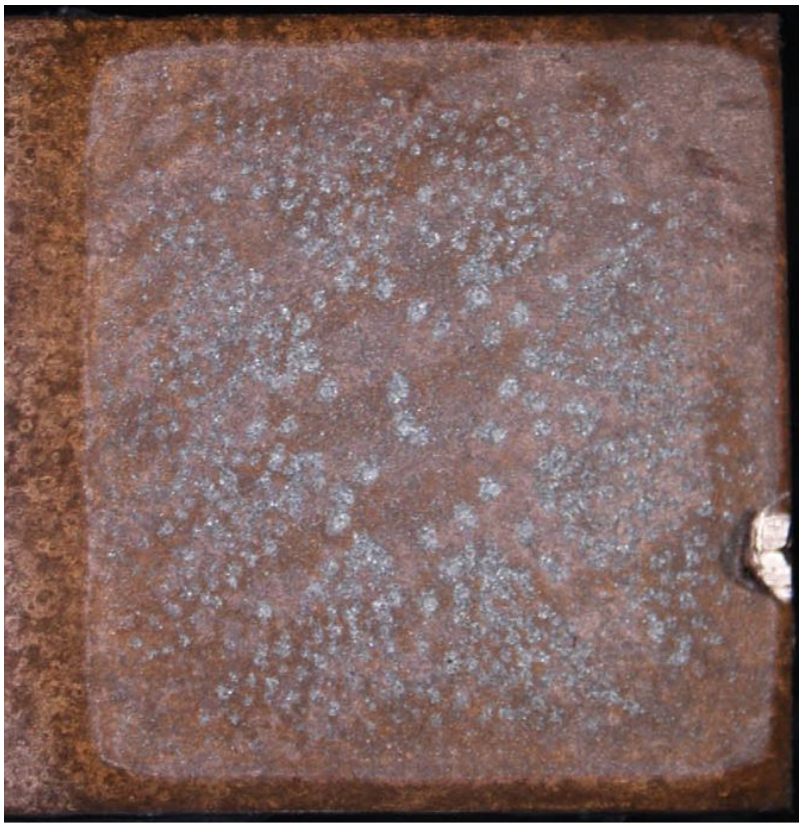

Figure 61: Dark residue obscuring the die pad surface.

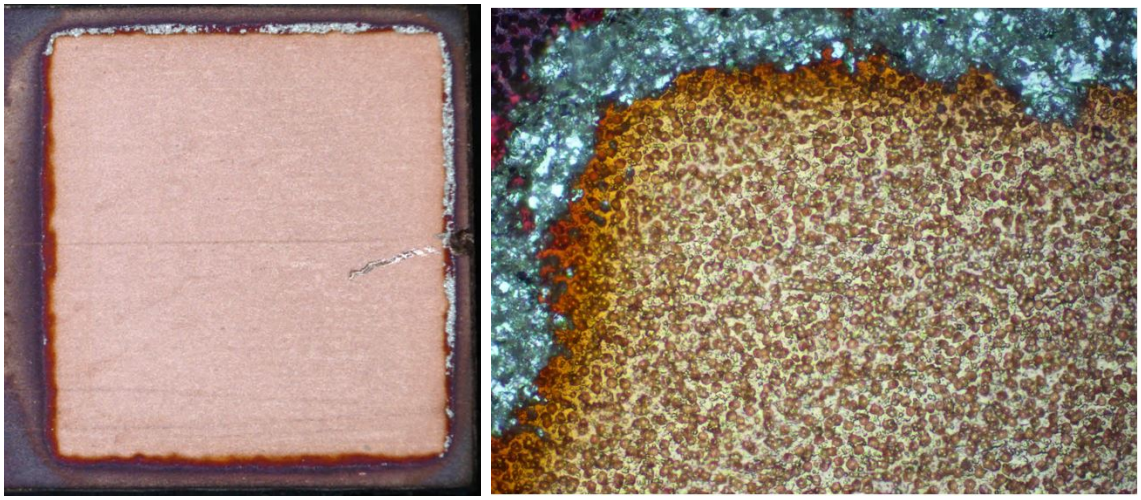

(a) (b)

Figure 62: (a) & (b) Bald die pad under ASIC, suggests adhesion failure.

Quantification of peel artefacts

Sometimes it is useful to understand the size of a defect in a sample in comparison with other similar defects in other samples, this kind of information can lead to

finding correlations which can help establish an understanding of the root cause. This section provides some measurement results and examples of how these can be compared and used. The purpose for this study was to demonstrate the method rather than identify a root cause.

The images of 8 samples were selected to be analysed using ImageJ software, firstly the ASIC area of each peel image was measured, followed by measurements of the ASIC area of the corresponding CSAM images. These were taken as reference areas for the remaining measurements. On both the peeled die pad and CSAM images the cracked areas were measured and divided by the respective ASIC areas, this left a crack area as a percentage of the ASIC area for image to image comparison.

Figure 63 is a plot that displays the comparison between the peel-measured cracks and the CSAM-measured cracks. It is clear that the peel-measured cracks give consistently higher area percentages than the CSAM measured cracks. Samples 6 to 8 display the largest difference between the two methods, but on average the difference in percentage was 4.95%, this is a significant amount. One reason for this difference is the ASIC area is not well defined in the CSAM images, and some estimation is required to determine it, therefore it is possible the ASIC area is over estimated which offsets the crack area percentage results.

The areas for measurement in the peel results were more defined and therefore easier to measure, thus a more reproducible and more accurate result. This is good for post-analysis purposes, however inconvenient for measuring crack amounts intervallically due to the destructive nature of the test, it also runs the risk of declaring more failures for a particular spec than the CSAM method would.

The numerical results can be seen in Table 9.

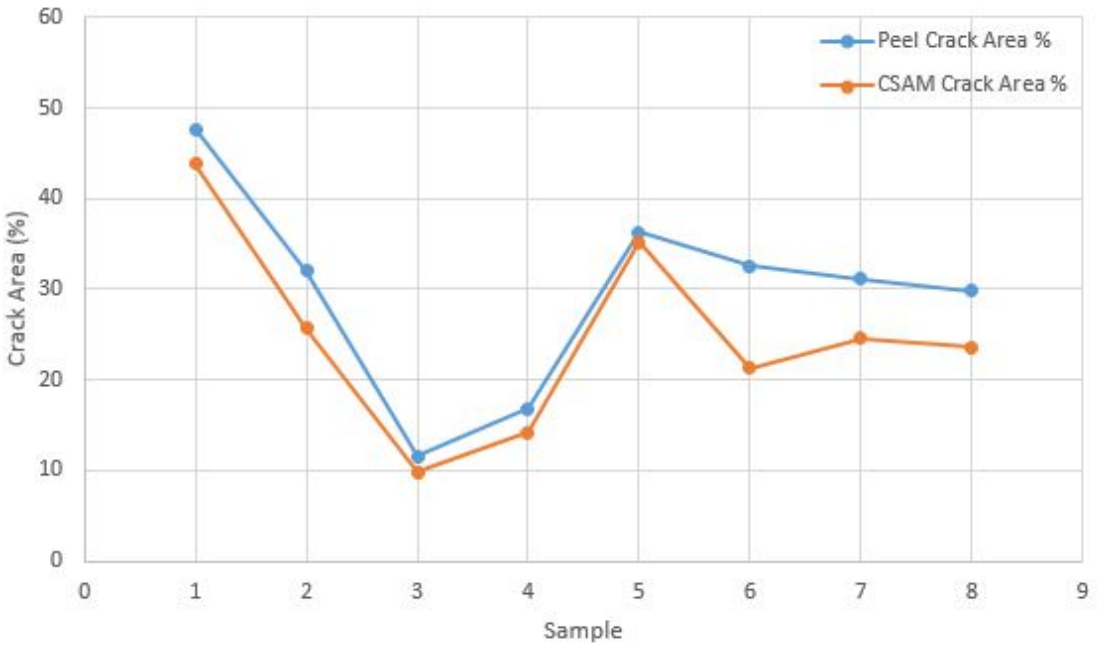

Figure 63: Comparison of peel-measured cracks vs CSAM-measured cracks.

Sample	Peel Crack Area (% ASIC Area)	CSAM Crack Area (% ASIC Area)	Difference (%)
1	47.69	43.85	3.84
2	31.99	25.66	6.33
3	11.50	9.77	1.73
4	16.78	14.16	2.62
5	36.24	35.20	1.04
6	32.56	21.31	11.24
7	31.16	24.57	6.58
8	29.81	23.55	6.25
		Average	4.95

Table 9: Comparison of peel-measured cracks vs CSAM-measured cracks, numerical results.

Another area which was analysed using the quantification method laid out in the Methodology section, was the outgassing areas. Of the 8 samples used, all of them displayed an orange hue around the ASIC. These orange areas were measured using the ImageJ software and were defined as a percentage of the ASIC area, this was again to allow for sample to sample comparisons. The outgas areas were plotted against the peel-measured crack areas for correlation analysis. Figure 64 and Table 10 display the graphical and numerical results respectively.

The overall results indicate no significant correlation between the two areas, however the points at the lower and upper ends of the range do display a little correlation. Further investigation of this area is out of the scope of this study, but could be explored further in a more in-depth study.

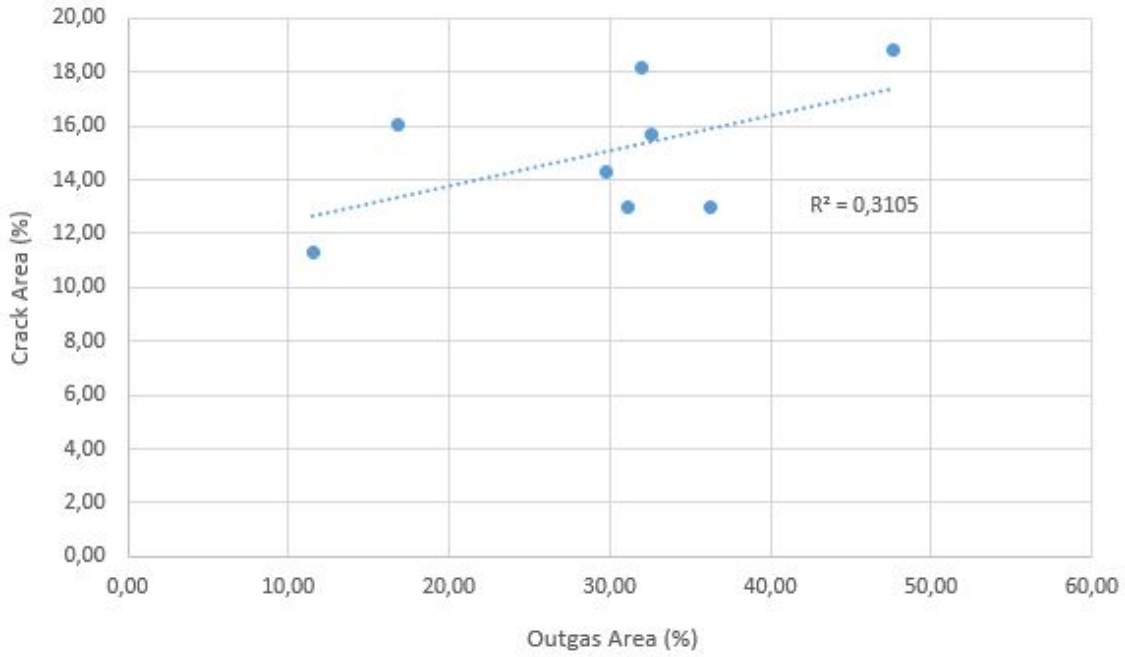

Figure 64: Comparison between outgassing amounts and the amount of ASIC adhesive cracking.

Sample	Peel Crack Area (% ASIC Area)	Outgas Area (% ASIC Area)
1	47.69	18.79
2	31.99	18.14
3	11.50	11.28
4	16.78	16.06
5	36.24	12.97
6	32.56	15.66
7	31.16	12.96
8	29.81	14.32

Table 10: Comparison between outgassing amounts and the amount of ASIC adhesive cracking, numerical results.

Correlation

It is important to find links between peel observations, cracking, and electrical output in order to fully understand the root causes of abnormal performance, for this reason a correlation analysis was established as part of this study to further demonstrate the application potential of the peel test herein. Results and observations from the correlation analysis are presented in this section.

3 samples from 5 different lots were cycled to TC2000, imaged with the CSAM, peeled, and than imaged under the optical microscope. Each sample had the same BOM, and process steps.

First of all the electrical results were analysed, plots of the offset drift in the X, Y, and Z channels for each lot can be seen in Figure 65. The samples were chosen based on their representation of overall trends within the lot. The rows represent the 5 lots, and the columns represent the X, Y, and Z channel results for the 3 samples from each lot.

It can be seen that the samples from lot 1 clearly display drift after TC1500 in all three channels. Lot 1 samples appear to have the worst drift out of all the lots tested. Drift is where the output diverges away from the zero line, most of the plots in the other lots display curves which only fluctuate minimally from the zero line, this is evidence of good reliability.

Other than lot 1, plots d and i display one drifting sample in the X and Z channels respectively, however the other channels are unaffected and the drifting parts do not display excessively steep diverges from the zero line after Reflow. This could be explained by an erroneous result at the FRESH test point, as the plots then appear to flatten out at subsequent test points. Also, plot l contains one sample (sample 4c) which displays a steep drift after TC1500.

Figure 66 contains a grid of CSAM and peel images for each sample from the correlation study. The rows represent the 5 lots, and the columns represent the 3 samples from each lot. It is clear from the electrical results that lot 1 had the worst electrical performance, this correlates directly with the CSAM images displayed in Figure 66, where the lot 1 parts clearly have a large cracked surface (solid yellow contrast area) at the bottom edge of the ASIC. The samples 2b, 3c, and 4c, which display some offset drift in the electrical results do not show any significant cracking in the CSAM images, instead the yellow areas appear to just be noise from the CSAM, but CSAM images have limited resolution and it can be difficult to distinguish

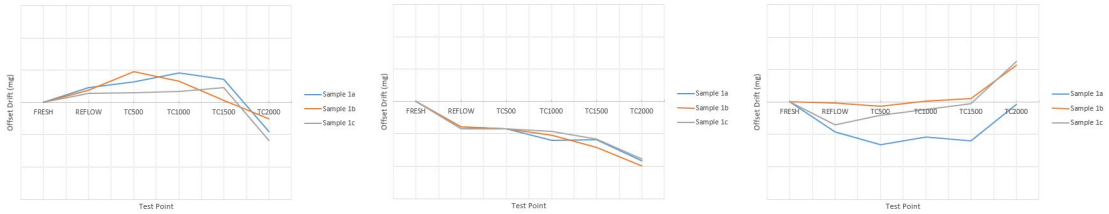

(a) X-Channel (b) Y-Channel (c) Z-Channel

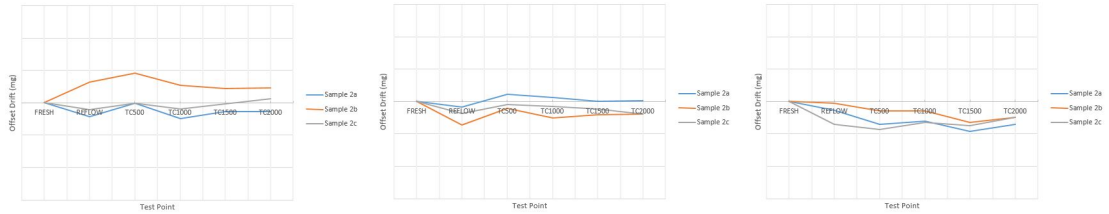

(d) X-Channel (e) Y-Channel (f) Z-Channel

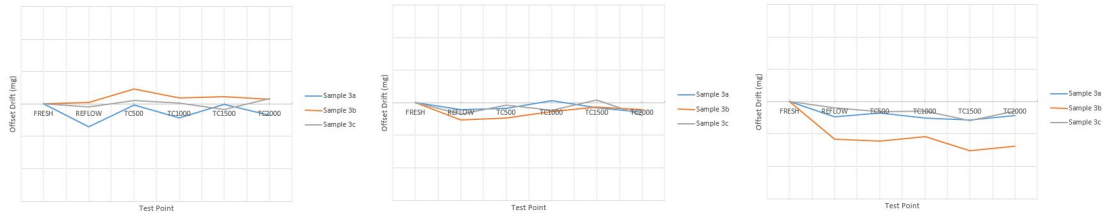

(g) X-Channel (h) Y-Channel (i) Z-Channel

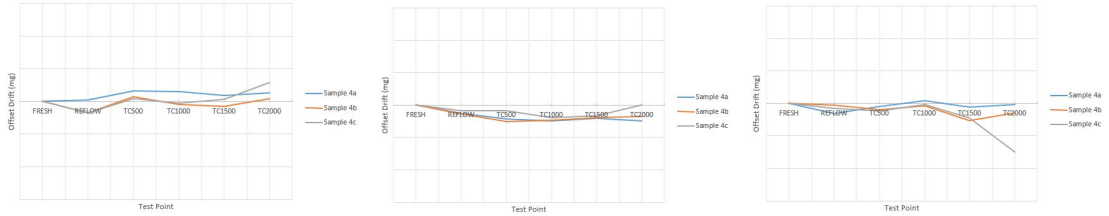

(j) X-Channel (k) Y-Channel (l) Z-Channel

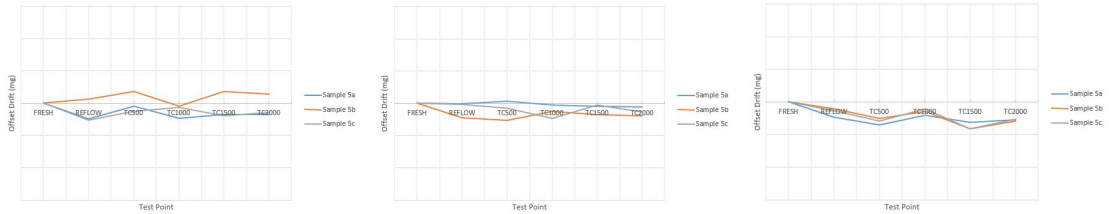

(m) X-Channel (n) Y-Channel (o) Z-Channel

Figure 65: (a)-(c) Lot 1, (d)-(f) Lot 2, (g)-(i) Lot 3, (j)-(l) Lot 4, (m)-(o) Lot 5.

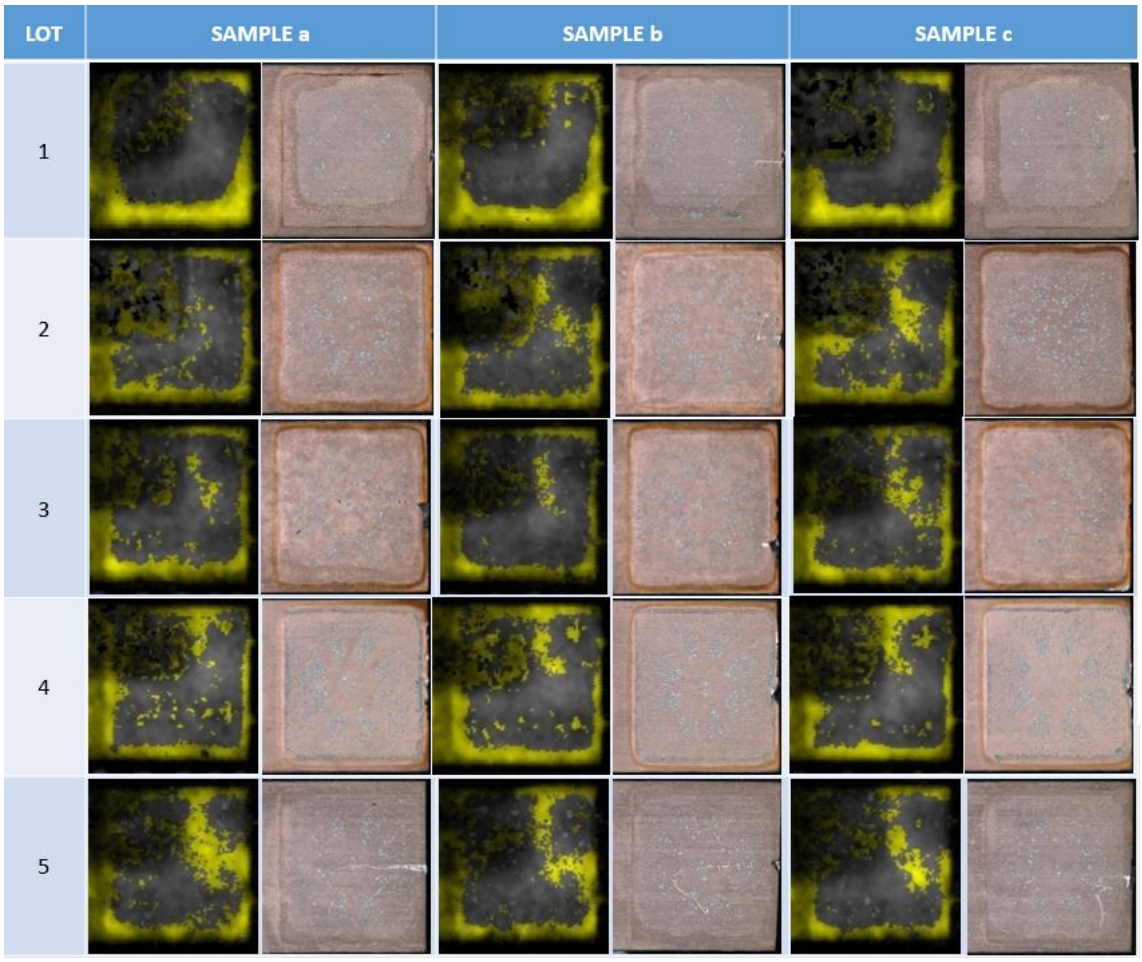

Figure 66: Compilation of CSAM and peel images to support the correlation analysis.

between noise and actual cracks with this filter setting. This filter setting was used because it provides the clearest definition of the ASIC adhesive cracks when the samples have had laser etching, which masks areas of the ASIC.

Sample 4b appears to show some cracking in the CSAM image, however no evidence of drift is visible in the plots. All the other CSAM images do not contain clearly cracked areas.

Moving onto the peel images, the side by side comparison with the CSAM images shows just how much more definition and information is available in the peel images. Also immediately visible is the lot to lot variation. Samples from the same lot appear similar in appearance with each other but different to samples from other lots. This is a strong indication of process variations during manufacture.

Starting with lot 1, the cracking at the bottom of the ASIC can be easily seen as a darker area in the peel images, which indicates a die pad interface crack. This area also appears to extend around the whole ASIC perimeter, which indicates the ASIC was cracking from all edges; a detail which cannot be seen in the CSAM images. Also, some possible areas of outgassing are visible around the ASIC, indicated by

the lighter patches on the die pad.

The lot 2 samples do not appear to show any significant cracking in the peel images, although some traces of minor cracks can be seen at the bottom edge of the ASIC in samples 2a and 2b, the largest areas are associated with 2b, which may correlate with the electrical drift seen in the corresponding X-channel electrical plot. Samples 2a and 2b have a hazy appearance and the ASIC edge appears quite faint when compared with 2c. It is important to note 2c is a sample from a different lead frame, which could account for the minor difference between these three images. All three images display an orange hue around the edge of the ASIC, in samples 2a and 2c this orange hue is thick and well defined, in sample 2b this orange hue is somewhat fainter.

The lot 3 samples appear to look similar to lot 2 samples, however sample 3a has a large area of die pad interface cracking at the bottom edge of the ASIC, although this is not clear in the CSAM image, it does correspond to an area of brighter yellow contrast. Some minor cracking can also be seen at the bottom edge of samples 3b and 3c, where the CSAM images look almost identical. 3a displays a larger crack than 3b, but it is 3b which has some drift in the Z-channel, not 3a, which would not correlate. As with the lot 2 samples, the overall area has a hazy finish, and similarly sized areas of orange hue are visible.

The lot 4 samples appear much cleaner in appearance than lots 2 and 3, this means the artefacts are more clearly defined in the images and not masked by haziness. No clear evidence of die pad interface cracking can be seen, however on all three samples there remains some silver-rich remnants of adhesive material around the ASIC perimeter, which might suggests there has been some cohesive cracking. Although, it is unclear whether this is a result of TC or a result of peeling as there is no clear evidence of cohesive cracking in the CSAM images. However, there is a thicker area of yellow at the bottom edge of the CSAM images which might correspond with the cracking seen, but 4b has the thinnest amount of adhesive residue present and the thickest yellow area in the CSAM image, this contradicts the yellow being indicative of cracking. 4b was the sample from this lot which displayed some Z-channel drift after TC1500, but there is nothing in the peel images that distinguishes this sample from the other two, which displayed no drift. The ASIC area is also surrounded by an orange hue in all three samples, similarly to lots 2 and 3.

The lot 5 samples appear similar in appearance to lot 1 samples and display similar evidence of die pad interface cracking around the edges of the ASIC area, albeit at a lesser extent than the lot 1 samples. When comparing the CSAM images of lot 5 with the other lots, there is less yellow visible in the ASIC area, however the yellow that is present corresponds with the cracked areas in the peel image. This is a good example of how CSAM images alone are not enough to clearly determine the presence and size of cracks. All three lot 5 samples do not display any significant drift in the electrical plots, which suggests a lack of correlation. The texture of the peeled surface appears different to the other lots, where in this case there is some haziness but in a striped pattern parallel to the peel direction. Similarly to lot 1, there are lighter areas around the ASIC which could indicate outgassing, rather than the orange hue present in lots 2,3 and 4.

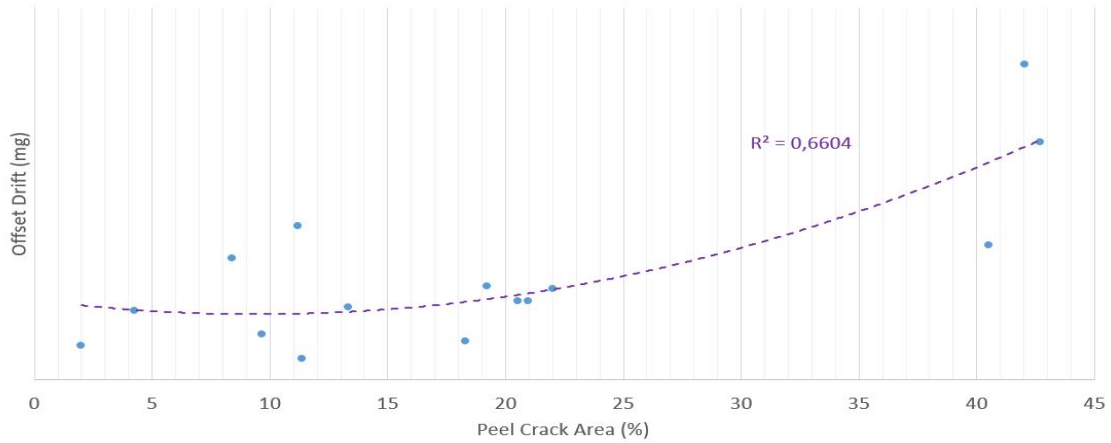

(a) X-Channel

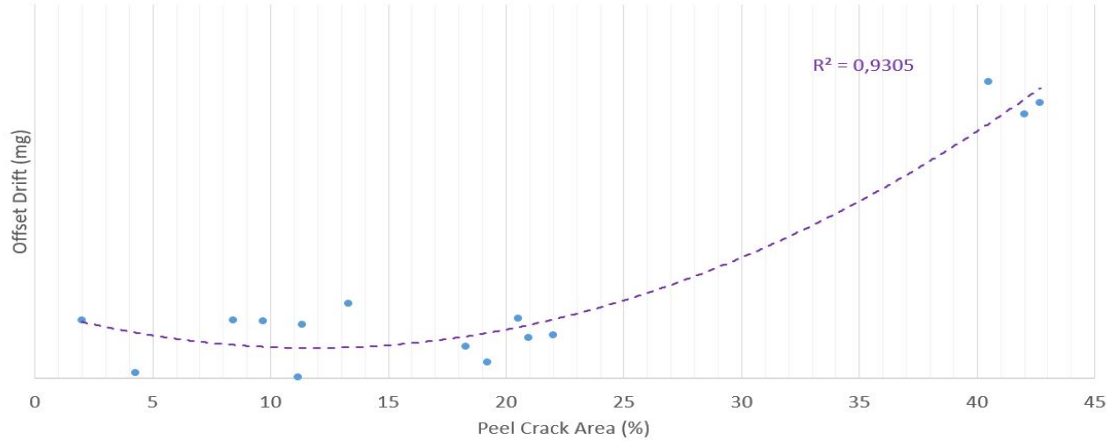

(b) Y-Channel

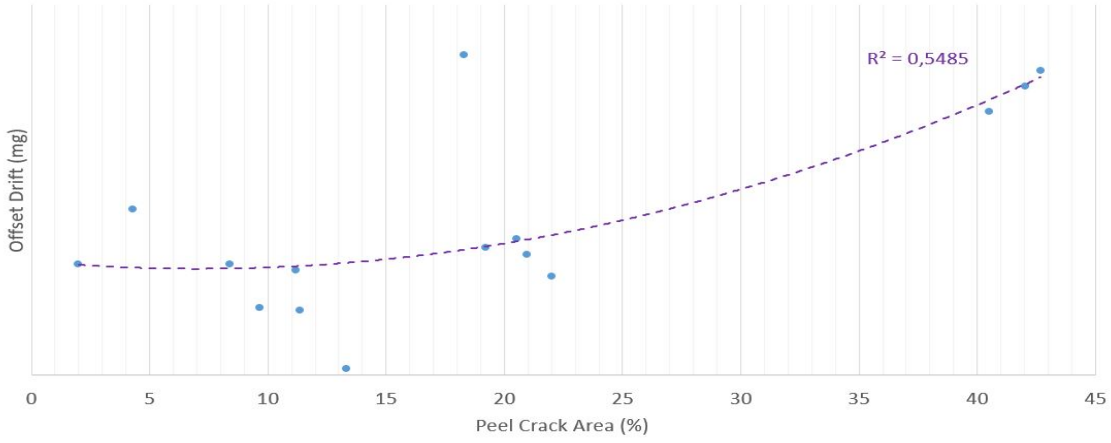

(c) Z-Channel

Figure 67: Offset drift vs Percentage crack area observed in peel images.

Measurements were also taken of the cracked areas visible in the peel images and plotted against the offset drift in X, Y and Z channels. The plots can be seen in Figure 67. Some correlation between the amount of cracking present and the amount of offset drift can be seen from the plots. Polynomial trend-lines were applied to the plots and the R^2 values for the X,Y and Z channels were, 0.66, 0.93, and 0.55 respectively. The Y-channel displayed the strongest correlation between the drift and cracking. There are clearly two populations seen in the plots, this is because lot 1 was the only lot which clearly displayed offset drift and significant cracking, whereas the cracking in other lots was less clear with minimal drift visible. The two populations result in an apparent non-linear nature in the plots, this resulted in polynomial trend-lines of the order 2 being applied.

The comparisons were not repeated for the CSAM images due to the lack of accuracy possible in the measuring of the unclear crack areas.

5 Discussion

The purpose of this thesis was to explore the practicalities of performing an adhesive peel test on mass-manufactured overmoulded inertial MEMS packages, and to analyse the resulting surfaces for useful information in relation to die attach adhesive cracking. The background explains how the reliability of inertial MEMS packages in the automotive industry is a critical aspect for safety, and how the thermally cyclic automotive environments subject the device to harsh conditions pushing its mechanical integrity to the limit, resulting in drifting electrical outputs. This has led to the requirement for TC testing during qualification, placing significant stresses on the material interfaces, which has been shown to cause various modes of cracking in the die attach adhesives. It was believed that a successful peel test would reveal more information of the cracked surfaces which would improve the understanding of the crack mechanics and could help identify the root causes.

A full surface and crack analysis was out of the scope of this study, but some analysis methods are explored, with descriptions of the observations and suggestions for the meanings behind them.

This section sets out to systematically review the core aspects of this thesis, starting with the de-capsulation and peel method, followed by the observations made during and after the test, and methods for analysing the peeled surfaces. Finally a discussion of the practicalities of this test and what it means for future crack analysis in this field, as well as suggestions for further development will be presented.

De-capsulation

Regardless of the peel method implemented, accessing the die pad was a necessary part of this study. However, the peel method influenced the selection of the de-capsulation method. A selection process was carried by way of a decision matrix, where eight different options were considered. These options ranged from grinding to machining to etching, with manual and automated examples. The decision matrix considered feasibility, accuracy, finish, repeatability and throughput. Not all methods were readily available in the lab for exploration, such as laser ablation, machine etching 2, or grinding with a jig, which immediately put them out of contention. However, it was important to score these methods for future consideration anyway, as they offer better control and accuracy, which could be beneficial for repeatable peel tests.

The highest scorer of the decision matrix was the grinding by hand method, which was an already established method in the lab, requiring no funds or outsourcing. The downfall with grinding by hand was the lack of control, accuracy, and therefore repeatability of some peel test methods. Initially the goal was to perform a quantifiable peel method which would need to be repeatable, therefore grinding by hand would not have been a sufficient enough de-capsulation method. After grinding the die pad thickness depends on the accuracy of the hand of the lab operator performing the grind, this lends itself to die pads of varying thickness and uneven surfaces after grinding, which would affect the peel forces, and hence introduce substantial errors

in the results.

For reasons other than de-capsulation methods, the quantification of the peel test was abandoned, this reduced the requirement for high accuracy during the de-capsulation, meaning that grinding by hand was considered a sufficient method. However, operator error was still a factor in the peel success, whereby over-grinding would lead to thin die pads which would fail to peel cleanly; with a "popping" motion. Besides the small percentage of failed peels, the de-capsulation method was not considered an important factor which affected the visual results of the peel, because lot to lot variation was clearly visible even though variation between the grinding of samples was not controlled.

If peel forces were to be measured, the de-capsulation method would need to be improved, reducing the error, in order to obtain results which would produce any correlation. An ideal de-capsulation method would leave the die pad completely intact, and remove the OM material such that the die pad sits proud of the OM surface, this could be achieved by laser ablation, milling, or etching with chemicals that would specifically target the OM compound and not the copper. Leaving the die pad proud of the OM surface would ensure the peel forces only need to overcome the adhesion to the die pad surface rather than the edges, giving a better indication of the adhesion quality between the ASIC adhesive and die pad, and lowering the overall peel force, making the glue attachment method more feasible. A proud die pad would also allow for other attachment possibilities for peeling which could improve the repeatability of the peel.

Peel Trials

The real crux of this study was implementing a peel attachment method which would not only facilitate the detachment of the die pad from the sample, but do so in a controlled and repeatable manner. The samples were not designed with peel testing in mind, therefore no provisions were in place for peel attachment, requiring retrospective implementation. De-capsulation methods were limited, which limited the amount of die pad exposure, limiting the attachment possibilities. Initially the samples were only ground up to the die pad backside, which just revealed a flat surface for peel attachment. This meant the connection between the machine performing the peel and the sample could only be some form of surface to surface attachment, for this reason it was decided to glue a screw to the die pad backside which could then be screwed into the peeling machine. The sample was grasped on both sides by a vice, and the machine applied a load to the screw until the die pad popped open.

It was soon clear that the force required to pop open the die pad was greater than the adhesion strength of the glue between the die pad and screw, which resulted in the screw detaching from the die pad before a peel was initiated. Three other glues were trialled with no success. To try and improve the situation the sample was ground from the tie bar edge up to the die pad, it was thought this would lower the peel force requirement, as the OM material would not be resisting the die pad from this edge. A few samples were successfully peeled with this method, but the majority failed, rendering the method unrepeatable, and therefore abandoned. It is

important to note here that different surface preparations of the die pad backside were not trialled in this study. It is possible that some alternate surface conditions may have improved the adhesion between the die pad and screw enough to complete the peel test.

Even if the glue method had worked, it was not necessarily a repeatable test. Firstly the screw was not specially designed and positioning the screw by hand would lend itself to placement error, introducing variation in the length between the peel initiation point and pivot point, which would affect the peel angle and leverage force. To help overcome this a specially designed screw with a flange would need to be used. The screw would then be positioned by placing the screw head surface on the die pad surface and then sliding towards the pivot point until the flange contacts the die pad edge, ensuring the peel location is always flush with the die pad edge. In this case the grinding of material up to the die pad edge would need to be carefully controlled to ensure the die pad lengths would be consistent.

Secondly, the modulus of the glue would introduce error into the test. It is suspected that the plasticity of the glue would interfere with the stress-strain curve, and introduce its own variation due to the bond line thickness and spread of the glue. Therefore the quantification would be limited to only finding the maximum load before onset of peel, which could be used for sample to sample comparison.

An alternative surface attachment method would be to weld or braze the screw onto the die pad backside. This method was not available in the lab and therefore not explored, however a weld would prove a solid connection between the screw and the die pad. The issue with this method is that welding or brazing requires enough heat to melt the filler metal, which could uncontrollably distort the lead frame and alter the adhesion properties of the ASIC adhesive, rendering the test unrepeatable.

The alternative to a quantifiable peel test was to peel the samples manually. This was achieved by embedding a knife into the exposed die pad edge between the die pad and OM material, and manually pulling the die pad away from the sample. This method lacked control in three main areas, peel application force, positioning of blade in sample, and peel application angle and follow through. Therefore, even if the peel force could be measured by way of a strain gauge attached to the knife, the results would not be reproducible. The lack of control also led to damage of the die pad surface, where the blade would leave a scratch during the peel follow through. However, this did not obscure and was easily distinguishable from other artefacts on the surface, therefore was not a cause for concern.

Even without controlling the peel itself, the visual results of the post peel surfaces were observed to have lot to lot variation, where samples within the same lot displayed similar appearances to each other, and those from different lots displayed variation in overall appearance. Mostly, differences in appearance between samples from the same lots were observed to be due to artefacts caused by TC induced cracking, or manufacturing processes, rather than the peel itself. For this reason, the visual peel results were considered reproducible and the peel test considered repeatable.

Various difficulties arose when trying to apply the knife peel method. One of the difficulties was a result of the malleability of the copper die pad, where upon peel application the die pad would deform under the pressure from the blade tip, causing

the blade to lose traction and slip before the peel had initiated. The problem here was that the knife would ideally be placed in the centre of the die pad edge to ensure an even peel, to restart the peel the knife needed to be re-positioned in the die pad edge, but away from the centre where the die pad had already been deformed, risking an uneven peel. Secondly, the very tip of the knife blade was very brittle which often resulted in fracture, leaving a less defined edge, making blade placement more difficult, which led to increased amounts of damage to the die pad, less control over the peel, and more deformation to the die pad edge.

The set up of the knife peel method was straight forward, as the sample could easily be clamped in a vice, although the small nature of the components led to difficulty aiming the blade, however magnifying binoculars could be positioned above the vice at the workstation which improved the visibility.

As this peel test method herein is not quantifiable, one of the initial goals of the study was a failure. However, the main overall goal of the study is to provide extra information for crack analysis. The study could continue because a manual peel test was implemented, which yielded successful peels, which revealed the desired surfaces for crack analysis, therefore in that regard the peel method can be considered a success.

Peel Results

This part of the discussion contains a review of the findings presented in the results section of this thesis. The purpose is to discuss the meanings behind the results and observations made with a focus on crack analysis, and examine the findings in relation to the main goals of this thesis; acquiring more understanding of defects for failure analysis.

Observational

The peel test yielded both successful and failed peels. A successful peel was defined in the results section, as a peel where the die pad separated from the OM cleanly with a popping action, without bending of the die pad or damage to the MEMS dies. Out of the samples tested, 6.7% of them were considered failures, for reasons such as the bending of the die pad, excessive damage to the die pad, or fragments of MEMS die remaining on the die pad surface. Peel-induced damages such as these prevented proper analysis from being carried out on the die pad surface due to obstruction of the non-peel-related artefacts. Although this was not considered a catastrophe for the peel testing carried out herein, it does reveal a risk that a sample can be irreversibly damaged using this method. Often failure analysis is carried out on "special" individual cases, if the sample is destroyed, without the required information obtainable, the failure analysis would be unsuccessful, therefore the failure rate of this test needs some improvement. The peel test also induced other damages to the samples which were considered less critical in peel success. These damages were often witness marks at the die pad edge, or scratches on the die pad surface.

The peel test was mostly a success with the two halves of the peel cleanly presented

after the peel. This allowed for analysis to be easily carried out on the surfaces which was the main goal of the study. The two halves of the peel revealed mirrored surfaces of each other, one half being the die pad surface, while the other was the OM material surface, these were shown in Figures 47 and 48 respectively. Both halves of the sample displayed the crack surfaces of the ASIC adhesive, and crack propagation areas around the ASIC area. The die pad side appeared to display more information than the OM side, particularly in the region of the die pad surface outside of the ASIC area. However, any surface interaction between the OM and the die pad could also be seen on the OM side.

The following are the main observational findings from the peel test, descriptions of what they could be, and reasons for them:

Adhesive crack at the ASIC interface:

A stand out feature of the die pad side peel images was cracking at the ASIC interface. This was characterised by a large amount of ASIC adhesive remaining of the die pad after the peel, as a consequence of the crack. The crack area at the ASIC interface was darker in contrast than areas that displayed cohesive cracking of the adhesive, this was due to the smooth nature of the adhesive at the ASIC surface, where the silver flakes would align with the ASIC surfaces, whereas in the cohesive areas the silver flakes were more randomly oriented, which consequently reflected more light under the microscope.

Similarly, on the OM side surface, the ASIC interface crack was easily seen, due to the ASIC backside being visible, characterised as a smooth looking surface. The cohesive zone of the crack can be seen around this area, with silver flakes clearly visible in the SEM images.

It is likely the cohesive zone is where the adhesive has fractured during the peel. It has been seen that TC-induced cohesive cracking usually presents itself when one inter-facial crack propagates to the other interface, in this case there was no lead frame interface cracking visible inbound of the cohesive zone. Interestingly, on the die pad side, the outer edges of the ASIC interface crack appear to be flush with the edge of the ASIC, where the adhesive fillet seems to have been peeled away from the die pad. There is a very small area of cohesive fracture between the ASIC edges and adhesive fillet, after which there is lead frame interface cracking at the bottom edge of the ASIC. It is possible this cohesive zone is also a result of the peel, where he fillet has detached from the lead frame, fracturing the adhesive, rather than being induced by the lead frame interface cracking.

It would be interesting to see whether below this ASIC interface crack is also lead frame interface cracking, however this is unfortunately impossible to see from this method. As there is no clear transition area between the lead frame interface crack and ASIC interface crack, it is likely the cracks are independent of each other. The square corners of the ASIC die and multiple material layers of differing coefficients of thermal expansion result in stress concentrations at

the corner at the ASIC interface, therefore this is the likely initiation point of the crack.

These crack areas correlate with areas of darker contrast in CSAM images, which is a good example of how these peel tests can be used to confirm CSAM findings.

Adhesive crack at lead frame interface:

Often in die side peel images there were darker patches visible around the ASIC edge. This is indicative of lead frame interface cracking. First of all, when examining the surface more closely with the SEM, the micro-pores of the lead frame surface in this area were filled with OM material, whereas the area between the micro-pores were completely clear of OM material, this suggested the crack propagated along the die pad surface, severing the OM bulk from OM globules inside the micro-pores.

Secondly, these areas correlated with areas of lighter contrast in the CSAM images, which has previously been confirmed to be lead frame interface cracking from cross section analysis.

It is possible this type of cracking also initiates at the corner of the ASIC due to stress concentrations, although the initiation point is not clear in the peel image. During TC testing, lighter contrast areas usually initiate approximately from the ASIC corner or edge area, then propagate along the ASIC edges, and towards the edge of the die pad away from the ASIC area. As seen in Figure 60, the crack visible in the peel image appears to follow the same progression.

Due to the lack of resolution in CSAM images it is difficult to see precisely whether the initiation point is in the ASIC corner or the ASIC adhesive corner, the peel image also does not show a clear initiation point and therefore the root cause remains unknown. However, in the peel image the ASIC area and crack area can easily be distinguished from each other, and the extents of the lead frame interface crack can easily be seen in the peel image which allows for accurate sample to sample comparison. It is interesting to note that the estimated crack initiation point occurs centrally within the bulk of the crack area, indicating the crack might have initiated and radially propagated outwards in all directions, including along the die pad where there is no adhesive, instead cracking through the OM material.

Also in Figure 60, inbound of the crack area is a line of silver-rich adhesive, which is a result of cohesive cracking. As the TC testing continues, the crack continues to propagate towards the centre of the ASIC area, where the cohesive cracking begins the crack surface has stop propagating along the die pad surface but instead begins to propagate through the adhesive bulk. It is suspected that this occurs due to cyclic fatigue.

Figure 56 displayed what the die pad interface crack looked like on the OM surface after peeling. The surfaces displayed a combination of areas covered with OM globules, which are spherically shaped bits of OM formed by the

micro-pores on the die pad, and areas where the globules have been severed from the surface. The surface with the broken globules corresponded exactly with the die pad interface crack on the die side peel, confirming the OM material remaining in the micro-pores.

Adhesive fillet perimeter:

The dark perimeter around the ASIC in the die pad side peel images appeared to be the outline of the adhesive fillet. The two SEM images in Figure 57 confirm the dark line was caused by remnants of ASIC adhesive. The main hypothesis for this was the tip of the adhesive fillet maintained enough adhesion to the die pad at the tip while the thickness of the adhesive in this area was very thin, causing it to be weak, resulting in fracture during the peel.

The adhesive outline is a useful artefact to have remaining on the die pad as it gives a clear impression of the ASIC adhesive area and allows for distinguishing between ASIC adhesive remnants and OM material remnants.

Voids:

In the ASIC area of the die pad side peel were clusters of circular ASIC adhesive remnants. These were the positions of voids in the adhesive. Usually voids occur due to air trapping or the shrinkage of the adhesive due to curing. It is clear these were voids because they lined up exactly with the void patterns seen in the X-ray images of the samples. Voids are essentially air gaps within the adhesive bulk, and when the peel was applied, the upper part and surrounding bulk of adhesive peeled away from the die pad but the bottom side of the adhesive surrounding the voids was left attached to the die pad, hence the remnants that can be seen.

Voids can easily be seen with X-ray imaging, therefore peel testing is an unnecessary test method for indicating the presence of voids. However, it is clear where there is ASIC adhesive left on the die pad at the location of a void, the void was within the thickness of the adhesive and not between the adhesive and the surface of the die pad or ASIC. Assuming the DA adhesive was free from bubbles upon application, this indicates the voids were formed after the DA process rather than during.

Die pad colouration:

The peeled die pads displayed various examples of discolouration around the ASIC area. First of all was the clean die pad area, this was characterised by a lighter area of contrast on the die pad. Under SEM it was confirmed the die pad and micro-pores were completely clean of any OM material. The corresponding area on the OM side of the peel showed intact OM globules, which had once sat inside the micro-pores, this shows the OM material was completely delaminated from the die pad in this area. As the clean area appeared to be emanating from the ASIC area, it is possible it was caused by the outgassing of organic gases during the curing of the adhesive [87].

It is unclear as to whether the delamination occurred due to outgassing after moulding forcing the OM material from the die pad, or whether the outgassing occurred pre-moulding, leaving a thin layer of residue on the die pad, which prevented adhesion of the OM material.

Another possibility is epoxy bleed-out. Epoxy bleed-out is a common occurrence in filled epoxies, where very fine amounts of colourless organic material leaks out of the adhesive into the surrounding area [88], which is in some ways similar to outgassing. Organic material spread onto the lead frame surface could also prevent proper adhesion between the OM material and the die pad.

As well as areas of lighter contrast on the die pad were areas of an orange hue emanating from the ASIC area, these areas were sometimes but not always clean of OM material, which suggests the cause is different to that of the lighter shades on the die pad. It is possible that one of these artefacts is caused by outgassing and the other is caused by epoxy bleed-out, which would explain the difference in appearance.

The orange hue and other areas of orange discolouration on the die pad are likely caused by tarnishing due to oxidation, however it is unclear what causes the area around the ASIC to tarnish. One possibility is that outgassing results in an air gap between the OM and the die pad which allows the die pad surface to oxidise.

The corresponding areas on the OM side of the peel also displayed discolouration. In this case there were rainbow tinted bands of colour, striped as though they are emanating away from the ASIC area. These colour bands could be caused by structural colouration of the light reflected, due to the changing thickness of a transparent thin film residue on the OM material. This is likely a layer of organic material on the surface, either due to outgassing or bleed-out. Epotek describes this phenomenon as a "halo ring" [88].

This kind of information about outgassing and bleed-out areas obtained from the peel tests could not obtained by other methods, it is therefore a useful addition to the analysis arsenal. Understanding these phenomena is crucial in rectifying the causes, for example, knowing the levels of outgassing from a sample, could help decide process parameters or lead to changes in wait times between die attach cure and over moulding. Additionally, the presence of organic compound on the die pad could be rectified by extra cleaning steps in between processes. With this in mind, the outgassing and bleed-out amounts could be interesting areas for further analysis, especially the measuring area of die pad affected for different amounts of adhesive and different wait times between processes.

OM residue on die pad:

Various areas of the peeled die pad displayed dark contrast compared with the clean areas. These areas were found to be where the OM material left residue on the die pad, confirmed by the SEM images. This was a similar finding to the area under a die pad interface crack, where the micro-pores were filled with OM material, however the difference is the areas which are purely OM residue with no crack present display OM material in the micro-pores and between the micro-pores, whereas the areas under the crack display OM residue only in the micro-pores.

These areas do not seem to offer too much information regarding adhesive cracking, however different amounts of OM material deposited on the lead frame between samples could suggest varying levels of surface interaction and adhesion between the OM material and the die pad. Most importantly though, the OM residue areas provide the boundaries of other interesting artefacts. These areas cannot be seen with traditional analysis techniques such as X-ray, CSAM, and cross section, which is another confirmation of the importance of the peel test.

Micro-pores under ASIC adhesive:

In the ASIC area after peeling, there was a darker residue left on the die pad. This could not be OM material as the area is obscured by the ASIC die and adhesive. It was suspected that this was the remnants of adhesive resin left in the micro-pores of the die pad after the peel, the dark appearance being due to the lack of silver filler.

The quality of adhesion between die pad and adhesive is not so easy to define from the images, but the presence of adhesive resin left in the micro-pores can be used as evidence of some level of adhesion. Similarly, A die pad which is completely clean under the ASIC adhesive is solid evidence of a lack of adhesion between die pad and adhesive. Figure 62 was a clear example of empty micro-pores under the adhesive and hence complete delamination. This type of failure could be caused by contamination of the die pad, preventing chemical adhesion, or a chemical mismatch between adhesive and substrate.

Clearness of die pad side images:

Some peeled die pad samples produced clear surfaces with well defined and easily recognisable artefacts and features, and some samples produced an extremely hazy surface, which somewhat obscured the features on the die pad, see Figure 61, and different amounts of haziness in between. It is not clear what causes these differences, but initially the effect looked similar to patches of OM material residue, however this cannot be possible over the ASIC area.

The effect of the haze is detrimental to the amount of information attainable from the peel samples, which is a problem for the peel test. Interestingly though, the level of haziness was consistent between samples from the same lead frame or batch, this suggests the reason behind the effect is not caused by the peel test itself, instead something related to the material interactions and processing parameters, however it is not clear what. This is an area that should be investigated further.

Quantification

The purpose of the quantification section was to examine and provide examples of how the visual artefacts could be translated into comparable numerical values. The importance of this lies in the way root cause analysis is often carried out, where variance in outputs are compared with variance of inputs. This requires linking the

output conditions to the input conditions. In the case of crack analysis, the output could be considered the size of the crack, after which comes the task of identifying the input conditions that lead to crack occurrence or increased crack size, by establishing correlations. In order to establish correlations, some kind of comparable value, usually numerical, needs to be measured and applicable to a range of different samples.

In this study two quantification methods were carried out, both of which revolve around the premise described in the Methodology section, and utilise the open source image processing software ImageJ. The difficulty with the samples herein was with the variance in image resolution between peel images and CSAM images, which affects the amount of pixels in any given area. In addition to this, there were subtle differences in magnification between the peel images, which would also affect the number of pixels seen. This meant that for each measurement a reference was required to be established which would remain consistent between samples, in this case the ASIC area was chosen.

The first method directly compared the measurement of peel images with CSAM images. The ASIC area was first measured in number of pixels in both images independently, then the crack areas were measured in pixels. For each image the crack areas were divided by the ASIC areas, this gave the crack size as a percentage of the ASIC area, and therefore a value which could be compared between the two images.

The percentage crack size was consistently and significantly larger in peel images than CSAM images by approximately 4.95%. This was due to several reason. Firstly the ASIC area is not as clearly defined in the CSAM images as it is in the peel images, and therefore the area is estimated. This leads to some error in the calculations, and likely over estimation. In addition to this, crack areas are more visible in the peel images and some areas visible in peel images are not visible in the CSAM images, and as a consequence a larger area was measured.

It would appear that measuring the crack areas from the peel images produced the most accurate results, which is important for sample comparisons, however consistently producing higher values is not necessarily desirable for specification reasons as a higher percentage of components would be recorded as failure, lowering the product yield.

The second method explored was a comparison between artefacts on the same samples. The samples chosen all displayed an orange hue around the ASIC, this was called outgassing for the sake of this study, but the cause is not entirely known. The total area of this orange hue was measured in pixels, this was then divided by the area of the ASIC, similarly to the crack, giving a value as a percentage of the ASIC area. Being a percentage of ASIC area meant the outgassing areas were comparable between samples, even though the outgassing did not actually occur in the ASIC area. These values were then plotted against the similarly calculated crack area percentages from the same samples.

The scatter plot did not display any clear correlation, however the extremes of the results do correlate, where the sample with the lowest crack area displayed the lowest outgas area and the sample with the highest crack area had the highest outgas area. There are too few samples over a too small range of cracking to establish a

correlation. The results in this case are inconclusive, but give a clear example of how the method could be used in future on a greater number of samples. The method has potential for utilisation in crack analysis and can also be applied to other visible artefacts.

Correlation

It is important to explore how the peel test being developed herein fits into the current analysis process and how the results link to or elaborate on the results obtained from other analysis methods. For this reason, a correlation study was carried out which directly compared the electrical, CSAM and peel results of 15 samples.

The samples were divided between five different lots, and the results were presented similarly. Lot 1 clearly displayed drifting in all three samples, whereas the other lots displayed mostly flat curves, bar a few outlier samples. CSAM images of the lot 1 parts clearly showed cracking at the bottom edge of the ASIC in all three samples, whereas the presence of cracking was unclear in the images of other lots. This was a clear example of correlation, but how did the peel images fit in?

First of all, the peel images displayed clear lot to lot variation between the samples, given by the visual similarities between samples of the same lot, but differences between the lots. This sort of detail was not present in CSAM images. Lots 1 and 5 were very similar in appearance in the peel images, both exhibiting a greyish hue with die pad interface cracking present, although worse cracking was visible in the lot 1 parts, however the CSAM images were completely dissimilar.

The other three lots had an orange tint hue about them rather than grey, it is also important to note the orange hue around the ASIC was present in these lots and not lots 1 or 5, which might explain why the samples appeared more orange. Lots 2 and 3 were very similar in appearance, even displaying a similar hazy pattern over the surface, whereas lot 4 samples were very clear in appearance with all artefacts clearly defined.

The drift and CSAM cracks visible in lot 1 clearly correlated with the die pad interface cracking in the lot 1 peel images, however the extent of the cracking was much clearer in the peel images. Some areas of cracking which were visible in the peels were not visible in the CSAM images, this sort of information could be valuable in correlating drifting to cracking, especially if these areas are not necessarily visible or distinguishable in the CSAMs.

The CSAM images generally displayed lots of yellow areas, which in some cases were obvious cracks, but in other cases just seemed to be noise as there was no clear correlation with the peeled samples. For example, lot 4 samples had large amounts of yellow at the bottom of the ASIC area, however in the peel images there is no clear evidence of this kind of crack, instead there are thin lines of adhesive material left on the die pad around the ASIC areas which indicates cohesive cracking, which is not visible in the CSAM images.

There was generally a lack of correlation between CSAM images and peel images in lots 2-5. Evident in lot 3 the CSAM images are almost identical, but all three samples displayed different amounts of cracking. Although, some cracking was present

in these samples, the cracking was not as severe as in lot 1. It is likely the crack severity was not enough to be clearly shown in CSAM images.

Likewise, the electrical results for lots 2-5 did not display much drift even though some cracking was present. The outlier parts did not display significant enough cracking which would set them apart from the other samples, with no correlation to the electrical results. This leaves the cause of the drifting unclear. Lots 1 and 5 appeared somewhat the same in hue with similar defect patterns in the peel images. However, lot 1 displayed considerably more cracking than lot 5. In addition the lot 1 samples were clearly drifting, whereas the lot 5 samples displayed no drift at all. Similarly to the CSAM images, a lack of crack severity may again have prevented the cracking from becoming evident in the drift plots.

The amounts of cracking visible from the peel images of all the parts were measured using the ImageJ software method. These were then plotted against the respective, X, Y and Z channel offset drift. The plots appeared to display correlation between the amount of cracking and amount of offset drift. The Y-channel displayed the strongest correlation from the data herein which might suggest the Y-channel is the most sensitive axis to cracking at the bottom edge of the die pad. Two populations of data were present in the plots, one population of low drift and low crack area, and a second population of high drift and high crack area. The second population was representative of the large amounts of cracking seen in the lot 1 parts and the clear offset drift. From this study there was a lack of data between the two populations to conclusively state what might have caused the non-linearity between the them. However, it is likely that there is a point when the amount of cracking surpasses a threshold, after which there is a steep increase in offset drift. This would explain why, even though similar in appearance, the lot 1 samples displayed significantly more drift than the lot 5 samples. Further study of more complete data sets would be required to confirm this possibility.

Even though the three test methods did not always correlate, when the electrical output was clearly drifting, there was a clear correlation between electrical, CSAM, and peel results. Generally, low amounts of cracking correlated with the electric results by displaying no drift. The destructive nature of the test means it can only be utilised as a post test analysis method. Considering the lack of detail displayed in CSAM images, it is clear the peel test would be a useful addition to the test chain simply due to the plethora of extra information acquirable. It has been shown in this study that there is variation between lots but very little variation within lots, this means there is also potential here to perform peel tests at the same test intervals as the electrical and CSAM measurements on samples from the same lots. The crack progression of samples in the lot can be monitored and studied, along side the electrical output. This would allow for measurement of the crack sizes at the different intervals, which would possibly indicate where most of the cracking occurs, whether during preconditioning, in early TC stages or late in the TC, and how this correlates with the electrical output. This could help get a clearer idea of how the defects develop within the sample, and the overall lifetime performance of the device.

What this Peel test means

It can be said that the peel test explored herein brings an additional dimension to crack analysis. A method was developed which could open over-moulded SOIC samples at the die pad and OM interface, revealing surface defects, interactions between the adhesive and substrate, as well as detailed three dimensional views of crack surfaces. This allowed for the gathering of lots of potentially useful information for crack analysis. The detail in the images enabled the implementation of numerical sample to sample comparison methods. Although the method is destructive of the sample, it fits into the crack analysis procedure in the place of CS analysis, which is also a destructive test method.

CS analysis is an established analysis method for crack analysis, but only two dimensional views of cracks can be obtained with little topographic information, whereas the peel test method has been proven to provide a larger and more informative overview of the crack surface and topography. For this reason peel testing could eventually replace CS analysis for studying cracks. Although, in this very primitive stage of the peel test implementation, CS analysis should be performed in parallel, because there are still many unknowns visible in the peel images such as, subtle areas which appear to be die pad interface cracks, but do not present themselves in CSAM images. CS analysis can be used to support the findings. There are also other disadvantages of the peel test, where the thickness of layers on the die pad are not so easily obtainable as they are with CS analysis. For example, the bond line thickness of the adhesive, which is an important control factor in the DA process, it would be impossible to ascertain this information with the peel test.

CSAM analysis has proven integral to analysing samples for cracking throughout the testing process. As this is a non-destructive test method, it cannot be replaced by the peel test, however the results herein have shown how the information provided by CSAM images is limited to only low resolution indications of cracks. This study also shows how the peel test is a very sensitive method for finding cracks, by providing evidence of how cracks were visible in peel images but not CSAM images. For this reason CSAM and peel testing should be used together, with CSAM images indicating the cracking at each test interval and the peel test for the detailed post-test-analysis.

The premise of the study was to achieve a peel test method which yields more information which can be used for crack analysis than currently available, not to necessarily identify the root causes themselves. This has been successfully achieved through the presentation of artefacts such as outgassing and epoxy bleed-out, as well as the three dimensional crack structures, and OM material interaction with the die pad surface, although further investigation of these artefacts is required to link them to crack formation, this test has certainly opened new avenues to explore. The information obtainable is vital as it can feed back into the design and processing of the samples through lessons learnt.

In a design sense, for example, if there appears to be too much presence of a defect such as epoxy bleed-out which might be linked to the initiation of cracking, then the results of peel testing could lead to the selection of a different die-attach adhesive which produces less bleed-out. Peel testing also allows for highly detailed

images of the surface quality of the lead frame, and how the micro-pores interact with the OM material and adhesive, potentially changing the formations of these micro-pores could have a substantial effect on the reliability of the adhesion. In a processing sense, the amounts of tarnishing, residues, and discolourations of the die pad can be altered by changing processing steps, controlling wait times, implementing new cleaning steps, the effect of altering these can be analysed through the peel test method.

What Next?

The samples used in this study were all identical, but the peel test method appears somewhat transferable to other similar over-moulded lead frame-based packages, such as quad flat packages and dual inline packages, due to the similarity in their construction. Sometimes the die pad can be securely connected to the outside leads and not completely freely floating in the OM material, as can be the case in the corners of some quad flat layout die pads for example, which can make getting a clean peel a little difficult. In some cases like this it may be possible to use grinding to overcome these difficulties. However, further investigation is required to confirm the method is fully transferable to other similar package times. It is quite likely that the method would need to be adapted on a design to design basis.

Pre-moulded SOIC packages unfortunately cannot be peeled in the same way. A separate method would be need to be developed in order to perform peel tests on pre-moulded packages. In this case the die pad is accessible, by removing the lid and protection medium, however, the elements are not surrounded by OM material, meaning there is nothing hold the them in place when performing a peel. It is likely the elements would require individual peeling one by one using a very delicate and precise method in order to achieve similar results to the peel test herein.

One failure of the study herein was to make the peel itself quantifiable, this was due to lack of a sufficient method to secure the die pad to a test machine. An area for future development and a large improvement to this test would be to solve this issue. One option to improve the glue method trialled herein would be to implement some form of surface preparation before gluing the screw to the die pad, this could possibly improve the adhesion and lead to a successful peel test. Alternatively, if the glue method still fails to produce successful peels, it is likely the de-capsulation method would need to be revised. If the die pad can be free from OM material on all four edges, leaving the die pad proud of the OM material, there would be less resistance to peeling. To achieve this, milling or laser ablation could be used, for example, but these methods come with costs. However with costs aside, with the die pad proud of the OM material perhaps the glue method would work, although the viability of the results is not guaranteed with glue.

An alternative to gluing, if a minimum of three edges are exposed, there are extra possibilities for attachment to the die pad. For example, a two-pronged tool with tapered edges, orientated parallel to the backside surface, which can grab the die pad from opposite edges by sliding onto and embedding in them, and support itself on the perpendicular edge, would have a secure attachment to three edges of

the die pad. After it is securely attached it could initiate the peel by being tilted by a machine, and the load required to tilt could be measured. For this a specially designed fixture may be required to support the sample during the peel.

Another alternative would be to automate the knife peel method by attaching the blade to a cantilever piezoelectric actuator, similar to that of an atomic force microscope (AFM). Difficulties would still remain in positioning the blade accurately and consistently, but the peel forces could be measured.

If the sample can be peeled in a controllable and automated manner, as per above, then not only would the failure rate decrease,the amount of damage inflicted to the samples would decrease, and there would likely be less variability between the samples caused by the manual peel, making them more consistent. However, the most important part of the peel test are the artefacts presented on the peeled surfaces, therefore, in addition to improving the peel test, future efforts should also focus on deciphering the unknown artefacts present. These artefacts could be caused by all manner of different things, such as, outgassing, bleed-out, tarnishing, and understanding them could be the key to preventing unwanted defects such as cracking.

6 Summary and Conclusions

The safety criticality of inertial sensors in the automotive industry demands component reliability through the most stringent of test procedures, and understanding the causes of adverse outputs, such as die attach adhesive cracking, is crucial in the device development. This study explored a new adhesive peel test method which could be implemented on such a device with the same build as it would have in-situ.

Initially various de-capsulation methods were explored and discussed, but the final choice was limited to grinding, due to availability in the lab, and the cost of implementing more advanced methods. One of the goals with the peel method was to be able to record the forces required to initiate the peel, it was believed this would provide useful information about the adhesion strength of the die attach adhesive, and could be used for correlation with cracking and delamination occurrences. However, a measurable peel test was eventually deemed unfeasible for this study, after a succession of peel failures.

It was then decided to adapt a manual peel method which would still separate the die pads from the samples and allow for surface analysis of the peels. The switch to a manual peel test meant that grinding was a sufficient de-capsulation method, whereas grinding may have introduced variability and error to the results of a measurable automated peel test.

The manual peel test mostly yielded successful peels, with only a few samples suffering damage which led to the scrapping of the sample. The successful peels clearly displayed cracked areas of adhesive at the ASIC interface and at the die pad interface, which could be easily identified with an optical microscope and a SEM. The cracked surfaces were examined, and the images captured the crack geometry and topography in three dimensions, allowing for detailed exploration of the crack morphology for failure analysis purposes.

The peeled images also displayed a wide array of other artefacts, which cannot be fully explained through initial observations and are out of the scope of this study, instead requiring future investigation. These artefacts provide interesting new avenues to explore for future crack root cause analyses.

As well as presenting the visual findings of the peel surfaces herein, quantification and correlation methods were explored and suggested with a mixture of results. The measuring of the peel surfaces proved to be a more accurate method than measuring CSAM images, and the measurements of peel artefacts could be done in such a way that sample to sample comparisons were possible. An initial study of comparing crack amount with amount of orange hue artefact was possible but did not yield any clear correlation between the limited number of samples trialled.

An overview of how the peel test could fit in with current analysis methods was carried out via a correlation study, where electrical, CSAM, and peel results were compared. The peel results were proven to support examples where large amounts of drift were recorded and large areas of cracking could be seen in CSAM images, as well as giving clear evidence of visual lot to lot variation which is not visible from electrical or CSAM results. The peel images also displayed evidence of cracking in samples which did not correlate with any of the other methods, suggesting it is a

more sensitive method for crack detection than the other two.

It was concluded that peel testing would be a useful post-analysis tool which can be used in parallel with CS analysis and CSAM analysis to determine the nature of cracking, and thus supply more weight to evidence for root cause analysis. However, for reasons of improving accuracy and repeatability, it was suggested that further development is required of the peel method herein to achieve automation and the measurability of the peel forces.

Bibliography

[1] A. Merdassi, *Ultra-clean Wafer-level Vacuum Encapsulated Inertial Sensors Using a Commercial Process*. PhD thesis, McGill University Libraries, 2017.

[2] M. Kraft and N. M. White, *MEMS for automotive and aerospace applications*. 2013.

[3] D. Suhl, "Thermally induced ic package cracking," *IEEE Transactions on Components, Hybrids, and Manufacturing Technology*, vol. 13, no. 4, pp. 940–945, 1990.

[4] S. Schröder, F. Niklaus, A. Nafari, E. R. Westby, A. C. Fischer, G. Stemme, and S. Haasl, "Stress-minimized packaging of inertial sensors by double-sided bond wire attachment," *Journal of Microelectromechanical Systems*, vol. 24, no. 4, pp. 781–789, 2015.

[5] E. Tatar, T. Mukherjee, and G. K. Fedder, "Stress effects and compensation of bias drift in a mems vibratory-rate gyroscope," *Journal of Microelectromechanical Systems*, vol. 26, no. 3, pp. 569–579, 2017.

[6] T.-M. I. Băjenescu, "Mems manufacturing and reliability," 2019.

[7] D. J. Fonseca and M. Sequera, "On mems reliability and failure mechanisms," *Journal of Quality and Reliability Engineering*, vol. 2011, 2011.

[8] V. Khanna, "Adhesion–delamination phenomena at the surfaces and interfaces in microelectronics and mems structures and packaged devices," *Journal of Physics D: Applied Physics*, vol. 44, no. 3, p. 034004, 2010.

[9] O. Grosshardt, B. Á. Nagy, and A. Laetsch, "Applying microscopic analytic techniques for failure analysis in electronic assemblies," *Applied Microscopy*, vol. 49, no. 1, p. 7, 2019.

[10] M. Uddin, M. Alam, Y. Chan, and H. Chan, "Adhesion strength and contact resistance of flip chip on flex packages—-effect of curing degree of anisotropic conductive film," *Microelectronics Reliability*, vol. 44, no. 3, pp. 505–514, 2004.

[11] J. Kim, T. Lee, T. Kim, and K. Paik, "The effect of anisotropic conductive films adhesion on the bending reliability of chip-in-flex packages for wearable electronics applications," *IEEE Transactions on Components, Packaging and Manufacturing Technology*, vol. 7, no. 10, pp. 1583–1591, 2017.

[12] M. Rezaee, L.-C. Tsai, M. I. Haider, A. Yazdi, E. Sanatizadeh, and N. P. Salowitz, "Quantitative peel test for thin films/layers based on a coupled parametric and statistical study," *Scientific Reports*, vol. 9, no. 1, pp. 1–11, 2019.

[13] T. Ferracin, C. Landis, F. Delannay, and T. Pardoen, "On the determination of the cohesive zone properties of an adhesive layer from the analysis of the wedge-peel test," *International Journal of Solids and Structures*, vol. 40, no. 11, pp. 2889–2904, 2003.

[14] M. Nase, M. Rennert, S. Henning, A. Zankel, K. Naumenko, and W. Grellmann, "Fracture mechanics characterisation of peelfilms," in *Deformation and Fracture Behaviour of Polymer Materials*, pp. 271–281, Springer, 2017.

[15] I. Mohammed, M. Charalambides, and A. Kinloch, "Modelling the interfacial peeling of pressure-sensitive adhesives," *Journal of Non-Newtonian Fluid Mechanics*, vol. 222, pp. 141–150, 2015.

[16] X. Niu, S. Nasser, C. Goodall, and N. El-Sheimy, "A universal approach for processing any mems inertial sensor configuration for land-vehicle navigation," *Journal of Navigation*, vol. 60, no. 2, pp. 233–246, 2007.

[17] H. Du and R. Bogue, "Mems sensors: past, present and future," *Sensor Review*, 2007.

[18] M. Perlmutter and S. Breit, "The future of the mems inertial sensor performance, design and manufacturing," in *2016 DGON Intertial Sensors and Systems (ISS)*, pp. 1–12, IEEE, 2016.

[19] R. Rao, "Prime faraday technology watch isbn 1-84402-020-7 an introduction to mems an introduction to mems (micro-electromechanical systems) prime faraday partnership prime faraday partnership."

[20] P. D. Milano, *Desing and simulation of capacitive accelerometers*. Available at http://www.mems.polimi.it/accelerometers.html.

[21] G. M. Projects, *Gyroscopes and Accelerometers on a Chip - Geek Mom Projects*. Available at https://www.scribd.com/document/345071032/Gyroscopes-and-Accelerometers-on-a-Chip-Geek-Mom-Projects.

[22] M. Perlmutter and L. Robin, "High-performance, low cost inertial mems: A market in motion!," in *Proceedings of the 2012 IEEE/ION Position, Location and Navigation Symposium*, pp. 225–229, 2012.

[23] J. Korvink and O. Paul, *MEMS: A practical guide of design, analysis, and applications*. Springer Science & Business Media, 2010.

[24] D. Xia, C. yu, and L. Kong, "The development of micromachined gyroscope structure and circuitry technology," *Sensors (Basel, Switzerland)*, vol. 14, pp. 1394–473, 01 2014.

[25] J. Marek, "Mems for automotive and consumer electronics," in *2010 IEEE International Solid-State Circuits Conference - (ISSCC)*, pp. 9–17, 2010.

[26] "Road vehicles – Functional safety," standard, International Organization for Standardization, Geneva, CH, Dec 2018.

[27] J. Marek, "Mems technology- from automotive to consumer," in *2007 IEEE 20th International Conference on Micro Electro Mechanical Systems (MEMS)*, pp. 59–60, 2007.

[28] C. J. Kahane, "Lives saved by vehicle safety technologies and associated federal motor vehicle safety standards, 1960 to 2012–passenger cars and ltvs–with reviews of 26 fmvss and the effectiveness of their associated safety technologies in reducing fatalities, injuries, and crashes," *Report No. DOT HS*, vol. 812, p. 069, 2015.

[29] F. Pieri, C. Zambelli, A. Nannini, P. Olivo, and S. Saponara, "Limits of sensing and storage electronic components for high-reliable and safety-critical automotive applications," in *2017 International Conference of Electrical and Electronic Technologies for Automotive*, pp. 1–7, IEEE, 2017.

[30] H. Tilmans, J. D. Coster, P. Helin, V. Cherman, A. Jourdain, P. D. Moor, B. Vandevelde, N. Pham, J. Zekry, A. Witvrouw, and I. D. Wolf, "MEMS packaging and reliability: An undividable couple," *Microelectronics Reliability*, vol. 52, pp. 2228–2234, Sept. 2012.

[31] M. K. Mishra, V. Dubey, P. Mishra, and I. Khan, "Mems technology: A review," *Journal of Engineering Research and Reports*, pp. 1–24, 2019.

[32] J. F. Breedis, P. Y. Chia, and Y. Goh, "Electronic packaging: Lead frame materials 73," in *Reference Module in Materials Science and Materials Engineering*, Elsevier, 2017.

[33] P. Lippens, *Low-pressure cold plasma processing technology*, p. 64–78. Elsevier, 2007.

[34] F. E. Andros and B. G. Sammakia, "Integrated circuit packaging," in *Encyclopedia of Physical Science and Technology*, pp. 883–896, Elsevier, 2003.

[35] W.-H. Li, "A study of plasma-cleaned ag-plated cu leadframe surfaces," *Journal of Electronic Materials*, vol. 39, pp. 295–302, 03 2009.

[36] S. Industries, *Shinko Industries - Lead Frames*. Available at https://www.shinko.co.jp/english/product/ic-package/leadframe/.

[37] H. Kuisma, A. Cardoso, N. Mäntyoja, R. Rosenkrantz, S. Nurmi, and M. Gall, "Fo-wlp multi-dof inertial sensor for automotive applications," in *2018 7th Electronic System-Integration Technology Conference (ESTC)*, pp. 1–7, IEEE, 2018.

[38] R. Components, *MEMS SOIC - RS Components*. Available at https://uk.rs-online.com/web/p/accelerometer-sensors/8212425/.

[39] S. Takeda, T. Masuko, N. Takano, and T. Inada, "Die attach adhesives and films," in *Materials for advanced packaging*, pp. 469–510, Springer, 2017.

[40] B. Mouawad, *Innovative power electronics assemblies using the "Spark Plasma Sintering" technique*. PhD thesis, 03 2013.

[41] P. Micro, *The economic manufacture of lead frames – a technical comparison*. Available at https://www.precisionmicro.com/the-economic-manufacture-of-lead-frames-a-technical-comparison/.

[42] Renyi Wang, R. Kuder, Bing Wu, G. T. Emmerson, and G. J. Seeley, "Understanding lead frame surface treatment and its impact on package reliability," in *52nd Electronic Components and Technology Conference 2002. (Cat. No.02CH37345)*, pp. 947–954, 2002.

[43] A. Lewis and A. Babiarz, "Conductive adhesive dispensing process considerations," in *NEPCON WEST*, pp. 335–349, Citeseer, 1999.

[44] D. Hollocher, S. Zhang, A. Sparks, S. Bart, W. Sawyer, P. Narayanasamy, C. Pipitone, J. Memishian, H. Samuels, S.-L. Ng, R. Mhatre, D. Whitley, F. Sammoura, M. Bhagavat, C. Tsau, K. Nunan, M. Judy, M. Farrington, and K. Yang, "A very low cost, 3-axis, mems accelerometer for consumer applications," pp. 953 – 957, 11 2009.

[45] H. Engineering, *Harwin Engineering - Mold Tool*. Available at http://www.harwinengineering.com.hk/gallery6.htm.

[46] S. S. T. Co.LTD., *IC Plating Chemicals - Plating pre-treatment > Chemical Deflash*. Available at http://www.sunstech.com.tw/index_en.php?action=products_in&cid=1&cid2=12&cid3=22.

[47] E. semiconductor manufacturing, *EEsemi - Lead Coating*. Available at https://www.eesemi.com/leadfinish.htm.

[48] B. Fang, W. Chou, and L. Ding, "An optimal calibration method for a mems inertial measurement unit," *International Journal of Advanced Robotic Systems*, vol. 11, no. 2, p. 14, 2014.

[49] M. Gheorghe, "Advanced calibration method, with thermal compensation, for 3-axis mems accelerometers," *SCIENCE AND TECHNOLOGY*, vol. 19, no. 3, pp. 255–268, 2016.

[50] T. Kose, K. Azgin, and T. Akin, "Temperature compensation of a capacitive mems accelerometer by using a mems oscillator," in *2016 IEEE International Symposium on Inertial Sensors and Systems*, pp. 33–36, 2016.

[51] P. Aggarwal, Z. Syed, X. Niu, and N. El-Sheimy, "A standard testing and calibration procedure for low cost mems inertial sensors and units," *The Journal of Navigation*, vol. 61, no. 2, p. 323, 2008.

[52] T. Gillespie, "Fundamentals of vehicle dynamics," 01 2000.

[53] D. Steckelberg, *Development of an internal combustion engine fuel map model based on on-board acquisition*. PhD thesis, 11 2016.

[54] C. R. Marra, F. M. Ferrari, S. Karman, A. Tocchio, F. Rizzini, and G. Langfelder, "Single-resonator, time-switched fm mems accelerometer with theoretical offset drift complete cancellation," in *2018 IEEE Micro Electro Mechanical Systems (MEMS)*, pp. 117–120, 2018.

[55] C. R. Marra, A. Tocchio, F. Rizzini, and G. Langfelder, "Solving fsr versus offset-drift trade-offs with three-axis time-switched fm mems accelerometer," *Journal of Microelectromechanical Systems*, vol. 27, no. 5, pp. 790–799, 2018.

[56] X. Zhang, S. B. Park, R. Navarro, and M. W. Judy, "Accurate assessment of packaging stress effects on mems devices," in *Thermal and Thermomechanical Proceedings 10th Intersociety Conference on Phenomena in Electronics Systems, 2006. ITHERM 2006.*, pp. 1336–1342, 2006.

[57] X. Zhang, S. Park, and M. W. Judy, "Accurate assessment of packaging stress effects on mems sensors by measurement and sensor–package interaction simulations," *Journal of microelectromechanical systems*, vol. 16, no. 3, pp. 639–649, 2007.

[58] A. E. C. C. T. Committee, "Failure mechanism based stress test qualification for integrated circuits," tech. rep., 09 2014.

[59] R. W. Johnson, J. L. Evans, P. Jacobsen, J. R. Thompson, and M. Christopher, "The changing automotive environment: high-temperature electronics," *IEEE Transactions on Electronics Packaging Manufacturing*, vol. 27, no. 3, pp. 164–176, 2004.

[60] R. Siregar, M. Adhitya, D. Sumarsono, N. Nazaruddin, G. Heryana, and F. Zainuri, "Study the brake performance of a passenger car based on the temperature that occurs in each brake unit," *AIP Conference Proceedings*, vol. 2227, 05 2020.

[61] W. Wang, Y. Yao, X. Long, and Z. Zhu, "Material and structural optimization of fatigue life of pbga under temperature cycling," in *2018 19th International Conference on Electronic Packaging Technology (ICEPT)*, pp. 477–481, 2018.

[62] A. A. O. Tay and Tingyu Lin, "Moisture diffusion and heat transfer in plastic ic packages," *IEEE Transactions on Components, Packaging, and Manufacturing Technology: Part A*, vol. 19, no. 2, pp. 186–193, 1996.

[63] S. E. test Chambers, *Two Zone Thermal Shock Test Chamber , Environmental Conditioning Thermal Test Chamber*. Available at http://www.climatic-chambers.com/sale-10893422-two-zone-thermal-shock-test-chamber-environmental-conditioning-thermal-test-chamber.html.

[64] W. Wang, Z. Chen, S. Wang, and X. Long, "Mechanics-based acceleration for estimating thermal fatigue life of electronic packaging structure," *Microelectronics Reliability*, vol. 107, p. 113616, 2020.

[65] S. Abdullah, F. Abdullah, A. K. Ariffin, and A. Jalar, "Thermal-mechanical analysis of a different leadframe thickness of semiconductor package under the reflow process," *American Journal of Applied Sciences*, vol. 6, 04 2009.

[66] G. Rabilloud, "Adhesives for electronics," in *Handbook of Adhesives and Surface Preparation*, pp. 259–299, Elsevier, 2011.

[67] H. Watanabe, N. Yamada, and M. Okaji, "Linear thermal expansion coefficient of silicon from 293 to 1000 k," *International Journal of Thermophysics*, vol. 25, pp. 221–236, 01 2004.

[68] A. A. O. Tay and T. Y. Lin, "Influence of temperature, humidity, and defect location on delamination in plastic ic packages," *IEEE Transactions on Components and Packaging Technologies*, vol. 22, no. 4, pp. 512–518, 1999.

[69] A.-Y. Park, S. C. Chaparala, and S. Park, "Risk assessment of the crack propagation and delamination of the cu-to-cu direct bonded (cudb) interface," *Microelectronics Reliability*, vol. 66, pp. 113–121, 2016.

[70] G. Kelly, *The simulation of thermomechanically induced stress in plastic encapsulated IC packages*. Springer Science & Business Media, 2012.

[71] A. A. O. Tay, G. L. Tan, and T. B. Lim, "Predicting delamination in plastic ic packages and determining suitable mold compound properties," *IEEE Transactions on Components, Packaging, and Manufacturing Technology: Part B*, vol. 17, no. 2, pp. 201–208, 1994.

[72] V. Gektin, A. Bar-Cohen, and J. Ames, "Coffin-manson fatigue model of underfilled flip-chips," *IEEE Transactions on Components, Packaging, and Manufacturing Technology: Part A*, vol. 20, no. 3, pp. 317–326, 1997.

[73] S. S. Manson, *Behavior of materials under conditions of thermal stress*, vol. 2933. National Advisory Committee for Aeronautics, 1953.

[74] L. F. Coffin Jr, "A study of the effects of cyclic thermal stresses on a ductile metal," *Transactions of the American Society of Mechanical Engineers, New York*, vol. 76, pp. 931–950, 1954.

[75] S. Bazhenov and A. Berlin, "Destruction of polymers and adhesion layers," *Polymer Science - Series D*, vol. 4, pp. 102–117, 04 2011.

[76] P. Aryan, S. Sampath, and H. Sohn, "An overview of non-destructive testing methods for integrated circuit packaging inspection," *Sensors*, vol. 18, no. 7, p. 1981, 2018.

[77] N. Kotwaliwale, P. Weckler, G. Brusewitz, G. Kranzler, and N. Maness, "Non-destructive quality determination of pecans using soft x-rays," *Postharvest Biology and Technology - POSTHARVEST BIOL TECHNOL*, vol. 45, pp. 372–380, 09 2007.

[78] P. Labs, *Priority Labs - XRAY Gallery.* Available at http://prioritylabs.com/engineering-services/x-ray/.

[79] P. Rework, *PDR ReWork - GenX-90P XRAY Machine.* Available at https://www.pdr-rework.com/genx-90-x-ray-system.

[80] A. Technology, *How it works Scanning Acoustic Microscopy (C-SAM).* Available at https://wpo-altertechnology.com/how-it-works-scanning-acoustic-microscopy-c-sam/.

[81] D. Zooker, M. Vizentovski, A. Fish, O. Keren, and Y. Weizman, "Vulnerability of secured iot memory against localized back side laser fault injection," pp. 7–11, 09 2017.

[82] P. Dobriyal, A. Kurella, and S. Southwick, "On-board package decapsulation techniques for failure analysis," in *Proceedings of Surface Mount Technology Association International Symposium*, 2015.

[83] S. D. Brandenburg and J. S. Tsai, "Methods to provide and expose a diagnostic connector on overmolded electronic packages," June 30 2009. US Patent 7,553,680.

[84] R. K. Lowry, "Laser decapsulation method," Jan. 1 2002. US Patent 6,335,208.

[85] R. R. Wurzbacher and S. B. Walchli, "System and method for decapsulating an encapsulated object," Feb. 5 2008. US Patent 7,326,305.

[86] J. V. Ellerson, L. J. Konrad III, R. J. Moore, and J. A. Varcoe, "Apparatus and method for selectively etching a plastic encapsulating material," Oct. 12 1993. US Patent 5,252,179.

[87] M. Khan, T. Tarter, and H. Fatemi, "Aluminum bond pad contamination by thermal outgassing of organic material from silver-filled epoxy adhesives," *IEEE Transactions on Components, Hybrids, and Manufacturing Technology*, vol. 10, no. 4, pp. 586–592, 1987.

[88] Epotek, *Understanding and Preventing Epoxy Resin Bleed.* Available at http://www.epotek.com/site/files/Techtips/pdfs/tip16.pdf.